

THE BONN MESON-EXCHANGE MODEL FOR THE NUCLEON-NUCLEON INTERACTION

R. MACHEIDT

Los Alamos National Laboratory, MS H850, Los Alamos, NM 87545, U.S.A.

and

Department of Physics, University of California, Los Angeles, CA 90024, U.S.A.

and

K. HOLINDE and Ch. ELSTER

*Institut für Theoretische Kernphysik der Universität Bonn, Nussallee 14–16, D-5300 Bonn,
West Germany*



NORTH-HOLLAND – AMSTERDAM

THE BONN MESON-EXCHANGE MODEL FOR THE NUCLEON-NUCLEON INTERACTION*

R. MACHELEIDT[†]

Los Alamos National Laboratory, MS H850, Los Alamos, NM 87545, U.S.A.

and

Department of Physics, University of California, Los Angeles, CA 90024, U.S.A.

and

K. HOLINDE⁺⁺ and Ch. ELSTER

Institut für Theoretische Kernphysik der Universität Bonn, Nussallee 14-16, D-5300 Bonn, West Germany

Received 6 October 1986

Contents

1. Introduction	3	8.2.2. The vertex form factors	38
2. Historical perspective	6	8.3. Final remarks concerning the results	39
3. Basic features and assumptions of the model	8	9. The parametrization of the nuclear force by one-boson-exchange terms	40
4. One-meson-exchange contributions	10	9.1. A relativistic OBEP in q -space (OBEPQ)	40
5. The 2π -exchange model	11	9.2. A nonrelativistic OBEP in r -space (OBEPR)	41
6. The πp contribution	19	9.3. Features of approximate representations of the nuclear force	43
7. Further 3π and 4π contributions	23	10. Some remarks concerning nuclear structure	44
8. Results for the full model and discussion	25	11. Summary, conclusions and outlook	46
8.1. Predictions for the NN data	25	Appendix A: Field-theoretical framework for mesons and baryons	47
8.1.1. NN scattering	25	Appendix B: Meson-exchange contributions in time-ordered perturbation theory	50
8.1.2. The deuteron and the low-energy scattering parameters	32		
8.2. The meson parameters	35		
8.2.1. The coupling constants	36		

* Supported in part by Deutsche Forschungsgemeinschaft.

[†] Formerly: Institut für Theoretische Kernphysik der Universität Bonn, Nussallee 14-16, D-5300 Bonn, West Germany, and TRIUMF, 4004 Westbrook Mall, Vancouver, B.C., Canada V6T 2A3.

⁺⁺ Also: Institut für Kernphysik, KFA Jülich, D-5170 Jülich, West Germany.

Single orders for this issue

PHYSICS REPORTS (Review Section of Physics Letters) 149, No. 1 (1987) 1-89.

Copies of this issue may be obtained at the price given below. All orders should be sent directly to the Publisher. Orders must be accompanied by check.

Single issue price Dfl. 63.00, postage included.

Appendix C: NN scattering	57	Appendix F: Coordinate space OBEP (OBEPF)	82
Appendix D: The deuteron	62	References	85
Appendix E: Relativistic momentum space OBEP (OBEPQ)	70		

Abstract:

We present a comprehensive field-theoretical meson-exchange model for the nucleon–nucleon (NN) interaction below pion production threshold consisting of all diagrams which we believe to be important. Fictitious terms, which characterized most boson-exchange models of the past, are strictly avoided. In particular, apart from the well-known one-pion and one-omega exchange, our model contains an explicit determination of the 2π -exchange contribution. In this 2π -exchange model we take into account virtual isobar excitation and direct $\pi\pi$ -interactions consistent with the empirical information from πN and $\pi\pi$ scattering. In addition, higher-order diagrams involving heavy-meson exchanges are included, especially the combination of π and ρ which proves to be crucial for a quantitative description of the low angular momentum phase shifts of NN scattering. Explicit predictions are given for NN scattering and for the deuteron. The overall description of the data is of excellent quality.

The comprehensive character of our model yields a definite prediction of the meson–nucleon (–isobar) vertex parameters (coupling constants and cutoff parameters of the vertex form factors). These result from our quantitative fit to the NN data and may in the future be related to QCD. The model provides a sound basis for addressing several important issues in nuclear physics, such as three-body forces, meson-exchange currents, charge symmetry and independence violations, relativistic effects and effects of the nuclear medium on the NN force in the nuclear many-body problem.

We also present a simple parametrization of the model by one-boson-exchange terms (in momentum as well as in coordinate space). This is convenient for practical purposes and may be useful in applications to nuclear structure physics.

1. Introduction

It is now widely believed that quantum chromodynamics (QCD) [1] is the fundamental theory of strong interactions. On that basis, the nucleon–nucleon (NN) interaction is completely determined by the underlying quark–gluon dynamics. However, due to the formidable mathematical problems raised by the non-perturbative character of QCD in the low-energy regime, we are still far from a quantitative understanding of the NN force from this point of view.

Closely related and of even broader relevance is the problem of the confinement of hadrons. Here, the intractability of low-energy QCD* is usually circumvented by the ad hoc introduction of (picking one of the most popular euphemisms in modern physics) “QCD-inspired” models, e.g. bag or potential models. There are naturally large uncertainties in the details of these models. For example, in the context of bag models, a crucial question is the size of the confinement radius R . Should R turn out to be small ($R \lesssim 0.5$ fm) as suggested by the little bag [3], there would be enough room for conventional hadrons like nucleons, mesons and isobars to represent the essential degrees of freedom for a wide range of nuclear physics phenomena, and meson exchange would be a valid picture. In that case, the appropriate procedure is to construct the nuclear force from meson–nucleon and meson–isobar vertices, these being understood as effective descriptions of complicated multi-quark reactions. Hadron masses, coupling constants and vertex form factors, which are the physical parameters of such a meson theory, are then left to be ultimately explained by QCD [4, 5].

Genuinely new quark–gluon processes, which do not belong to the class of diagrams represented by meson exchange, may occur only for overlapping hadrons. Therefore, their role depends decisively on the hadron size. As discussed, for small R ($\lesssim 0.5$ fm) they should have a negligible influence provided the consideration is restricted to phenomena involving comparatively low energies and momentum transfer, such as NN scattering up to a laboratory energy of about 300 MeV and nuclear binding energies. In this case, the introduction of meson–nucleon (–isobar) vertex form factors would be a sufficient accounting of the inner structure of the hadrons and its consequences.

* Presently the only promising treatment of low-energy QCD is lattice-gauge theory [2]. However, because of computational restrictions on present-day computers, lattice QCD is not (yet) a practical tool for everyday nuclear physics.

The situation may be substantially different if the bag radius is large ($R \gtrsim 0.8$ fm) as is suggested by the MIT-bag [6] or the cloudy-bag model [7]. In a naive interpretation these radii may tolerate just the pion, leave no room for the heavier scalar and vector bosons, and instead require the inclusion of genuine quark-gluon-exchange processes as dominant contributions. The question of whether such processes can indeed quantitatively take over the empirically established role of higher-mass exchanges (mainly building up the short-range part of the NN force) has been studied by various groups in recent years [8–16]. We believe that this is still an open question. Although there seems to be no problem in obtaining sufficient repulsion at short range, all known models of this kind create either too little or no intermediate-range attraction (which is sometimes artificially cured by adding a suitable attraction arising from scalar boson exchange). Moreover, it has not yet been demonstrated convincingly that such models can supply the proper ratio of spin-orbit strength to central repulsion. In addition to uncertainties inherent in the nonrelativistic potential models (as, e.g., the questions of nucleon size, the effect of configuration mixing or the choice of the quark–quark interaction) there is a much more serious problem: Namely, the quark–quark spin-orbit interaction, which provides the NN spin-orbit force in such calculations, seems to be suppressed in baryons, since corresponding spin-orbit splittings have not been seen in the excited states of the nucleon [17]. Thus, we are as yet far from a quantitative and consistent description of the one- and two-baryon system using such potential models.

An alternative approach to low-energy QCD is offered by the Skyrme model. Following a proposal by 't Hooft [18], QCD is generalized from SU(3) to an $SU(N_c)$ gauge group, with N_c the number of colours. In this generalization, $1/N_c$ is the coupling constant. If one assumes confinement, then, in the large N_c limit, QCD is supposedly equivalent to a local meson field theory. Furthermore, in this theory it can be shown that baryons arise as soliton solutions of the meson field equations [19], an idea which was advanced by Skyrme [20] about twenty years ago. In this “Skyrme” model the exact size of the bag radius does not play a decisive role and can, in fact, be rather small [21]. This feature is most beautifully described by the magic picture of the “Cheshire cat” [22] (here, the bag wall) which tends to fade away when examined closely, leaving behind only its grin (here, the confinement) [23]. Vector bosons can be introduced into the Skyrme model in a natural way [24]. More details of this approach to low-energy QCD are given in the Zahed–Brown review [25].

Thus, from the point of view of models which in some sense may claim to approximate QCD, there are strong theoretical indications that *meson theory** is the appropriate concept for the NN interaction and for the domain of nuclear physics in general.

In addition, there is traditionally strong phenomenological evidence for the meson-exchange picture of nuclear forces and for the presence of mesons in nuclei [26]. The peripheral partial waves in NN scattering furnished early evidence of the one-pion exchange (see section 2 for references) and, more recently, the asymptotic D/S state ratio of the deuteron provided further proof for the reality of the pion in the two-nucleon system [27]. Moreover, it is well known that meson-exchange current contributions are crucial in several reactions involving very light nuclei, such as the radiative capture of protons by thermal neutrons, the electrodisintegration of the deuteron near threshold at backward angles and the magnetic form factor of ${}^3\text{He}$ [26]. In fact, meson exchange is at present, and in the foreseeable future, the only quantitative model for the NN interaction (apart from purely phenomenological treatments, of course). Such a representation of the nuclear force, provided by an

* We should note that nowadays the term “meson theory” is strictly speaking incorrect, since a “meson theory” in the fundamental sense of the word “theory” does not exist. (QCD may turn out to be a theory.) However, for historical reasons, this term is well established – due to the fact that originally it was really believed to be a theory – and that is why we will continue using it. More correctly, one should speak of something like an “effective meson model”.

underlying physical picture, is needed as a starting point for a consistent description of the large field of nuclear structure physics including the important subtleties due to mesonic and isobar degrees of freedom.

Motivated by the arguments given above we present in this paper a model for the NN interaction which is based solely on nucleons, isobars and mesons, these being treated on an equal footing. We develop this model step by step starting with the long-range contributions and gradually proceeding to shorter ranges. At each step we make a quantitative comparison with empirical data.

In developing this model, it is our principal intention to work on as broad and well-founded a basis as possible and to use an approach that is “complete” insofar as it includes all processes within the framework of meson theory which reasonably contribute to the NN interaction in the energy region below pion production threshold. In addition, the derivation is intended to be reliable and unambiguous from the field-theoretical point of view.

Let us state in more detail what we mean by some of these points. First and most obviously, we want to use only existing mesons (and not include any fictitious ones). Secondly, apart from the well-known one-particle exchange, we will also include multi-meson exchange and, thus, go far beyond the traditional one-boson-exchange model. It will be important to consider correlated as well as uncorrelated multi-particle exchange. Thirdly, in view of the relationship between the mass of the exchanged meson(s) and the range of the corresponding force we will start with the long-range component. Step by step, we will then include all relevant diagrams with increasing exchanged mass up to the cutoff mass used in the meson–nucleon vertex functions. The use of such “cutoffs” is natural in the light of the discussion given above. They suppress meson exchange for small distances. In fact, such form factors were originally introduced into meson theory, in a purely ad hoc way, to supply sufficiently rapid falloff of potentials at high momenta so that a solution of the scattering equation could be obtained. Now, due to the extended quark structure of hadrons, the form factor is a theoretically well-founded concept since it is related to the finite size of the hadron. Anticipating part of our results: We obtain cutoff masses in the range of 1.2–1.5 GeV. Consequently we include diagrams up to a total exchanged mass of about 1 GeV.

Finally, we will be concerned with some of the subtleties of field theory (more about this in section 3). We avoid nonrelativistic approximations and take meson retardation (recoil effects) into account.

There are many reasons why we pursue this thorough and comprehensive approach to the NN interaction. First there is a rather basic motivation: one wants to know if, and to what extent, meson exchange alone is able to provide a quantitative model for the NN interaction. Further, this field-theoretical approach provides an unambiguously defined off-shell behaviour of the nuclear force. The underlying formalism allows for a consistent extension of meson exchange up to intermediate energies, i.e. above pion production threshold. Furthermore, the set of diagrams contributing to the NN interaction forms a sound basis for a consistent generalization to three-body forces and meson-exchange-current contributions to the electromagnetic properties of nuclei (e.g., the deuteron and ^3He). Moreover, the explicit field-theoretical description of the processes contributing to the nuclear force provides a basis for the consideration of relativistic effects and of medium effects on the nuclear force when applied in the nuclear many-body problem. The model is also essential for the consideration of charge independence and charge-symmetry breaking of the nuclear force due to the mass differences between the charged states of mesons, nucleons and isobars. Finally, the NN interaction implied by the NN interaction due to G -parity can be determined in an unambiguous way.

The paper is divided into eleven sections and six appendices. After a historical retrospection in section 2, we present the basic features and assumptions of our model in section 3. The explicit

construction begins with the single-particle-exchange mechanisms in section 4. Section 5 contains our model for the 2π -exchange contribution, which we compare with results from dispersion theory. Combined with the single-particle-exchange contributions of section 4, it already provides a good description of the higher angular momentum phase shifts. In the next section, we demonstrate the importance of πp contributions for a quantitative fit of the phase shifts in the lower partial waves. We also show that the σ -boson used in one-boson-exchange models represents an effective description of 2π (apart from ρ) plus πp exchange. In section 7 further (irreducible) 3π and 4π exchanges are considered and arguments for the convergence of the diagrammatic expansion are discussed. In section 8 we present the resulting NN data (phase shifts up to 300 MeV nucleon laboratory energy, deuteron and effective range parameters and also some observables of NN scattering). We also discuss the values of the meson parameters (coupling constants, masses and cutoff parameters) which have been obtained in describing the NN data and compare them with information obtained from other sources. Section 9 contains a simple parametrization of our model in terms of one-boson-exchanges. These are given in momentum as well as in coordinate space and should be convenient for applications in nuclear structure physics. In section 10 we indicate some of the particular and favourable consequences, to which our model may lead in nuclear structure. Finally, section 11 contains a summary and some conclusions.

2. Historical perspective*

The meson theory of nuclear forces has a long history. Therefore, before going into the details of the present work it appears appropriate to provide the historical background. We briefly review the major ideas and previous efforts in the field. Especially, we want to stress the important developments of which our work is a continuation. Also, the relevance of the present study may become more apparent by comparison with the numerous attempts of the past.

Historically, the principal idea underlying our concept goes back to Yukawa's fundamental hypothesis, stated in 1935, that the nuclear force is mediated by massive-particle exchange [29]. Though, over the years, the basic understanding of that idea has undergone modifications (namely, from a more fundamental to a more effective view), the principal motivation has remained the same ever since. Massive particle exchange suggests itself as a particularly adequate tool for describing the empirically known properties of the NN interaction. With regard to the finite range of the nuclear force, this aspect is reflected in the relationship between the mass of the exchanged particle and the range of the corresponding force, for which Wick [30] provided a specially plastic picture.

The original Yukawa-idea of a scalar field interacting with nucleons was soon extended to vector (Proca [31]) and then to pseudoscalar and pseudovector fields (Kemmer [32]). Mixed theories, in particular the combination of vector and pseudoscalar fields, were already considered in the 1940s by Møller and Rosenfeld [33] and by Schwinger [34]. The inclusion of a pseudoscalar field was suggested by the discovery of the quadrupole moment of the deuteron [35], the sign of which was given correctly by the exchange of an isovector, pseudoscalar boson. This led to the conjecture that such a meson was very likely to exist (Pauli [36]) long before the pion was found and its spin and parity determined [37].

After the discovery of the pion in 1947/48 [38] more systematic work started, for which Taketani, Nakamura and Sasaki [39] (TNS) set the framework in 1951. They proposed to subdivide the range of the nuclear force into three regions. The far-sighted character of this proposal becomes evident from

* For a more detailed historical review see the corresponding chapter of ref. [28].

the fact that nowadays, particularly in view of QCD-inspired approaches to the nuclear force, this subdivision is still physically most meaningful. TNS distinguish a “classical” (long-range, $r \gtrsim 2$ fm; r denotes the distance between the centres of two nucleons), a “dynamical” (intermediate range, $1 \text{ fm} \lesssim r \lesssim 2$ fm) and a “phenomenological” or core (short-range, $r \lesssim 1$ fm) region. The classical region is dominated by one-pion exchange. In the intermediate range the two-pion exchange is most important, although heavier-meson exchange (like ω) also becomes relevant. Finally, in the core region many different processes play a role. There are multi-pion exchange, heavy mesons of various kinds and (from today’s point of view) genuine quark-gluon exchange.

The TNS program is of utmost theoretical and practical importance. It allows for a stepwise exploration of the nuclear force and permits, if necessary and suggested by theory, a different derivation for different parts of the force. Thus, when developing an approach to the NN interaction, one does not have to face the whole problem with all its complexities at once.

In the 1950s the one-pion exchange became well established as the long-range part of the nuclear force. The evidence came from small-angle NN scattering (or high angular-momentum states) [40] and from the deuteron [41]. Tremendous problems occurred when the 2π -exchange contribution to the NN interaction was first attacked. Various approaches pursued in the 1950s, the best known being those by Taketani, Machida, Onuma [42] and by Brueckner and Watson [43], differed substantially from each other, both conceptually and quantitatively. None was doing well in comparison to experiment. In particular, it turned out to be impossible to derive a sufficiently strong spin-orbit force from 2π -exchange [44, 45].

The experimental discovery of heavy mesons in the early 1960s, especially vector bosons, broke finally the deadlock situation in meson theory left by the previous decade. The existence of vector mesons had been suggested already from the empirical evidence for a strong short-ranged spin-orbit force and from the electromagnetic structure of the nucleon [46]. The next phase started: one-boson-exchange (OBE) models [47]. The basic assumption of these models was that multi-pion exchange could be represented in an adequate way by the exchange of appropriate multi-pion resonances. Thus, it was hoped that the uncorrelated multi-pion-exchange contribution (apart from iterative contributions which are generated by the unitarizing equation) was negligible. This assumption was certainly too extreme, especially since the existence of a low-lying 2π S-wave resonance has never been confirmed experimentally [48]. Still, the great merit of the OBE model is that it demonstrates clearly the importance of vector bosons and correlated particle exchange in general. It further provides a simple parametrization of the nuclear force, which can account quantitatively for the empirical NN data using very few parameters [49–54]. The success of the OBE model also reveals why the pion program of the 1950s failed: correlations (interactions) between pions had not been considered.

However, as indicated above, conceptually the OBE model was not satisfactory. More “complete” approaches to the nuclear force problem were finally pursued along two lines: by dispersion relations and in the framework of field theory.

In the dispersion-theoretical approach to 2π -exchange, πN and $\pi\pi$ data are used to construct the NN amplitude, which is obtained on the energy shell. Correlated, as well as uncorrelated 2π -exchange, is automatically included. After early work on this concept in the 1960s by many groups [47, 55], NN potentials based in part on this approach were developed in the 1970s, in particular by the Stony Brook [56, 57] and the Paris group [58–60]. To obtain a full nuclear force, the dispersion-theoretical 2π -exchange contribution is complemented by OPE and ω -exchange, as well as by an arbitrary phenomenological short-range potential. In the case of the Paris potential, the final result is parametrized by means of static Yukawa terms [60].

However, such a simplified representation of the nuclear force is insufficient in many areas of nuclear physics. If one takes the concept of meson exchange seriously, an explicit description of the processes contributing to the NN interaction is necessary. As already mentioned in the introduction, this is required for a consistent calculation of pion production processes as well as three-body forces and meson-exchange currents. Also, a well-defined off-shell behaviour and medium effects on the nuclear force when inserted into the many-body problem are natural consequences of meson exchange. Only a field-theoretical approach can account for these.

Work along the field-theoretical line was taken up in the late 1960s by Lomon and collaborators [61, 62]. They evaluated the 2π -exchange Feynman diagrams for nucleons and represented their result in the framework of the relativistic three-dimensional reduction of the Bethe–Salpeter [63] equation suggested by Blankenbecler and Sugar [64]. In this way the ambiguities which beset the field-theoretical work of the 1950s were avoided. In subsequent work [62], the correlated 2π S-wave contribution was studied as well. A similar field-theoretical model, in which, however, the anti-particle contributions were suppressed, was developed by Nutt and Wilets [65]. Yet, neither group included processes involving the Δ -isobar in intermediate states. These are known to contribute substantially to the nuclear force [66]. Furthermore, nonresonant 3π - and 4π -exchange must be considered since their range is about that of ω -exchange, the latter being included in all models.

For a decade or so, our group in Bonn has pursued a program that includes all relevant diagrams in a field-theoretical model. In the early period [51–53], a relativistic three-dimensional equation was used together with the principle of minimal relativity [67]. The later treatment has been based on relativistic, time-ordered perturbation theory [68, 69] (see section 3 and appendices A and B for details). Step by step, all 2π -exchange diagrams including those with virtual isobar excitation [70–74] and, finally, also the relevant diagrams of 3π - and 4π -exchange [71, 75, 76] have been evaluated. In this paper, we give a summary of our model, results and conclusions.

3. Basic features and assumptions of the model

Our general scheme is to treat nucleons, isobars and mesons on an equal footing. Therefore, we start from a field-theoretical Hamiltonian H containing, as interaction part, nucleon–nucleon–meson and nucleon–isobar–meson vertices (but not a nucleon–nucleon potential). Antinucleons are not included from the beginning, mainly for the following reasons: It has been shown by Zuilhof and Tjon [77], in a covariant calculation based on (one-boson-exchange) Feynman diagrams and the Bethe–Salpeter equation [63], that the contribution from negative-energy states is quite small, provided that pseudovector (gradient) coupling is used for the $NN\pi$ vertex. This phenomenon is known as “pair suppression” since the early 1950s [57], for which the evidence was first seen in the empirical πN scattering length. Also, the pseudovector coupling is suggested as an effective coupling (Weinberg Lagrangian [78]) because of chiral invariance. Furthermore, according to quark-model arguments [79], the nucleon–antinucleon (NN) vertex may be considerably suppressed compared to the NN vertex. (In fact, in their subsequent work [80], the Utrecht group also omits negative-energy contributions. This leads to a considerable simplification.) Our assumption of pair suppression is not necessarily in contrast to recent work on the so-called Dirac approach to nuclear physics [81–83]. Though it has been shown that the success of this approach can be attributed to small anti-particle contributions [84, 85], which appear to be crucial for spin observables in N –nucleus scattering and nuclear matter saturation, these subtleties play no role in the NN problem.

In contrast to refs. [77, 80] we treat H in relativistic time-ordered (old-fashioned) perturbation theory [68, 69] (see also appendices A and B). This corresponds to standard many-body theory and, thus, leads to a well-defined transition from the two- to the many-body problem. Since one of our goals is to provide a meson exchange NN interaction suitable for application in nuclear structure, this procedure is more appropriate than that of refs. [77, 80].

The couplings for the various mesons in fig. 1(a) are given in terms of their interaction Lagrangian densities by

$$\begin{aligned}\mathcal{L}_{NNps} &= \frac{f_{ps}}{m_{ps}} \bar{\psi} \gamma^5 \gamma^\mu \psi \partial_\mu \varphi_{ps}, & \mathcal{L}_{NNs} &= g_s \bar{\psi} \psi \varphi_s, \\ \mathcal{L}_{NNv} &= g_v \bar{\psi} \gamma_\mu \psi \varphi_v^\mu + \frac{f_v}{4m} \bar{\psi} \sigma_{\mu\nu} \psi (\partial^\mu \varphi_v^\nu - \partial^\nu \varphi_v^\mu),\end{aligned}\quad (3.1)$$

for pseudoscalar (π, η), scalar (σ, δ) and vector mesons (ρ, ω), respectively. m is the nucleon and m_α the meson mass; ψ the nucleon and φ_α the meson field operators. Note that for isospin $I=1$ mesons φ_α is to be replaced by $\tau \cdot \varphi_\alpha$ with τ_i the usual Pauli matrices. Correspondingly, the vertices in fig. 1(b) are described by

$$\mathcal{L}_{N\Delta\pi} = \frac{f_{N\Delta\pi}}{m_\pi} \bar{\psi} T \psi_\mu \partial^\mu \varphi_\pi + \text{h.c.}, \quad \mathcal{L}_{N\Delta\rho} = i \frac{f_{N\Delta\rho}}{m_\rho} \bar{\psi} \gamma^5 \gamma_\mu T \psi_\nu (\partial^\mu \varphi_\rho^\nu - \partial^\nu \varphi_\rho^\mu) + \text{h.c.}, \quad (3.2)$$

where ψ_μ is the field operator describing the Δ -isobar and T the isospin transition operator; h.c. stands for hermitian conjugate. For more details concerning the formalism see appendices A and B.

A form factor F_α is applied to the vertices (fig. 1(a), (b)). It is parametrized in the conventional form

$$F_\alpha(k^2) = \left(\frac{\Lambda_\alpha^2 - m_\alpha^2}{\Lambda_\alpha^2 + k^2} \right)^{n_\alpha}, \quad (3.3)$$

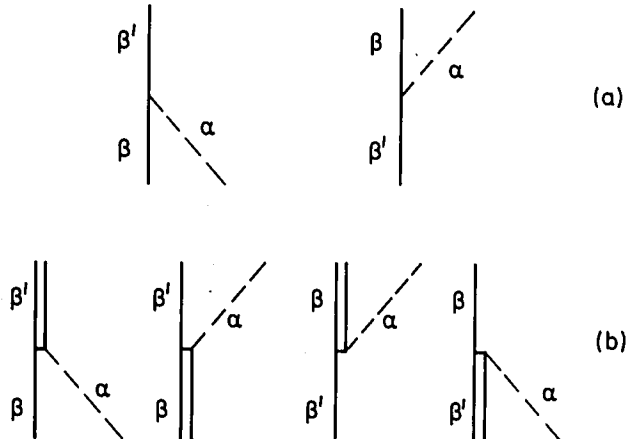


Fig. 1. Meson-nucleon-nucleon (a) and meson-nucleon-isobar (b) vertices. The single line denotes a nucleon, the double line a Δ -isobar and the dashed line a meson.

with k the three-momentum transfer, Λ_α the so-called cutoff mass and $n_\alpha = 1$ or 2 depending on the specific coupling. The form factor suppresses the contribution of high momenta, i.e. small distances. As discussed, the presence of such a form factor is dictated by the extended (quark) structure of the hadrons. The parameter Λ_α , which governs the range of suppression, can be directly related to the hadron size. However, since the question of hadron size is still very much open, we will adjust Λ_α to fit the empirical NN data. The extended structure of hadrons also has the following obvious consequences: Because the meson mass exchanged between two nucleons determines the range of the corresponding contribution to the NN force (higher mass implying shorter ranges), one should restrict oneself to meson exchanges with a total exchanged mass below a certain value, typically on the order of the cutoff mass Λ_α . As it turns out that Λ_α must have values in the range 1.2–1.5 GeV in order to fit the data, it is reasonable and consistent to include all relevant exchanges up to a mass of about 1 GeV. Moreover, as the hadrons are not fundamental fields, the vertex functions (see appendices A and B) cannot be rigorously derived from an underlying interaction Lagrangian; they should, in fact, be considered as a semi-phenomenological ansatz. However, we stress that this ansatz contains only physical parameters (coupling constants *and* cutoff masses) and has the required transformation properties as prescribed by the spin and parity of the meson exchanged which, in turn, essentially determine (apart from slight off-shell ambiguities) the form of the vertex functions.

The exact, energy-dependent meson propagators, which we apply here in the framework of time-ordered perturbation theory, differ from the static ones used in most conventional descriptions of the nuclear force, by characteristic meson retardation or recoil terms (see appendix B, eqs. (B.7) and (B.8)). These terms vanish on-shell but have an important off-shell effect: they tend to suppress higher momenta. Consequently, higher-order diagrams, in which large intermediate momenta are involved, are reduced. For example, all uncorrelated 2π -exchange diagrams (see section 5) are smaller by at least a factor two when meson retardation is taken into account. For that reason static models either drastically overestimate those diagrams or have to apply unrealistic form factors. Also, in our model, the strength of the tensor force due to one-pion exchange (OPE) is typically diminished compared to models using a static pion propagator, as for example phenomenological models like the Reid [86] potential. (Models which use the full Bethe–Salpeter equation [54, 77] keep these recoil effects also and thus have a small tensor force comparable to that of our model.) Since the amount of tensor force has a large impact on results in nuclear structure physics, it is crucial to keep these recoil terms. Whether this is done in a covariant way, as in the Bethe–Salpeter equation, or in time-ordered perturbation theory, as in our model, is essentially immaterial.

Following the guidelines stated in this chapter, we present and discuss, in the next four sections, the various diagrams which we include in our model for the energy-dependent NN potential $V(E)$. Their analytic structure and evaluation has already been described extensively in previous articles [70–76]. We give the starting expressions in appendix B and refer to the references for further details. We introduce the various contributions systematically by going from the lowest order of the meson-exchange process to those of multi-pion exchange. In this way we demonstrate clearly the relevance and necessity of the separate contributions.

4. One-meson-exchange contributions

We start with the well-established one-pion and one-omega exchange, see fig. 2. (The ρ -meson, a 2π -resonance, is included in the next section which deals with the 2π -exchange model.) The pion provides the long-range (essentially tensor) force; the omega (a 3π -resonance with a mass of 783 MeV)

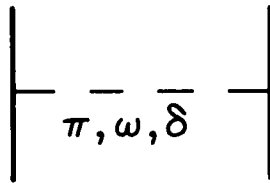


Fig. 2. Single-meson exchanges included in our model.

is mainly responsible for the short-range repulsion and the spin-orbit interaction*. The parameters (coupling constants, cutoff masses) will be fixed and discussed later. We include also the scalar, isovector δ -meson (4π -resonance, mass 983 MeV) which is needed for a consistent description of both S-wave phase shifts. It is a very small contribution.

We leave out $\eta(549)$ - and $\eta'(958)$ -exchange. Due to the pseudoscalar nature of their coupling, the contribution of these particles (which are very heavy compared to the pseudoscalar pion) is small. In addition, their coupling constants are small, a fact which is predicted by the quark model** and confirmed in phenomenological studies analyzing NN scattering with forward dispersion relations [87].

Also, we do not include some mesons with a mass around or slightly below 1 GeV, namely the $\phi(1020)$ and $S^*(975)$. These mesons, providing in any case rather short-ranged exchanges, have a considerable $s\bar{s}$ -content (with s denoting the strange quark) and, therefore, their coupling to the nucleon is suppressed according to the Zweig rule [88].

There are many mesons above 1 GeV, particularly in the area of 1200–1300 MeV, e.g., the $f(1274)$ or the $A_1(1275)$ [89]. For reasons of chiral invariance the A_1 -meson, which is the chiral partner of the ρ -meson, has been considered by some authors [90]. However, there are several reasons why we leave out all contributions arising from the exchange of mesons heavier than 1 GeV. First, their (short-ranged) contribution is masked to a considerable extent by the strong short-range repulsion originating from ω -exchange. Second, as discussed previously, the cutoff masses, which determine the range of the form factors at the meson–nucleon vertices, will turn out to be 1.2 to 1.5 GeV. Obviously, it does not make sense to take meson exchange seriously in a region in which modifications due to the extended structure of the hadrons are applied.

In summary, the simple exchanges in fig. 2, essentially π and ω , already explain important features of the two-nucleon force: the (long-ranged) tensor force and the short-ranged repulsion, together with a sizable spin-orbit contribution. But one important property of the nuclear force is still missing, namely the intermediate-range attraction. On the one-boson-exchange (OBE) level, such a contribution could be generated by a scalar-isoscalar meson with a mass of 500–600 MeV, which, unfortunately, does not exist [89]. The intermediate-range attraction is provided by 2π -exchange contributions, which are introduced and discussed in the next section.

5. The 2π -exchange model

Our model for the 2π -exchange contribution to the NN scattering T -matrix is shown in fig. 3. The essential features of the model are that it contains the contributions from nucleon resonances (isobars)

* For a thorough introduction and a more detailed discussion of the various boson-exchange contributions and their role in NN, the interested reader is referred to ref. [28].

**See appendix B to chapter X of ref. [57].

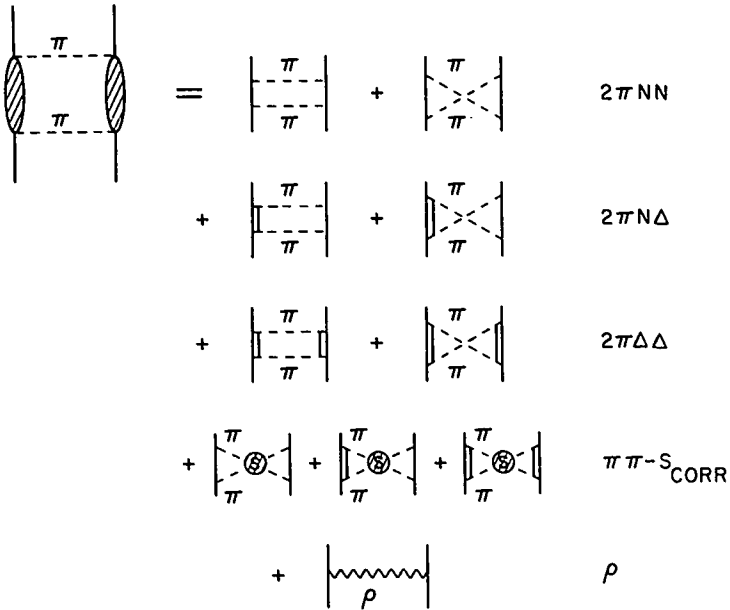


Fig. 3. Our model for the 2π -exchange contribution. The second line from the bottom represents the correlated S-wave contribution taken from ref. [91]. Line notation as in fig. 1.

as well as direct $\pi\pi$ interaction, phenomena which are well known from empirical πN scattering and other related processes.

The lowest-lying so-called Δ -resonance (spin $J = 3/2$, isospin $I = 3/2$) with a mass of 1232 MeV [89] is of particular importance. There are, of course, analogous processes involving higher-mass πN -resonances, like e.g. the $P_{11}(1470)$, the Roper, and the $F_{15}(1688)$ [89]. Because it has been shown by several authors that their contributions are rather small [91–93], we restrict ourselves to the $\Delta(1232)$ in our model, especially since we stay below the pion production threshold. Note that we view the Δ -isobar not as an empirical P_{33} resonance (built up by Chew–Low-type diagrams in πN scattering) but as a genuine particle in the quark model sense. The main motivation for this point of view is that we want (and have) to include crossed-box diagrams (without running the risk of double counting) and corresponding processes involving π - and ρ -exchange (see next section). Below pion production threshold, part of the dressing of the Δ can be conveniently taken into account by using the empirical Δ -mass.

The six upper diagrams in fig. 3 represent uncorrelated 2π -exchange. The various crossed-box diagrams shown were left out of most field-theoretical models of the past, simply because they are difficult to evaluate. However, they must be taken into account for two essential reasons: first, they are nonnegligible (see fig. 8, below), and, second, they provide an almost isoscalar character for the 2π -exchange contribution (at least in higher angular momentum particle waves), which is suggested by results from dispersion theory [94].

In addition, we have to consider corresponding correlated 2π -exchange processes since it is well known that a strong interaction between two pions does exist. If the two pions are in a P-wave state, this gives rise to the ρ -meson. On the other hand, the $\pi\pi$ S-wave interaction does not lead to a resonance. However, Durso et al. [91] have shown that the correlated $\pi\pi$ S-wave contribution (second line from the bottom in fig. 3) can be well approximated by the exchange of a scalar-isoscalar boson

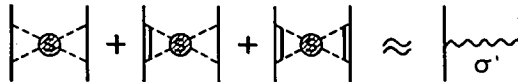
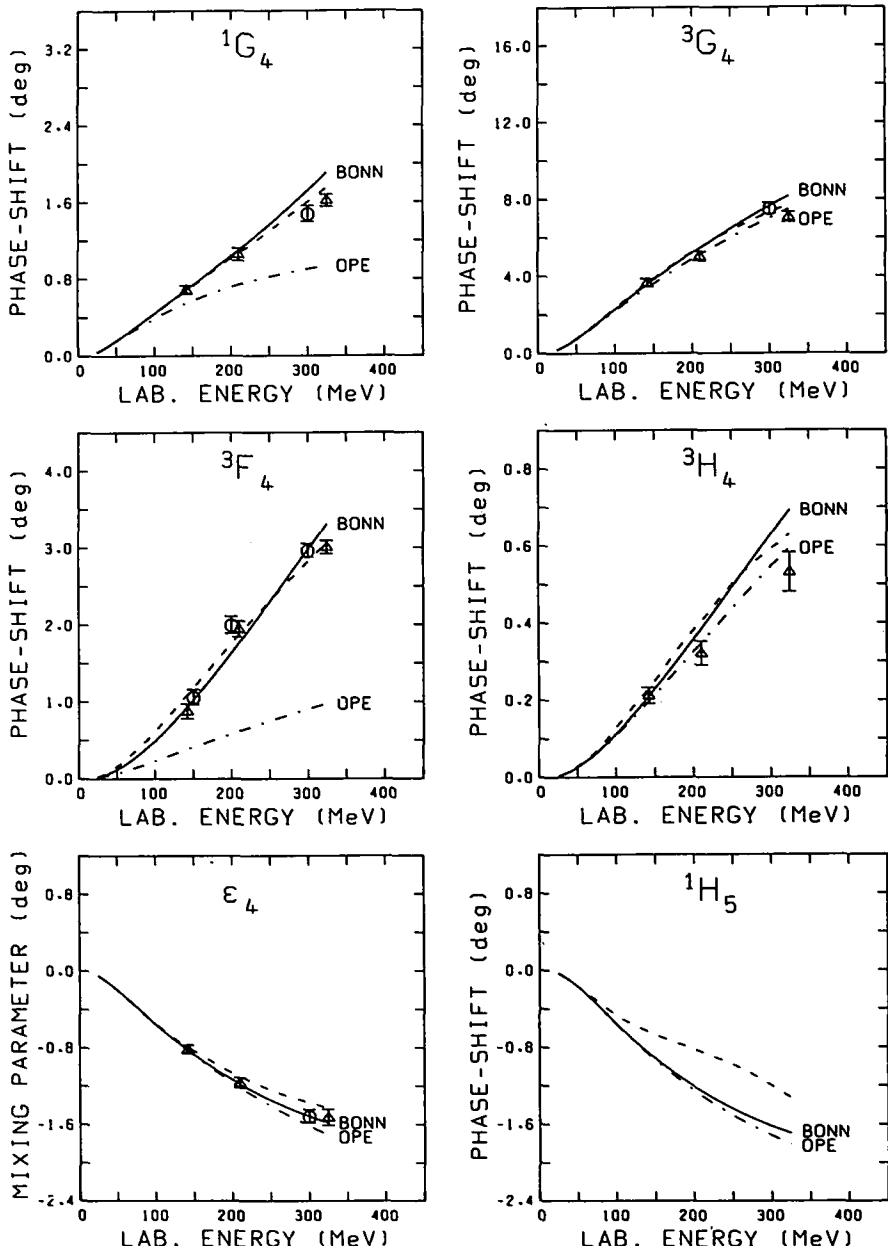
Fig. 4. Correlated 2π S-wave contributions building up σ' -exchange.

Fig. 5. NN phase-shift predictions of our model in higher partial waves. The full line labeled "BONN" contains all contributions from our model for the 2π -exchange, as shown in fig. 3 and discussed in the text, plus one-pion and one-omega exchange ($g^2/4\pi = 5.7$). The energy-dependent phase-shift analysis of Arndt et al. [95] is displayed by the dashed curve; energy-independent analyses are given from the latter group (octagon) and from Bugg and coworkers [96] (triangle). The dashed-dotted curve denotes the one-pion-exchange (OPE) contribution.

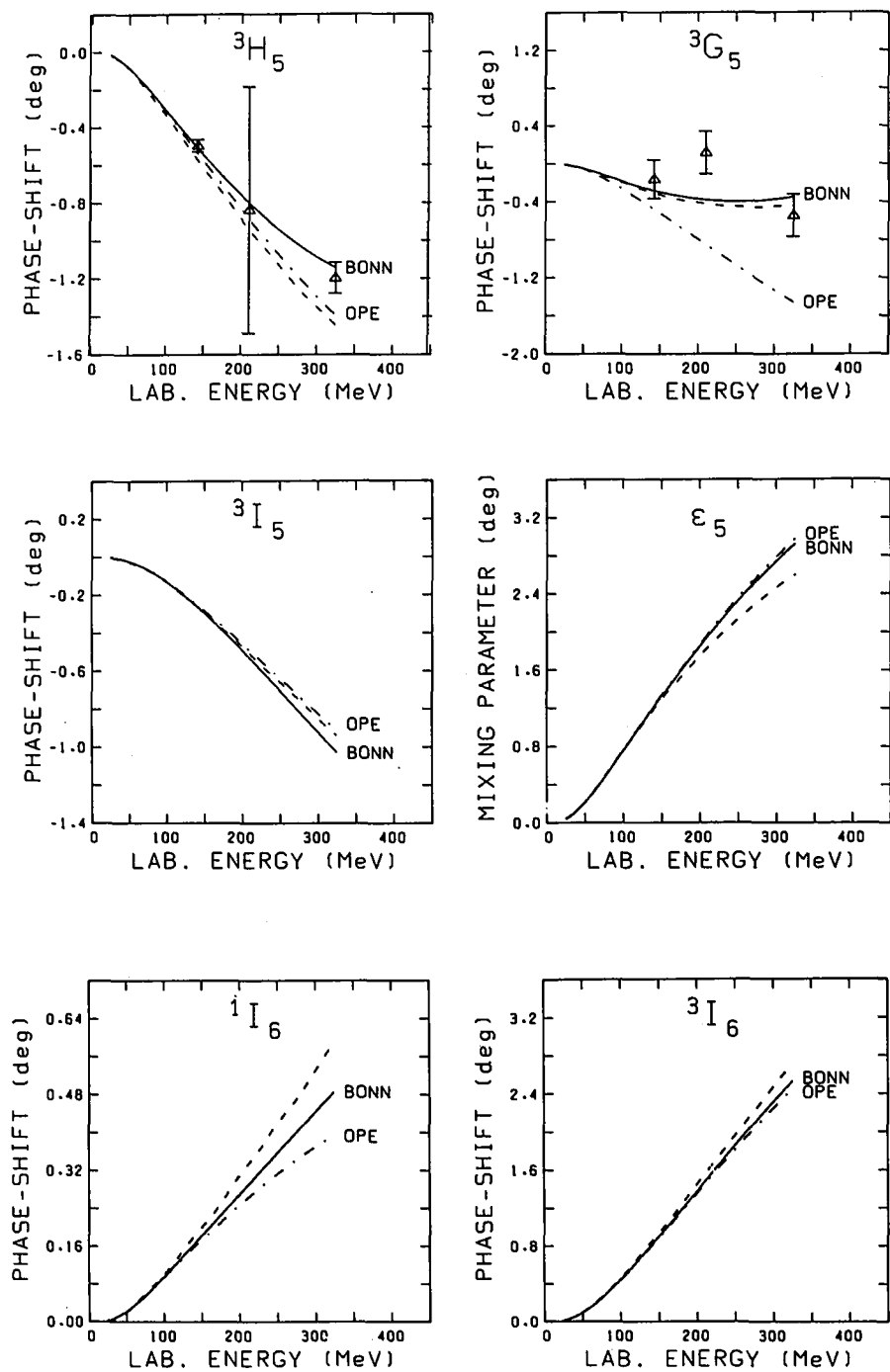


Fig. 5 (cont.)

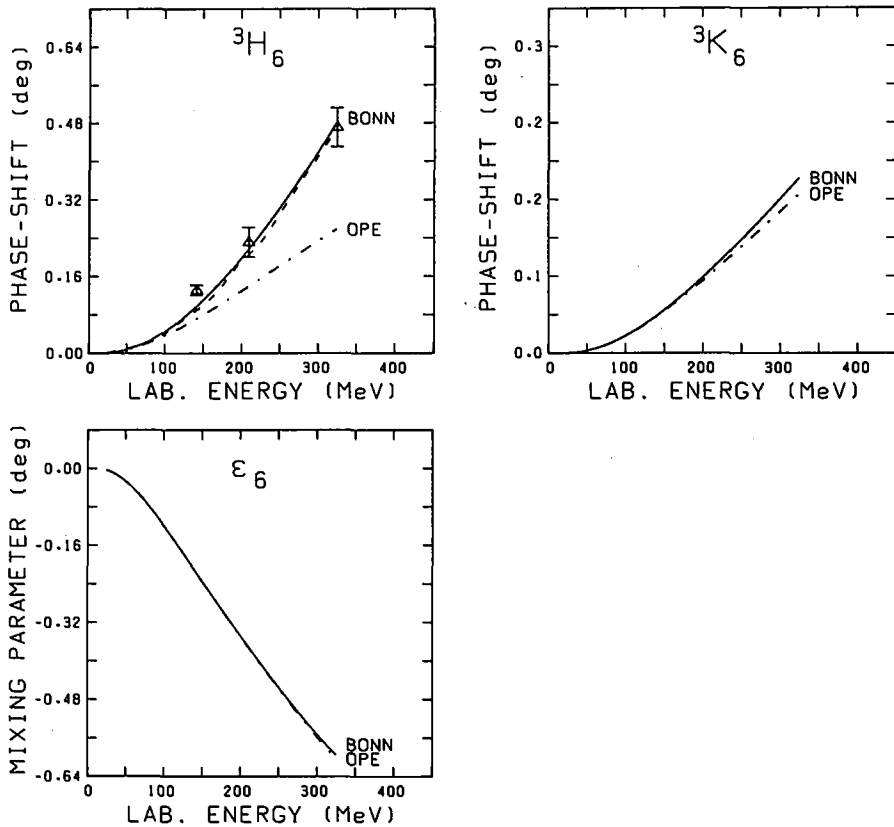


Fig. 5 (cont.)

with a broad mass distribution which we denote by σ' (fig. 4). According to ref. [91], this correlated 2π -exchange contribution provides about 2/3 of the total 2π -exchange, a result which we confirm later. Note that in ref. [91] the $\pi\pi$ S-wave interaction contained in the diagrams of fig. 4 has been determined from the empirical $\pi\pi$ S-wave phase shifts. Thus, σ' is introduced in a well-defined way in contrast to the σ_{OBE} typically used in one-boson-exchange models [49–54]. (In ref. [50], σ_{OBE} has been introduced with a width derived from $\pi\pi$ -scattering data; however, the strength of the coupling has been taken as a free parameter to be adjusted to the empirical NN data).

This model for the 2π -exchange contribution (with $g_\pi^2/4\pi = 14.4$, $f_{\text{N}\Delta\pi}^2/4\pi = 0.224$, $m_\pi = 138.03$ MeV; $g_p^2/4\pi = 0.55$, $f_p/g_p = 6.1$, $m_p = 769$ MeV, $\Gamma_p = 154$ MeV; $g_{\sigma'}^2/4\pi = 10$, $m_{\sigma'} = 662.5$ MeV, $\Gamma_{\sigma'} = 524.5$ MeV), supplemented by single π - and ω -exchange ($g_\omega^2/4\pi = 5.7$), provides a realistic description of the long- and intermediate-range part of the NN interaction. This is confirmed in fig. 5, which shows higher angular momentum NN-scattering phase shifts (total angular momentum $J = 4\text{--}6$) predicted by our model in comparison with those from empirical phase shift analyses [95, 96]*. The theoretical phase shifts have been obtained from the Born approximation (taking the lowest-order term only in the R -matrix eq. (C.2)), which is an extremely good approximation for these high angular momentum partial waves. (Note that the second iteration of the one-pion-exchange (OPE) is included

* Throughout this work we use “bar” phase shifts (see ref. [97] and appendix C.2); furthermore, we will always compare our predictions with the analyses of refs. [95] and [96] using the notation introduced in fig. 5.

in the 2π -exchange model). As mentioned earlier, the σ' -parameters are consistent with ref. [91]. The ω -coupling has been taken from phenomenological studies by Hamilton and Oades [98] using fixed-s dispersion relations; it is in agreement with SU(3) arguments from the naive quark model [57]. We stress that since the results in fig. 5 are sensitive only to the long-range part of the NN amplitude, they are completely independent of form factor parameters. In fact, in these calculations form factors have been used only for the evaluation of the fourth-order box diagrams describing the uncorrelated 2π -exchange; the results do not change even when the relevant cutoff masses are varied over a wide range.

As expected, OPE is dominant in almost all partial waves shown. In some states (3F_4 , 3H_6), however, the 2π -exchange contribution is quite appreciable; ω -exchange is negligibly small throughout, apart from the 3F_4 wave, see fig. 8 below. For convenience we give the precise values for the theoretical phase shifts in table 1. These might be of use in future phase shift analyses and for other purposes.

An alternative way to derive the 2π -exchange contribution to the NN interaction is by means of dispersion theory, in which empirical πN - and $\pi\pi$ -scattering information is used in order to evaluate the amplitude $NN + 2\pi$ [56–60]. We perform a quantitative comparison with the results from this latter approach. For this purpose, we consider sufficiently high angular momentum phase shifts of NN scattering such that there is no cutoff dependence in the results: neither due to form factors in our model nor due to cutting off dispersion integrals, as done in refs. [56–60]. Figure 6 demonstrates an obvious qualitative agreement between both approaches. (The discrepancies between the two dispersion-theoretical results in fig. 6 may be due to differences in the πN input [100], to uncertainties in the cutoff of the dispersion integrals or ambiguities in the analytic continuation of the πN amplitude).

As explained, the *correlated* 2π -exchange in $\pi\pi$ S-wave has been included by the exchange of a scalar boson with a broad mass distribution derived in the work of ref. [91]. In fact, this contribution can be even further approximated by a zero-width scalar exchange. This is demonstrated in fig. 7. Of

Table 1

NN bar phase shifts* (in degrees) for higher angular momentum states predicted by the model explained in this section with the meson parameters given in the text

E_{lab} (MeV)	25	50	100	142	150	200	210	300	325
1G_4	0.041	0.158	0.441	0.685	0.733	1.038	1.101	1.719	1.907
3G_4	0.179	0.759	2.275	3.559	3.795	5.200	5.466	7.628	8.160
3F_4	0.022	0.120	0.496	0.932	1.023	1.635	1.764	2.968	3.308
5E_4	-0.049	-0.199	-0.552	-0.822	-0.869	-1.131	-1.178	-1.512	-1.582
3H_4	0.004	0.026	0.113	0.209	0.229	0.357	0.384	0.626	0.693
1H_5	-0.033	-0.172	-0.558	-0.864	-0.917	-1.209	-1.259	-1.619	-1.694
3H_5	-0.015	-0.086	-0.311	-0.512	-0.549	-0.762	-0.800	-1.084	-1.143
3G_5	-0.009	-0.052	-0.185	-0.286	-0.302	-0.373	-0.381	-0.374	-0.348
5E_5	0.039	0.215	0.756	1.236	1.325	1.849	1.948	2.736	2.927
3I_5	-0.003	-0.024	-0.131	-0.266	-0.295	-0.491	-0.533	-0.921	-1.029
1I_6	0.003	0.022	0.095	0.168	0.182	0.270	0.287	0.443	0.486
3I_6	0.012	0.095	0.445	0.825	0.900	1.380	1.476	2.309	2.528
3H_6	0.001	0.007	0.045	0.098	0.110	0.197	0.216	0.419	0.482
5E_6	-0.004	-0.027	-0.120	-0.215	-0.234	-0.347	-0.369	-0.551	-0.596
3K_6	0.000	0.003	0.018	0.040	0.045	0.079	0.086	0.160	0.182
3K_7	-0.001	-0.012	-0.069	-0.139	-0.153	-0.245	-0.264	-0.425	-0.466
3I_7	-0.001	-0.007	-0.043	-0.090	-0.099	-0.164	-0.177	-0.287	-0.315
3K_8	0.000	0.001	0.007	0.018	0.020	0.040	0.044	0.094	0.110

* For the definition of the term bar phase shift see ref. [97] and appendix C.2.

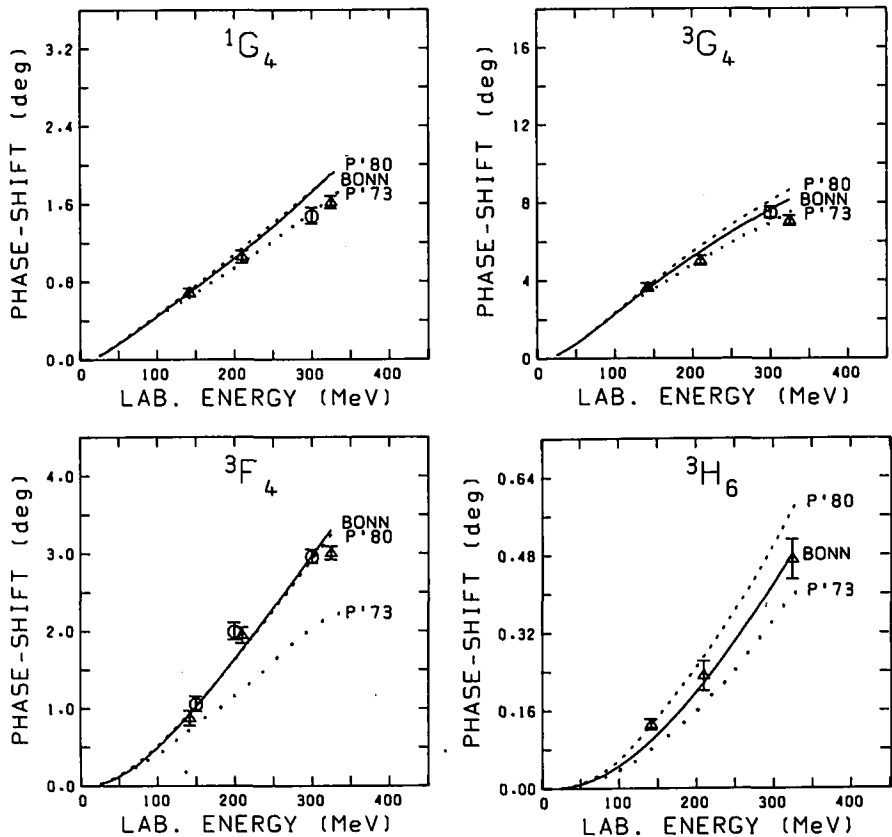


Fig. 6. Comparison of our model with results from dispersion theory. Full line (BONN) as in fig. 5. The dotted lines show results from dispersion-theoretical calculations of the 2π -exchange, P'73 from ref. [99] and P'80 from ref. [60]. All curves contain, in addition to the 2π -exchange, OPE and one-omega exchange. Empirical data as in fig. 5.

course, the parameters of this “sharp” σ' -exchange have to be readjusted, namely $g_{\sigma'}^2/4\pi = 5.7$, $m_{\sigma'} = 550$ MeV. In this sense, the mass distribution plays only a small and unimportant role. Note that the width of the ρ can be completely neglected, i.e. a sharp ρ can be used without changing the parameters. In the calculations of the following chapters, we use the zero-width prescription for both σ' and ρ .

In the traditional OBE model, the correlated and uncorrelated 2π -exchange, i.e. all the diagrams of fig. 3 (apart from the iterative process with NN intermediate states and the one-rho exchange), are effectively described by the exchange of a (sharp or broad) σ_{OBE} with suitably adjusted parameters. As seen also in fig. 7, this simple and convenient prescription is quite adequate for high partial waves. Here, typical values ($g_{\sigma_{\text{OBE}}}^2/4\pi = 9.2$, $m_{\sigma_{\text{OBE}}} = 550$ MeV) have been used. A comparison with the parameters of (the sharp) σ' shows that roughly 2/3 of the intermediate-range attraction is provided by correlated 2π -exchange, the rest being due to the uncorrelated processes. This is also apparent from fig. 8, in which, for the example of the 3F_4 -wave, the effect of the separate contributions is demonstrated. Furthermore, it is evident from that figure that the $N\Delta$ contributions play the most prominent role among the uncorrelated processes. Noniterative diagrams, i.e. essentially crossed-box diagrams, are clearly as important as the iterative ones.

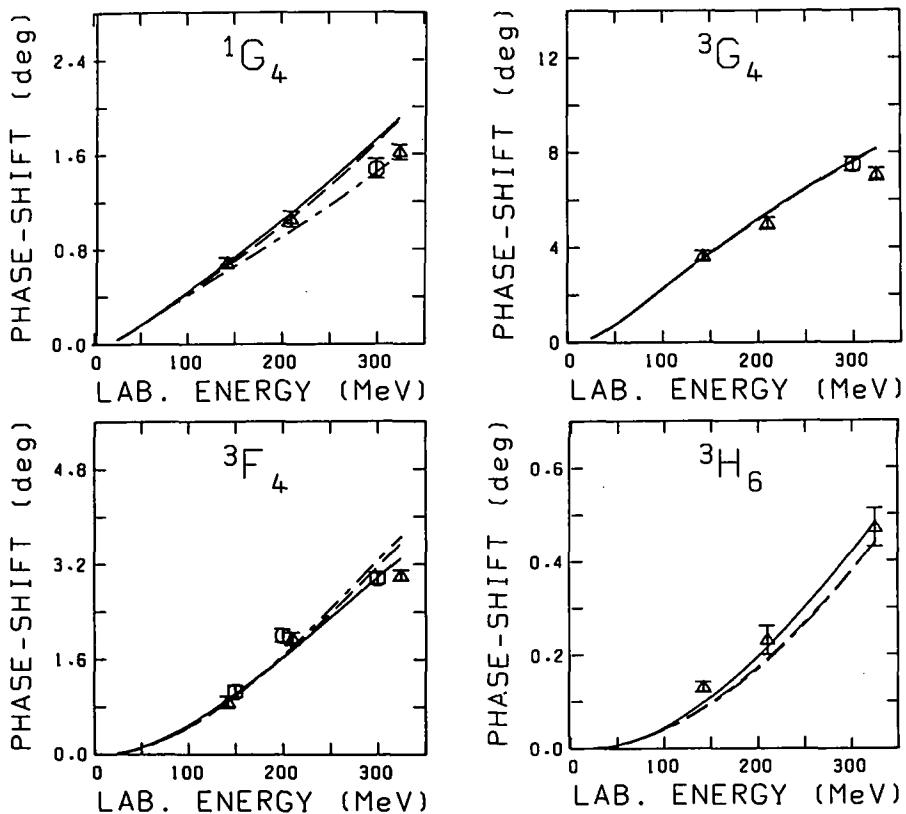


Fig. 7. Comparison of different treatments of σ -like contributions to the nuclear force. The full line (same as in fig. 5) contains the result for our 2 π -exchange model (fig. 3) with a broad (correlated) $\pi\pi$ S-wave contribution. In the dashed line this broad distribution is replaced by a zero-width scalar exchange whereas in the dashed-dotted line the whole 2 π -exchange of fig. 3 (apart from the iterated OPE and one-rho exchange) is replaced by σ_{OBE} -exchange. The parameters are given in the text.

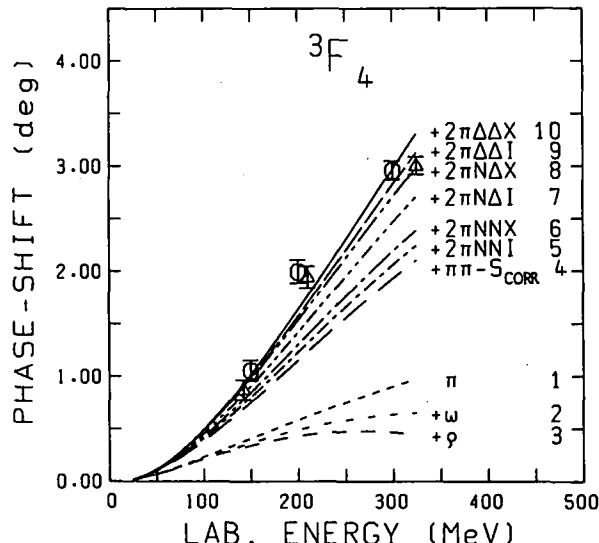


Fig. 8. The effects of the individual contributions to the NN interaction in the case of the 3F_4 phase shift of NN scattering. The contributions are added up successively in the order given on the right of the curve labels. The basic notation for the different parts of the 2 π -exchange is explained in fig. 3. Furthermore, "X" stands for the noniterative part of a contribution (i.e. stretched-box plus crossed-box diagrams, see appendix A); "I" denotes the iterative part.

6. The $\pi\rho$ contribution

In the last section we have successfully checked our 2π -exchange model in high angular momentum partial waves, which are sensitive to the long and intermediate range of the nuclear force only. We now proceed to states of lower angular momentum. This will clearly exhibit the need for the inclusion of additional (short-ranged) processes. A correct determination of low angular momentum NN scattering phase shifts requires going beyond Born approximation, i.e. iterating the potential to all orders. Therefore, in all following calculations we solve the scattering equation (C.2) and, consequently, leave out iterative contributions in the kernel (the “potential”) since these are now generated by the equation. Also, from now on, we will have to use form factors at all vertices because the ranges become shorter and integrations over large intermediate momenta are involved.

From the (incomplete) model developed thus far (which consists of one-meson and 2π -exchange only, but provides a quantitative description of the high partial wave phase shifts) we obtain now, for low angular momentum partial waves, the following result. The 2π -exchange contribution appears, in general, too attractive and a consistent and quantitative description of all phase shifts can never be reached – for any possible choice of the cutoff parameters Λ_α . This is no surprise. Various meson-exchange contributions which should be taken into account according to the rules of the game stated in section 3 have been neglected thus far.

From one-boson exchange it is known that the π - and ρ -mesons play the role of opponents because their tensor forces have opposite sign. It is therefore tempting to include next the π and ρ two-boson-exchange diagrams expecting them to counterbalance corresponding 2π contributions. Figure 9 displays the processes to be considered in analogy to the diagrams of uncorrelated 2π -exchange.

Anticipating the results to be shown and discussed below, the $\pi\rho$ contribution reduces the over-attraction, and, at the same time, improves considerably the consistency of the simultaneous description of all low angular momentum phase shifts (particularly the P-waves). Still, in addition, the ω -coupling constant has to be increased in order to reach a quantitative description of the data. The resulting parameters of this model, which consists of one-meson and 2π - plus $\pi\rho$ -exchange, are given in appendix B.3, table 9. Note that for both the $\pi N \Delta$ - and $\rho N \Delta$ -coupling we take values derived from the πNN - and ρNN -couplings through relations based on quark flavour SU(3) (see section 8.2.1). The

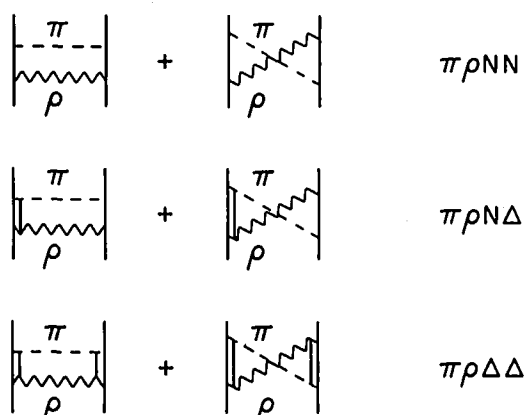


Fig. 9. $\pi\rho$ contributions to the NN interaction.

model provides a satisfactory description of the NN scattering phase shifts in all partial wave states and for the deuteron and low-energy parameters as well. Due to their short range, the additional πp contributions together with the increased ω -exchange have a negligible influence on high partial wave phase shifts and, thus, do not destroy the quality of the description reached in the last section with the one-meson plus 2π -exchange model.

The above results are shown and explained in detail in fig. 10, for some important partial waves. First, the figure displays the good quality of the description reached with the present model. Second, it demonstrates the compelling need for the inclusion of πp contributions. If they are omitted, taking in a first step the ω -coupling strength* to be the same as that employed in the former model for high partial waves, i.e. $g_\omega^2/4\pi = 5.7$, the over-attraction in all partial waves is clearly demonstrated (curve “ 2π

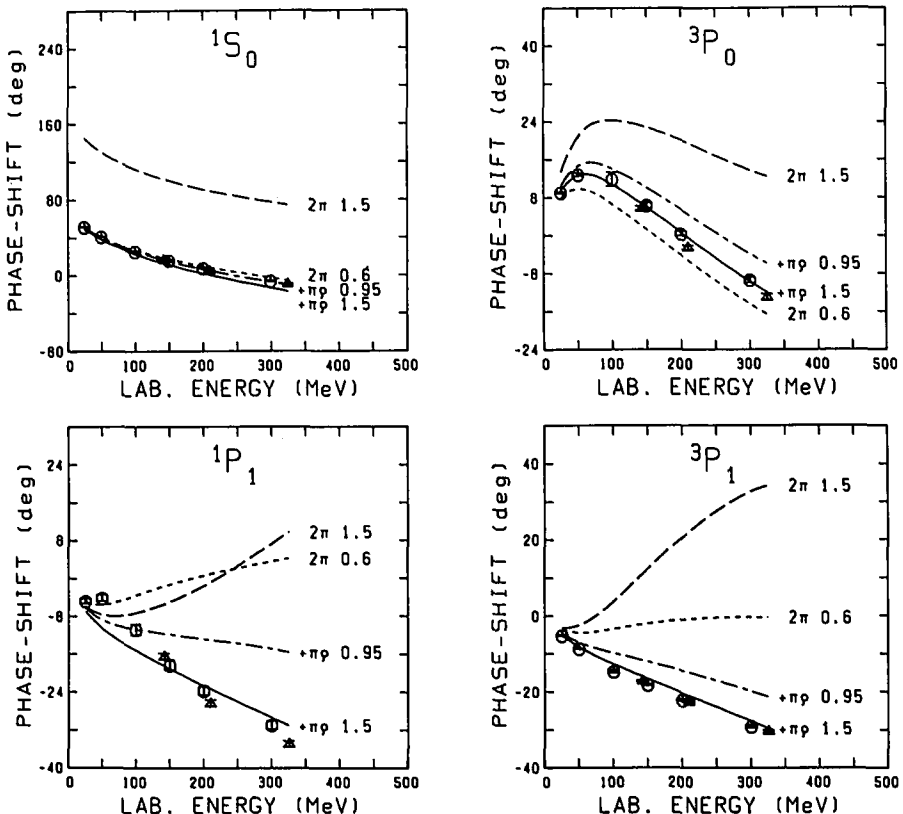


Fig. 10. Some low angular momentum phase shifts, demonstrating the need for πp contributions and increased ω strength. The solid line shows the result for the model discussed in section 6 with the parameters given in appendix B, table 9. For the long-dashed curve (“ $2\pi 1.5$ ”) the πp contributions are omitted, and $g_\omega^2/4\pi = 5.7$, this ω -coupling being used in all nonsolid curves (see the text for further explanations). For the short-dashed curve (“ $2\pi 0.6$ ”) $\Lambda_{NN\pi}$ and $\Lambda_{N\Delta\pi}$ are changed to 0.6 GeV. The dashed-dotted curve is obtained when πp -exchange (fig. 9) is added, choosing $\Lambda_{NN\pi} = \Lambda_{N\Delta\pi} = 0.95$ GeV.

* In the presence of a form factor, we define the coupling strength $g_\omega^2/4\pi$ to be $(g_\omega^2/4\pi) \cdot F_\omega^2(k^2=0)$ since this is the quantity which characterizes the strength of the contribution in lower partial waves. In other words, $g_\omega^2/4\pi = 5.7$ provides roughly the same strength as $g_\omega^2/4\pi = 5.7$ for a model without a form factor. For higher partial waves, however, it is the coupling constant which governs the behaviour. Since $g_\omega^2/4\pi = 5.7$ implies (for the specific form factor used) $g_\omega^2/4\pi \approx 10$, the strength in higher partial waves is increased. However, this is of no practical significance since ω -exchange, due to its short-range nature, has little influence on higher partial waves.

1.5"). As the contributions are now sensitive to the cutoff parameters, one may argue that the description might be considerably improved by a better choice of the cutoff masses. It turns out that this is not the case. If we reduce both $\Lambda_{NN\pi}$ and $\Lambda_{N\Delta\pi}$ to 0.6 GeV (curve "2 π 0.6" in fig. 10), the overall attraction is indeed reduced, as expected. However, a consistent description of all P-phases cannot be achieved. The 3P_0 phases are already too small whereas the 3P_1 phase shifts are still far too large. Also, it is obviously not possible to improve the 1P_1 phase shifts. In a next step, we add πp -exchange, keeping ω -exchange the same as before and choosing $\Lambda_{NN\pi} = \Lambda_{N\Delta\pi} = 0.95$ GeV in order to get a quantitative description of the 1S_0 phase shifts. The curve " πp 0.95" then demonstrates the basic feature of πp -exchange. Although the results do not yet fully agree with the empirical data, they have improved considerably since now, with a correct description of the 1S_0 -wave, all the P-waves are described consistently, though slightly too high. In a final step, we have to increase the strength of ω -exchange (to roughly double its value) in order to achieve a simultaneous lowering of the P-waves. Note that in spite of the fact that ω - and πp -exchange provide repulsion in general, they differ considerably in detail. For example, as seen clearly in fig. 11 (see also ref. [76]), πp -exchange is strongly repulsive in 3P_1 , but slightly attractive in 3P_0 . Speaking in terms of t-channel quantum numbers, the reason for this is that not only the 1^- , but also other channels, e.g. the 0^- -channel, obviously provide important contributions to πp -exchange; ω -exchange is about equally repulsive in all states of equal angular momentum. Summarizing, let us stress again our important finding: both effects, πp -exchange *and* an increased ω -strength, are needed to get a quantitative description of the NN scattering data.

The fact that the πp contribution is of relevance was pointed out previously by Durso et al. [94]. However, those authors suggested the πp contribution as a substitute for part of the ω contribution, which is always rather large in OBE models (in fact, about the same as in the present model) when compared to the SU(3) prediction*. Obviously, this suggestion is not realistic for two reasons. First, as we have seen above, the πp contribution does not act precisely like one- ω exchange; in fact, it varies tremendously from state to state, which is not true for the ω -exchange or the short-range repulsion in the NN interaction in general. Second, the over-attraction of the 2 π -exchange in low partial waves is such that, in addition to a rather large ω -coupling, further repulsion is needed. Therefore, the role of the πp contribution is to counterbalance the 2 π -exchange, and not to partially provide the basic short-range repulsion of the NN interaction. The deeper reason for the intimate counterplay between the 2 π and πp process is probably that they provide also nonnegligible contributions in t-channel quantum numbers other than 0^+ or 1^- (which are usually emphasized). These other contributions are also needed for an accurate description of the NN data; however, their amount (due to partial cancellations) assumes a realistic size only in the combination 2 π plus πp .

At this stage of the development of our model, it is instructive to readdress the question of what the fictitious scalar-isoscalar σ_{OBE} in former OBE models stood for. We saw in the last section that σ_{OBE} -exchange represents a good effective description of the total (uncorrelated plus correlated S-wave) 2 π -exchange contribution. However, this is true only for higher partial waves (corresponding to long ranges). For lower partial waves σ_{OBE} should, in fact, replace the sum of 2 π - and πp -exchange since the model of this section, i.e. one-meson-exchange plus 2 π - together with πp -exchange, has an ω -coupling strength comparable to OBE models. This is confirmed in fig. 11: σ_{OBE} -exchange, with precisely the same parameters as in the last section**, now in general underestimates the 2 π -exchange considerably, but reasonably accounts for the sum of 2 π and πp contributions. This is not in contradiction with the

* See section 8.2.1 and ref. [57], appendix B to Chapter X.

** $g_{\sigma_{OBE}}^2/4\pi = 9.2$; $m_{\sigma_{OBE}} = 550$ MeV; $\Lambda_{\sigma_{OBE}} = 2$ GeV.

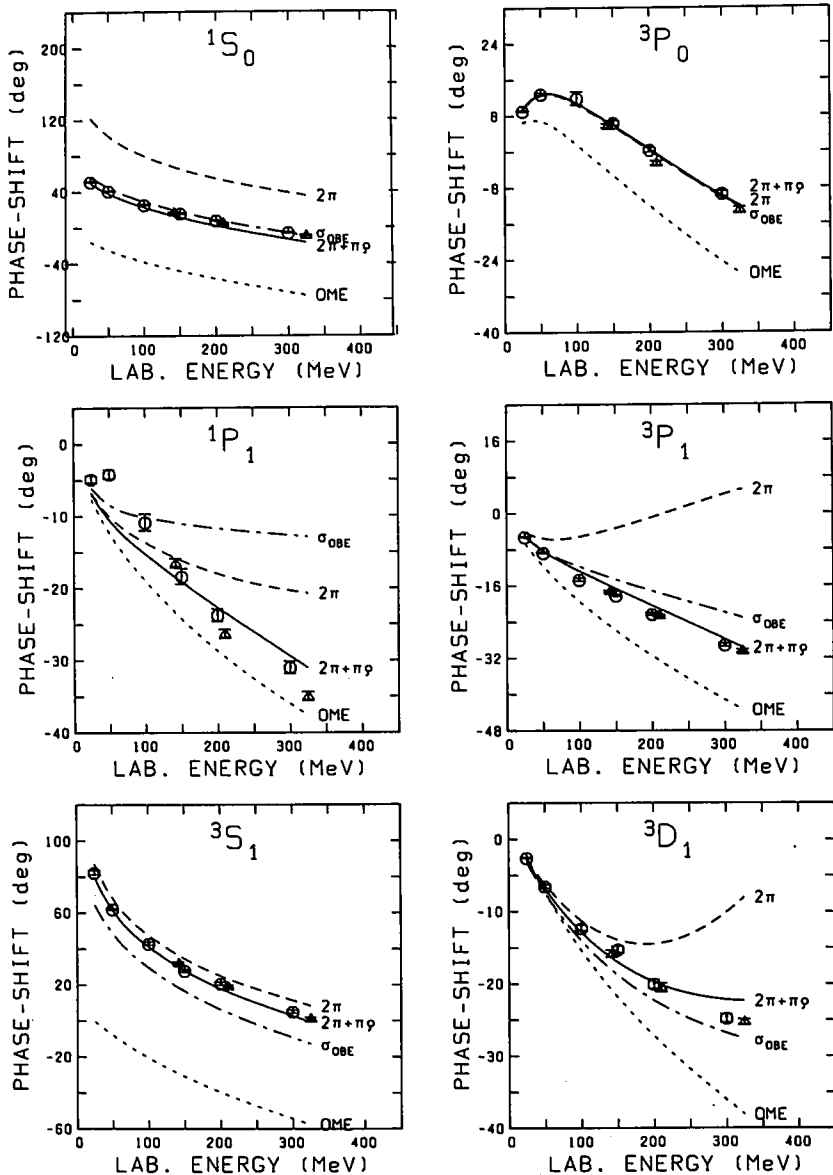


Fig. 11. The approximation of $(2\pi + \pi\rho)$ -exchange by a σ_{OBE} -boson in low partial waves. The dotted line (OME) consists of the one-meson-exchange contributions of π , ρ , ω and δ . The dashed line is obtained by adding the 2π -exchange contribution to OME. The solid curve denotes the complete model of section 6 (i.e. it is the same as the solid line in fig. 10), with the parameters given in appendix B, table 9. The dashed-dotted curve is obtained when σ_{OBE} -exchange ($g^2_{\sigma_{\text{OBE}}}/4\pi = 9.2$, $m_{\sigma_{\text{OBE}}} = 550$ MeV, $A_{\sigma_{\text{OBE}}} = 2$ GeV) is added to OME. All curves contain all possible iterations by the scattering equation.

result found in the last section. For high partial waves, the $\pi\rho$ contribution is simply negligible because of its short range. Finally, we would like to point out that although σ_{OBE} -exchange obviously gives a fair account of the physics of $2\pi + \pi\rho$ exchange there are some deficiencies connected with this simple picture. First, the quality of the fit is, in fact, inferior to that of the full model. Second, probably more important, Pauli-blocking and dispersive effects in the uncorrelated exchanges, which should occur

when such an interaction is applied to the many-body system, cannot be taken into account within the OBE model. In addition, there are many more important subtleties in nuclear physics which cannot be treated in the OBE approximation (see the Introduction).

7. Further 3π and 4π contributions

In the last chapter we have seen that the $\pi\rho$ diagrams are an essential contribution to the NN interaction. This shows that it is important to consider not only resonant 3π -exchange (like the ω) but also other 3π contributions.

Now, we should realize that there are more 3π -exchange processes, of comparable range. For example, a pion can be combined with other correlated as well as with uncorrelated 2π -exchange. Guided by our rule that diagrams up to an exchanged mass of about 1 GeV should be relevant, we have to consider such processes, too. Again, however, we should take advantage of the counter structure between π - and ρ -exchange and, in addition, between correlated $\pi\pi$ S-wave contributions (providing attraction) and (repulsive) ω -exchange. The combined consideration of these phenomena is known to lead to strong cancellations, which should persist in higher orders. (In fact, as we shall see below, these cancellations become even stronger in higher orders.)

Of course, it would be a horrible task to evaluate all of the relevant diagrams explicitly. In fact, we do not believe this to be worth the effort, since their combined effect will turn out to be quite small. Fortunately, we can obtain a reliable estimate of part of these contributions by making use of a fact we found in the last section; namely, to a reasonable extent, σ_{OBE} -exchange effectively describes 2π - (apart from ρ) plus $\pi\rho$ -exchange. As seen from fig. 12, it is then tempting to approximate the diagrams between the solid and the dashed line*, representing part of additional 3π and 4π contributions, by noniterative $\pi\omega$ - and $\pi\sigma_{\text{OBE}}$ -exchange. (Note that the parameters of σ_{OBE} are fixed and taken from the earlier consideration.)

It turns out that the individual contributions (i.e. $\pi\omega$ - resp. $\pi\sigma_{\text{OBE}}$ -exchange) are already quite small. Moreover, they cancel each other to an appreciable extent. However, there is one remarkable feature: a noticeable piece of the intermediate-range tensor force, arising from the contributions represented by $\pi\sigma_{\text{OBE}}$ -exchange, survives the cancellation due to $\pi\omega$ -exchange. As a consequence, the addition of these contributions to the model of the last section leads, after small readjustments of the parameters, to more consistent values for the πNN and $\pi\text{N}\Delta$ cutoff masses; namely 1.3 and 1.2 GeV as compared to 1.5 and 1.1 GeV before. The quantitative description of the data is also further improved. Therefore we include these contributions in our final model, although we are aware of the fact that (i) due to the presence of σ_{OBE} , the model loses some of its beauty** and (ii) because of technical complexities, processes of comparable range (and probably of a comparable magnitude which, however, is quite small) have to be omitted.

The resulting phase shifts and parameter values will be given and discussed in detail in the next section. Here, we demonstrate some features which are relevant to the present discussion. Figures 13(a),(b) show the separate contributions to the final result for the 3P_2 phase shifts. As stated before, $\pi\sigma_{\text{OBE}}$ and $\pi\omega$ are individually quite small and cancel each other almost completely (curve "ALL").

* Note that our model developed so far consists of the diagrams above and to the left of the dashed line.

** We stress again that we do not view σ_{OBE} as a physical particle, but only as a convenient tool to simplify the treatment of higher-order processes to the right of and below the dashed line of fig. 12.

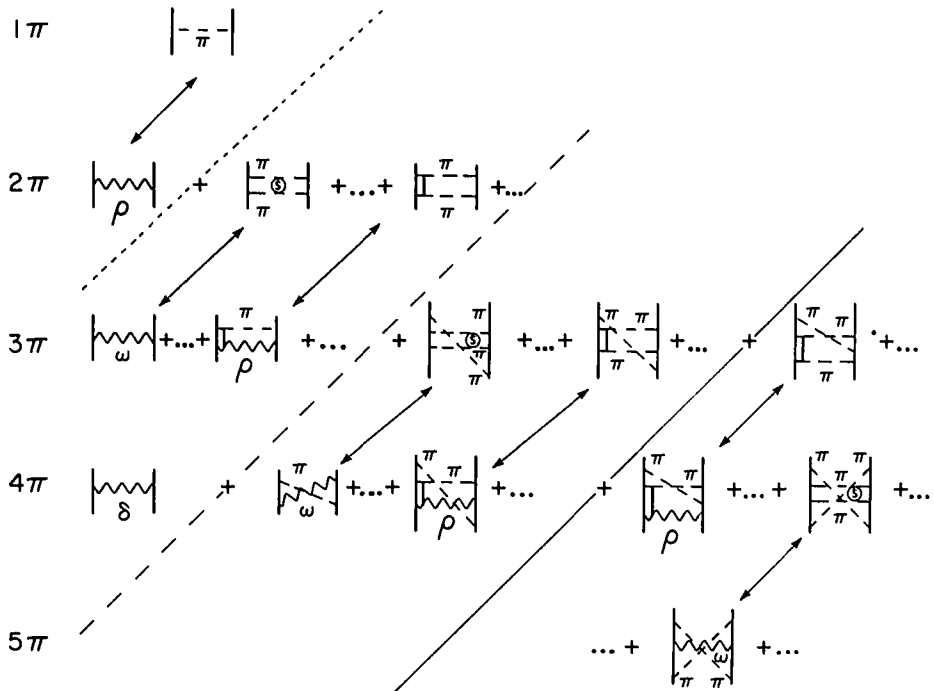


Fig. 12. Diagrammatic expansion of the meson-exchange NN interaction. All diagrams above and left of the solid line are included in our full model. The arrows point to terms which should be grouped together.

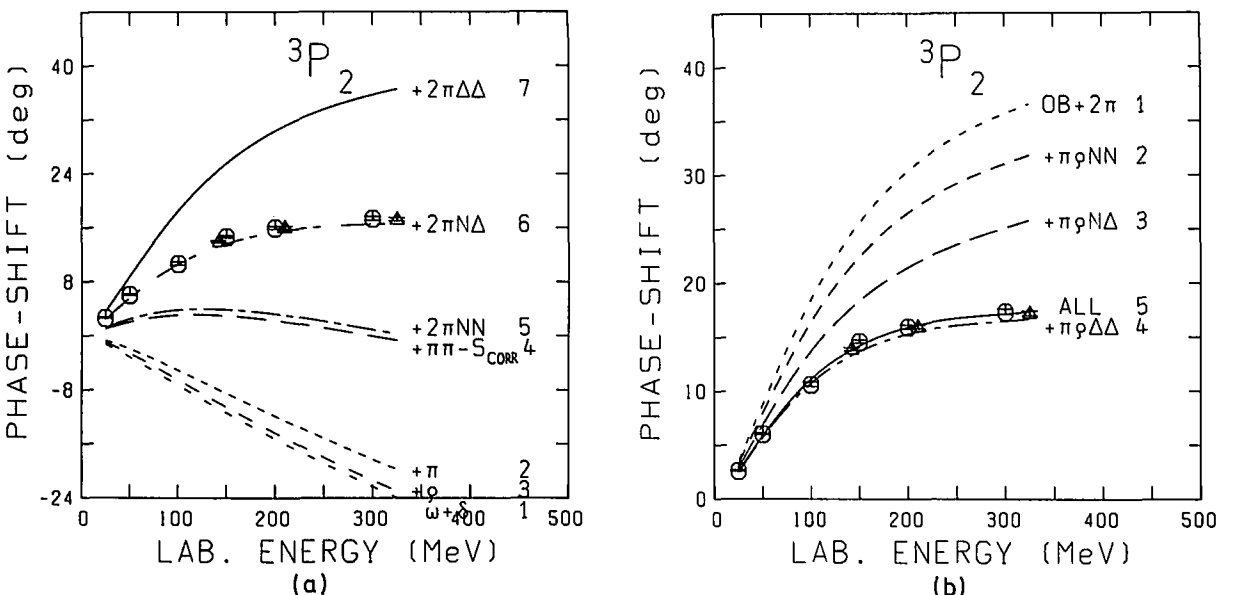


Fig. 13. The effects of the individual contributions to the NN interaction in the case of the 3P_2 phase shift. The contributions are added up successively in the order denoted to the right of the curve labels. The notation for the different parts of the 2π - and πp -exchange is explained in fig. 3 and fig. 9, respectively: (a) contains single-meson and 2π -exchange whereas (b) contains, in addition, πp - and $\pi\sigma_{\text{OBE}}$ - plus $\pi\omega$ -exchange ("ALL"). Note that all curves contain all possible iterations by the scattering equation; therefore iterative contributions with NN intermediate states are left out from the kernel and consequently also from the contributions denoted by $2\pi\text{NN}$ and $\pi\phi\text{NN}$. The parameters are given in table 4.

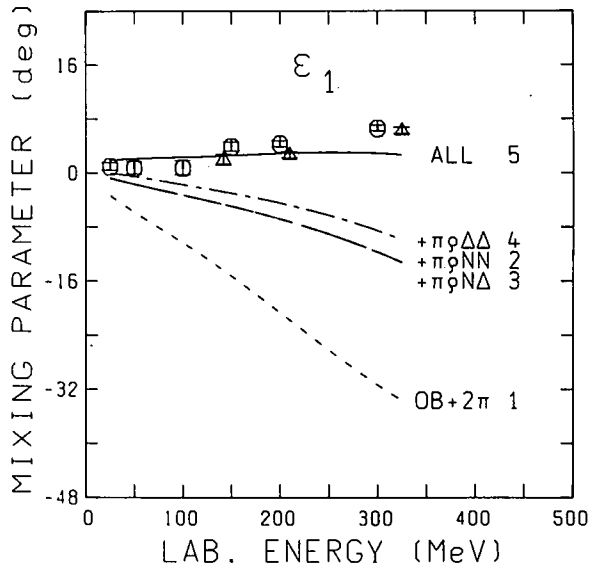


Fig. 14. ε_1 mixing parameter. Notation and comments as in fig. 13.

Thus, there is obviously a strong convergence of the diagrammatic expansion, provided only that the diagrams are grouped in a suitable way as dictated by the physics of the NN problem and indicated in fig. 12. Figure 13 also demonstrates once again the comparable importance of NN, N Δ and $\Delta\Delta$ contributions, for 2π - as well as $\pi\sigma$ -exchange.

Figure 14 (curve “ALL”) shows the net effect of combined $(\pi\sigma_{\text{OBE}} + \pi\omega)$ -exchange on the ε_1 mixing parameter, indicating a sizable increase in the amount of intermediate-range tensor force.

8. Results for the full model and discussion

In this section we present and discuss the results predicted by our final model which we will subsequently call the full model. It has been defined in the last section and fig. 12; the meson parameters are given in table 4 below and discussed later.

8.1. Predictions for the NN data

8.1.1. NN scattering

We start with the NN scattering* phase shifts shown in fig. 15 and tabulated for several energies in table 2. Our predictions for the phase shifts are in excellent agreement with the latest phase shift

* We should note that throughout the present work we assume charge independence and perform our quantitative fits to the neutron–proton data, for $T = 0$ as well as $T = 1$ states. Therefore, we use the average of the proton and neutron mass for the nucleon and an average pion mass (see table 4 below). The p-meson and the Δ -isobar mass are treated equivalently. Yet it is worth mentioning that our model does indeed provide a sound basis for a reliable evaluation of the charge independence violation of the two-nucleon interaction due to the charge dependence of the parameters (in particular, the mass difference between the charge states of nucleons, deltas and mesons). Though we are not concerned with this aspect in this paper, we note that, in a detailed calculation published elsewhere [101], it has been shown that the charge-independence violating difference between the proton–proton (without Coulomb distortion) and the neutron–proton scattering length can be explained, on the basis of our model, by the mass differences between the charge states of the nucleon and the pion.

analyses by Arndt and collaborators [95] and by Bugg and coworkers [96]. The quality of our fit is comparable or even better than that provided by the best known (semi-) phenomenological potentials [86, 49, 50, 60] in spite of the very few (physical) parameters in our model. All meson-theoretical potentials known to us, see e.g. refs. [49–54] and [60], have a problem with the 3D_2 or 3D_3 phase shifts, which for higher energies are too large as predicted in those models. The fact that these phase shifts are described correctly by our model can be traced to the inclusion of the $\pi\rho$ diagrams.

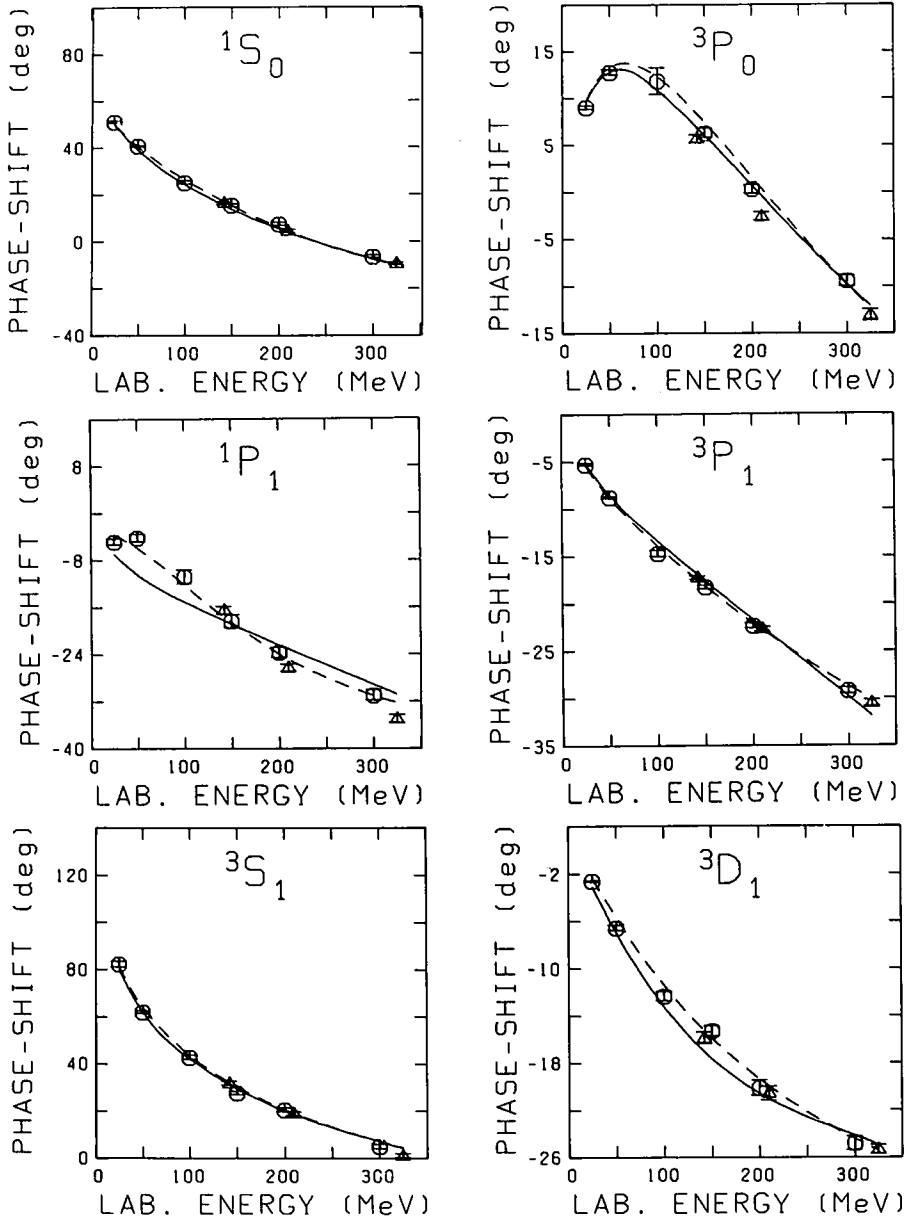


Fig. 15. Phase shifts of NN scattering. The solid line represents the result predicted by our full model. The dashed line refers to the energy-dependent phase-shift analysis of Arndt et al. [95]. Error bars denote the energy-independent analysis of Bugg and coworkers [96] (triangle) and of Arndt et al. [95] (octagon).

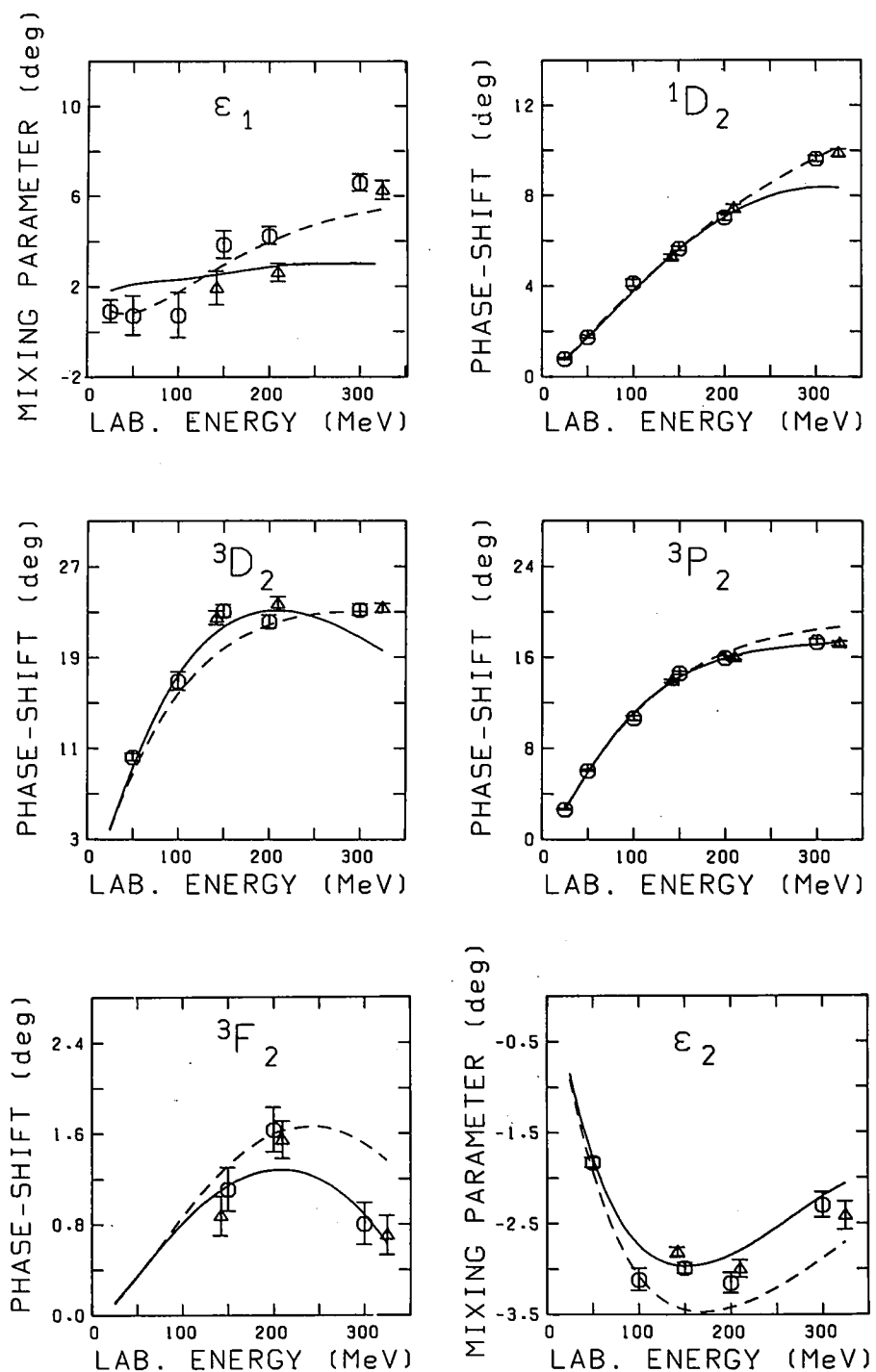


Fig. 15 (cont.)

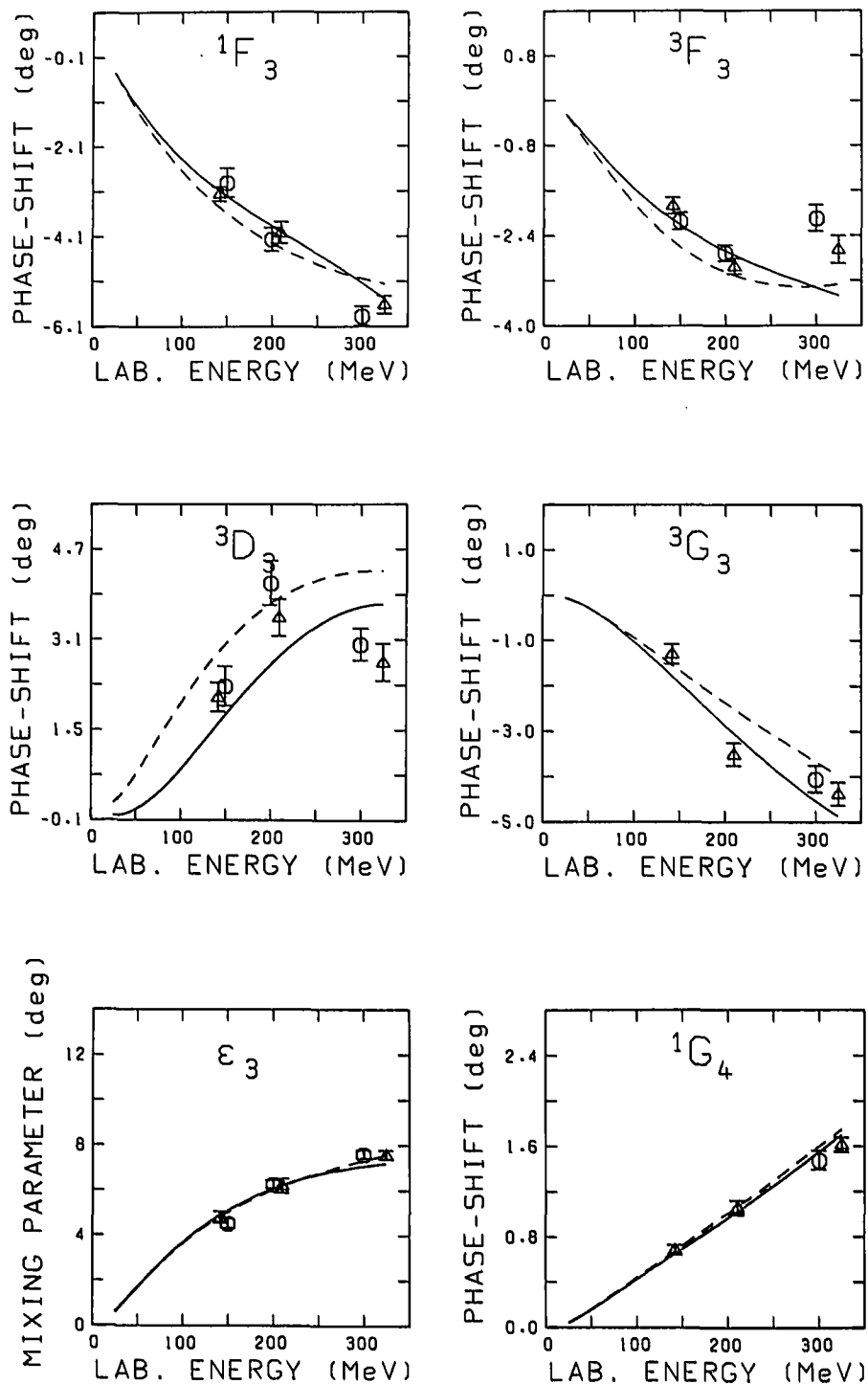


Fig. 15 (cont.)

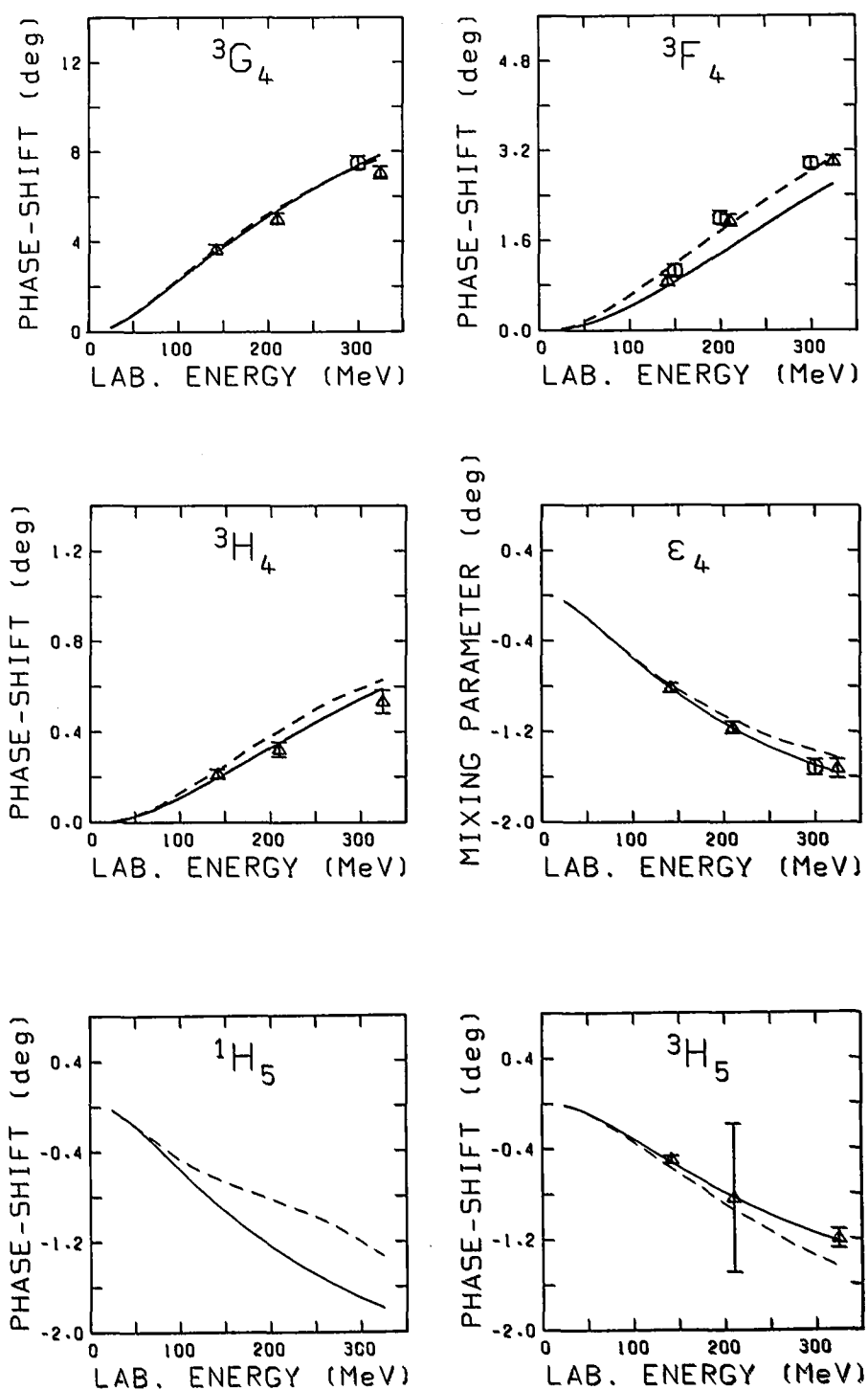


Fig. 15 (cont.)

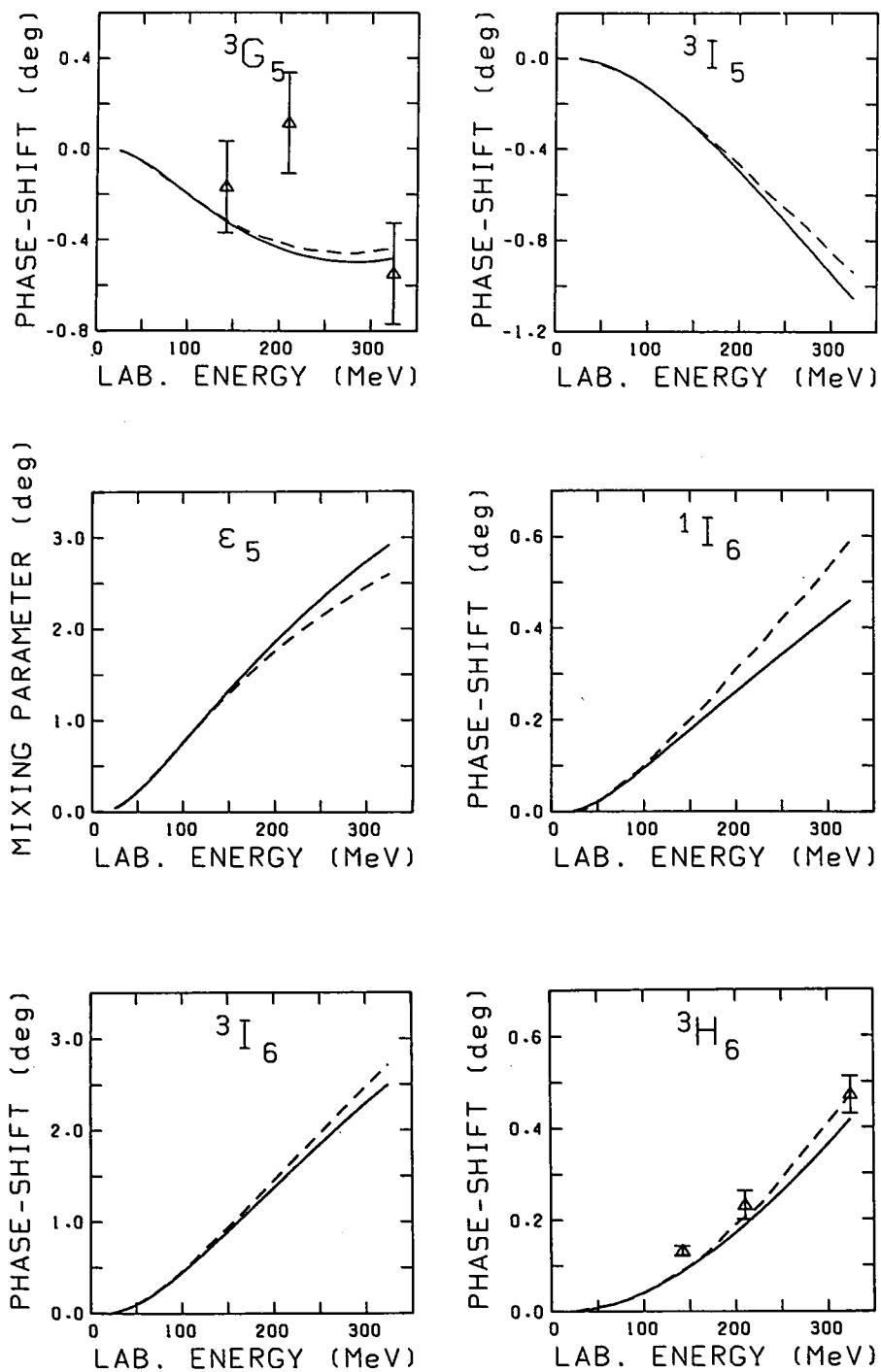


Fig. 15 (cont.)

Table 2
NN bar phase shifts (in degrees) predicted by our full model

E_{lab} (MeV)	25	50	100	142	150	200	210	300	325
1S_0	50.030	39.149	24.358	15.248	13.724	5.304	3.809	-7.622	-10.222
3P_0	9.573	12.788	10.882	6.854	6.015	0.656	-0.413	-9.662	-12.086
1P_1	-6.902	-10.484	-15.110	-18.304	-18.884	-22.407	-23.096	-29.170	-30.843
3P_1	-5.174	-8.526	-13.378	-16.952	-17.617	-21.729	-22.546	-29.871	-31.903
3S_1	80.301	62.185	42.268	31.386	29.637	20.305	18.704	7.058	4.537
ε_1	1.820	2.082	2.292	2.499	2.542	2.818	2.869	3.190	3.054
3D_1	-3.031	-6.980	-13.252	-17.040	-17.636	-20.621	-21.076	-23.425	-23.855
1D_2	0.722	1.723	3.763	5.343	5.615	7.042	7.266	8.322	8.351
3D_2	3.883	9.268	17.411	21.216	21.678	23.091	23.121	20.836	19.595
3P_2	2.540	5.886	11.137	13.858	14.240	15.925	16.150	17.217	17.334
ε_2	-0.849	-1.774	-2.740	-2.959	-2.965	-2.842	-2.795	-2.232	-2.056
3F_2	0.108	0.345	0.811	1.100	1.141	1.279	1.280	0.874	0.632
1F_3	-0.445	-1.201	-2.392	-3.101	-3.217	-3.878	-4.003	-5.149	-5.499
3F_3	-0.239	-0.715	-1.581	-2.127	-2.215	-2.677	-2.755	-3.335	-3.475
3D_3	-0.015	0.088	0.793	1.607	1.764	-2.653	2.805	3.648	3.706
ε_3	0.582	1.696	3.682	4.915	5.109	6.080	6.229	7.081	7.192
3G_3	-0.056	-0.278	-1.024	-1.788	-1.939	-2.873	-3.054	-4.518	-4.856

A remark concerning the ε_1 mixing parameter is in place. It may appear that our model predicts the ε_1 too high for low energies and too low for high energies. However, there is doubt if the results for ε_1 from the phase-shift analyses can be trusted for $E_{\text{lab}} \lesssim 100$ MeV. In that energy range, most realistic potentials predict ε_1 above the analysis. Note also that within a phase shift analysis the 1P_1 is closely related to the ε_1 . Notably, the 1P_1 result from the phase shift analysis for $E_{\text{lab}} \lesssim 100$ MeV disagrees with all theoretical predictions. Most likely, this is not just an accident. In the intermediate energy range ($E_{\text{lab}} \approx 140$ –210 MeV) there are obviously discrepancies between the two phase shift analyses with which we compare our results. We find precise agreement with the analysis of the BASQUE group (Bugg and coworkers [96]). At higher energies ($E_{\text{lab}} \gtrsim 250$ MeV), several points have to be kept in mind. First, the nuclear force at these energies is of no relevance to conventional nuclear structure calculations*. Second, one enters the region in which pion production starts and therefore the description of the NN interaction by the present model becomes inadequate. Third, the results for ε_1 produced by phase shift analyses have been subject to drastic changes over the past 20 years and the error bars given by the analyses are probably greatly underestimated.

Furthermore, when comparing different theoretical results one has to be aware of the following “technical” point: though in theory the ε_1 is in principle related to the tensor force, it also depends strongly on the 3S_1 and 3D_1 phase shifts; namely we have

$$\tan 2\varepsilon_1 = 2R_{D,S}^1 / (R_{S,S}^1 - R_{D,D}^1), \quad (8.1)$$

with $R_{L',L}^1$ denoting the relevant R -matrix elements (see appendix C.3, eq. (C.25)). For example, an increase in the 3S_1 phase shift will lower ε_1 even when the $R_{D,S}^1$ matrix element, which depends on the strength of the tensor force, is kept unchanged. Our value for the 3S_1 phase shift at $E_{\text{lab}} = 325$ MeV is 4.5°. This is in excellent agreement with the energy-dependent analysis of Arndt [95]. Furthermore, an accurate fit of the phase shifts for $E_{\text{lab}} = 100$ –210 MeV leads automatically to our value at 325 MeV by

* Note that the Fermi momentum at nuclear matter density is equivalent to $E_{\text{lab}} \approx 125$ MeV.

extrapolation. Note, however, that most existing NN potentials predict for the 3S_1 phase shift at 325 MeV a value $\approx 0^\circ$ (in disagreement with modern data). A lowering of the 3S_1 phase shift by $\approx 4^\circ$ results in an increase of ϵ_1 by about 2° (without change of tensor force). This “renormalizing” effect of 3S_1 on ϵ_1 should be kept in mind when predictions for the mixing parameter by different theoretical models are compared.

Finally, experimentally one measures NN observables (and not phase shifts). Therefore the real test of the quality of an NN interaction is the comparison with these data. For our model this is done in fig. 16. It is seen that for laboratory energies ranging from 25 MeV up to 325 MeV an excellent description of the data is achieved including those spin observables the ϵ_1 is very sensitive to.

8.1.2. The deuteron and the low-energy scattering parameters

In table 3 the deuteron and low-energy parameters are given and compared with experimental values. First, let us draw the attention to the rather small value for the D-state probability of the deuteron, P_D , a characteristic feature of our model. The P_D is a measure of the strength of the tensor force. $P_D = 4.25\%$, which is predicted by our model, indicates a weak tensor force. As this part of the nuclear force is of utmost relevance in nuclear structure (see section 10), we like to discuss the theoretical foundation of our prediction in more detail here. Our low P_D can be explained in a systematic way as follows: let us start by considering an (unrealistic) model, which would result in the maximal tensor force possible within the meson-exchange picture. Such a model would assume point-like hadrons (and consequently a point-like $NN\pi$ vertex, i.e. *no* vertex form factor) and, furthermore, it would not include the p-meson. The result would be $P_D \approx 6.6\%$. Not surprisingly, the Reid soft-core potential [86] predicts $P_D = 6.5\%$. The introduction of the p (but still keeping the $NN\pi$ vertex almost point-like) reduces P_D to 5.8% (see e.g. HM1 [52], which uses $A_\pi = 2.5$ GeV corresponding to a quite small nucleon radius of $R \approx 0.25$ fm, see section 8.2.2). Remarkably, most (semi-)phenomenological potentials commonly in use predict a P_D of about that value (e.g. Sprung [49]: 5.9%; Paris [60]: 5.8%; Argonne [113]: 6.1%; Nijmegen [50]: 5.4% and 6.4%). However, to emphasize the important physical point implied: if one believes in a nuclear potential with $P_D \approx 5.5\text{--}6.5\%$ (and uses it), then (at least in the framework of meson theory) one has to believe in extremely small nucleons and pions. However, nowadays with the growing empirical and theoretical evidence for a definite substructure of hadrons, this is hard to believe. Also, it has been impossible to create nonnegligible tensor force by other processes than meson exchange. The introduction of a $NN\pi$ vertex form factor, with a cutoff mass of 1.3 GeV (equivalent to a nucleon radius $R \approx 0.5$ fm) results in $P_D \approx 4.5\%$ (see the OBEP presented in section 9). Finally taking into account meson retardation further reduces P_D below 4% which is partly compensated by contributions from 3 π - and 4 π -exchange providing moderate intermediate range tensor force (see section 7). This explains our final result of $P_D = 4.25\%$.

In fact, since a decade there are empirical indications from the forward deuteron photodisintegration [114] and from electron–deuteron scattering [115] that the P_D is low ($\approx 4.5\%$).

In spite of the small P_D , the quadrupole moment, Q_d , is rather large and is reasonably close to the empirical value*. Of course, one should not expect exact agreement since meson-exchange-current corrections are known to contribute an additional amount of about 0.005–0.014 fm² [116] to Q_d . In fact, in our model the meson-exchange-current contributions are well-defined and it would therefore be a challenging task for the future to consistently evaluate them. This applies to the quadrupole moment

* The ability to combine a small P_D with a large Q_d is a characteristic feature of an energy-dependent potential; this was already observed with the HM2 potential [53].

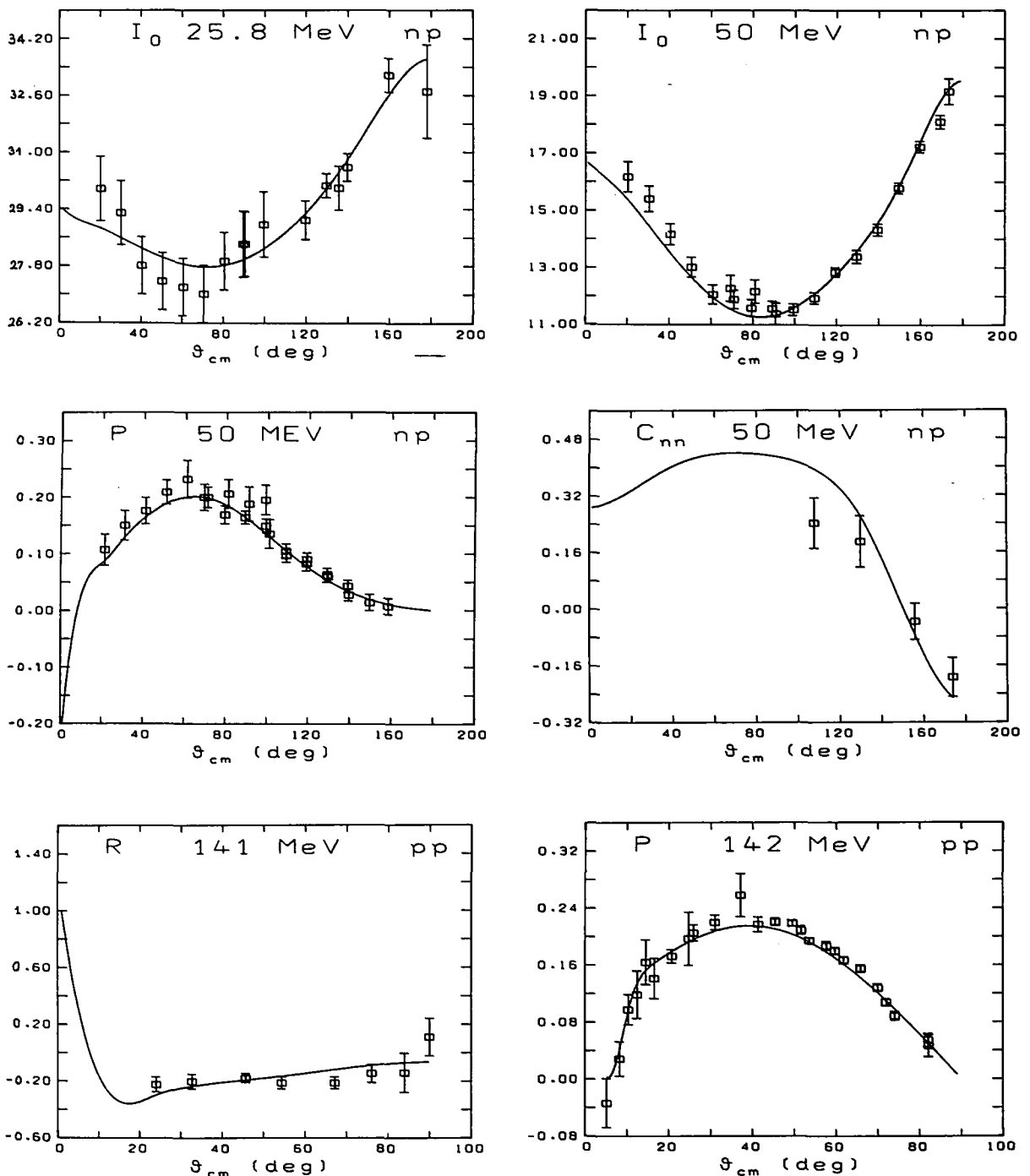


Fig. 16. Some observables of NN scattering. The solid line denotes the predictions by our full model. The energy in the laboratory system is given for each case. For references for the experimental data see ref. [102]. (Notation: np neutron–proton, pp proton–proton, I_0 differential cross section, P polarization, D depolarization, R rotation parameter, A_t , D_t and R_t polarization transfer parameters, C_{nn} spin correlation parameter. For notation and further explanations see also refs. [102, 103]).

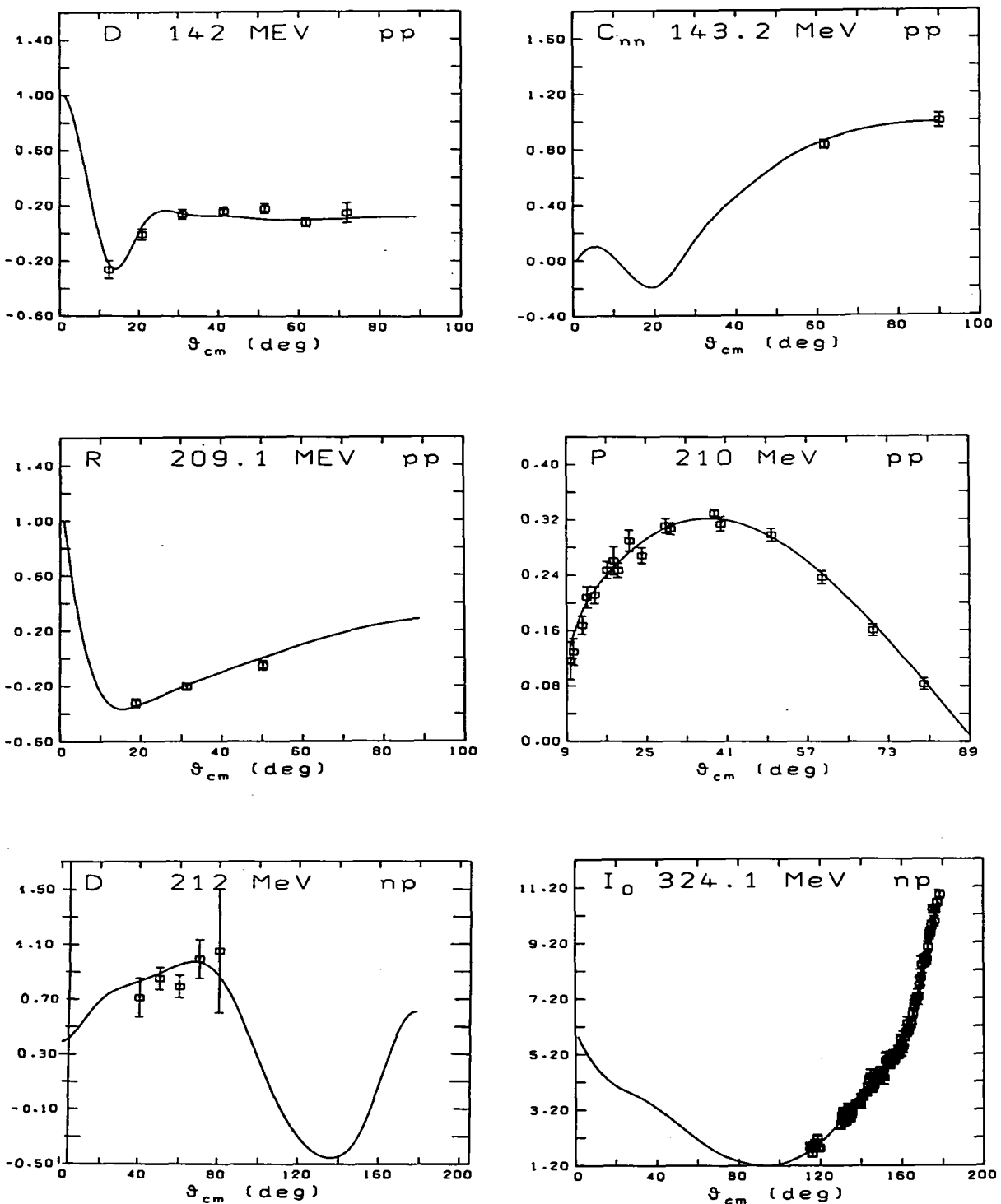


Fig. 16 (cont.)

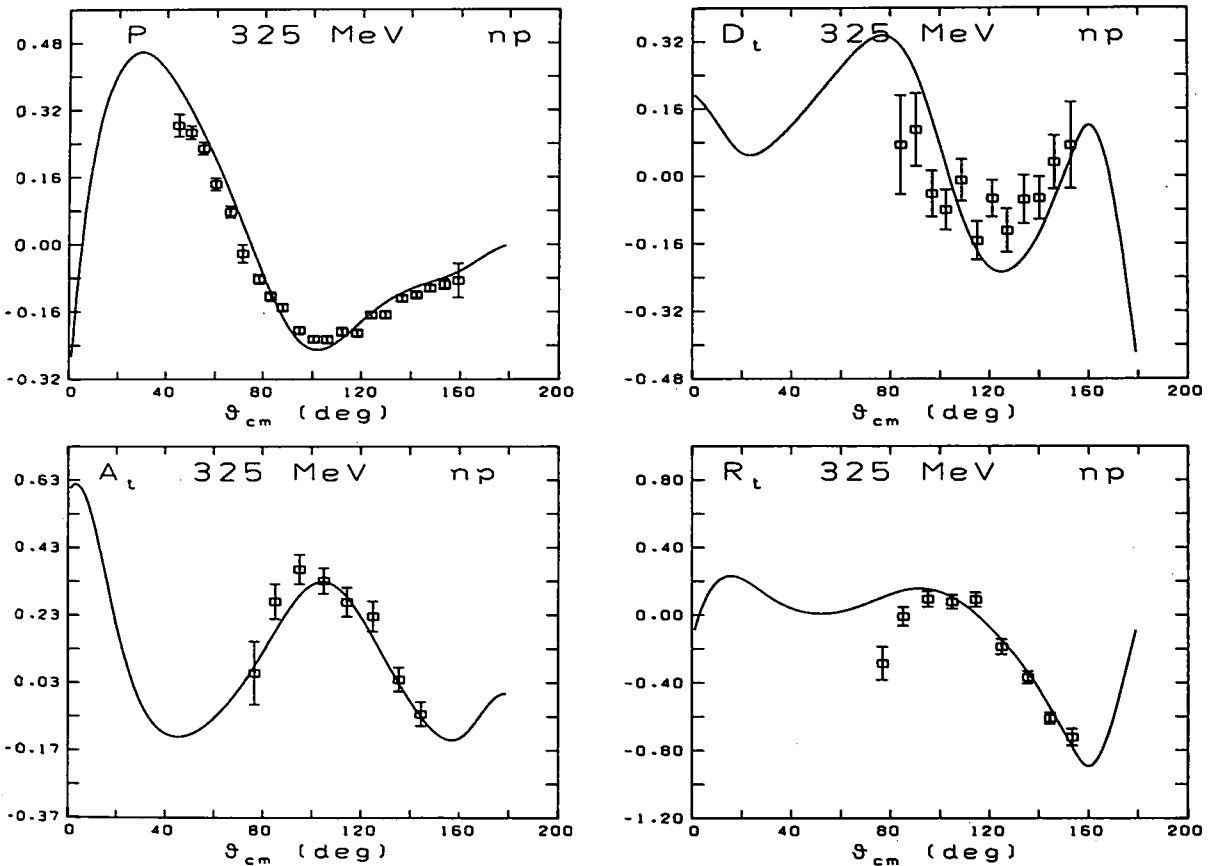


Fig. 16 (cont.)

and the magnetic moment as well as to the form factors and the root-mean-square radius of the deuteron. As Q_d is mainly determined by the outer-range part of the deuteron D-wave, the large Q_d in conjunction with small P_D implies that the outer-range part of the tensor force is hardly suppressed: obviously, meson retardation, being an off-shell effect, influences only the short-range part of the interaction. Furthermore, if the NN data are to be reproduced quantitatively, $\Lambda_{NN\pi} = 1.3$ GeV used by us is a lower limit for that parameter. Again, this suppresses only the short-range part (within 1 fm in coordinate space). For that reason, our model is able to reproduce the rather large experimental value for the asymptotic D/S state ratio (D/S) resulting from the analysis of the experiments by Ericson and Rosa-Clot [27]. An additional reason for our large values for Q_d and D/S is given by small, but crucial contributions to the intermediate-range tensor force from the 3π and 4π contributions discussed in section 7. Finally, we mention the extremely good reproduction of the triplet low-energy parameters, which usually pose a problem in simple boson-exchange models [50–52, 117]. For numerical values for the deuteron wave functions and a practical parametrization, we refer to appendix D.3.

8.2. The meson parameters

The meson parameters used in our model are given in table 4, together with some information about

Table 3
Deuteron and low-energy scattering parameters predicted by our full model (Theory) and from experiment (Experiment)

	Theory ^a	Experiment ^b	References	
Deuteron:				
binding energy ε_d (MeV)	2.22465	2.224644 ± 0.000046	Houk [104]	
		2.224575 ± 0.000009	van der Leun [105]	
D-state probability P_D (%)	4.249	(5 ± 2) ^c		
quadrupole moment Q_d (fm ²)	0.2807	0.2860 ± 0.0015	Reid [106] Bishop [107]	
		0.2859 ± 0.0003	Bishop [107]	
magnetic moment μ_d (μ_N)	0.8555	0.857406 ± 0.000001	Lindgren [108]	
asymptotic S-state A_s (fm ^{-1/2})	0.9046 ^a	(0.8846 ± 0.0016)	Ericson [27] ^d	
asymptotic D/S-state D/S	0.02668	0.0271 ± 0.0008	Ericson [27]	
root-mean-square radius r_d (fm)	2.0016 ^a	1.9635 ± 0.0045	Bérard [109]	
		1.9660 ± 0.0068	Simon [110]	
$\Delta\Delta$ -probability (%)	0.500			
neutron-proton low-energy scattering (scattering length a , effective range r):				
1S_0 : a_s (fm)	-23.749	-23.748 ± 0.010	Dumbrajs [111]	
	r_s (fm)	2.766	2.75 ± 0.05	Dumbrajs [111]
3S_1 : a_i (fm)	5.427	5.424 ± 0.004	Dumbrajs [111]	
	$r_i = p(0, 0)$ (fm)	1.755	1.759 ± 0.005	Dumbrajs [111]

^a In the theoretical results given here, the meson-exchange-current corrections (MECC) are not yet included and, therefore, the nucleonic wave function has been normalized to unity. In a more refined consideration, the Δ and mesonic components should be separated out of the total wave function. This would, on the one hand, reduce the normalization of the pure nucleonic wave function and, consequently, also the theoretical predictions for some deuteron properties (as e.g. Q_d , μ_d or r_d); but, on the other hand, MECC have to be added, which will, at least partly, (over)compensate the reduction. The probability for the non (-pure) nucleonic component in the deuteron turns out to be 3.79% in our model. Reducing the normalization of the wave function by this percentage implies $A_s = 0.8873$ (there are no MECC for A_s) and $r_d = 1.9257$ fm (there are MECC for r_d). This “renormalization” of the wave function is intimately related to the energy-dependence of our full model (see also appendix D.2). For predictions from our energy-independent meson-exchange model see table 6.

^b The experimental values for some of the deuteron properties are controversial; for a discussion see refs. [27] and [112]. We have doubled experimental errors estimated by the theorist Ericson [27].

^c There is no direct experimental access to P_D .

^d The “experimental” value for A_s is model-dependent. In general, for its derivation energy-independence of the nuclear force is assumed which however is not true for our full model.

the coupling constants from other sources. We will discuss the coupling constants first and then turn to the cutoffs.

8.2.1. The coupling constants

The πNN coupling constant is essentially fixed by the deuteron properties, particularly the Q_d and the D/S, which both depend most sensitively on the pion coupling. The very satisfactory results for the deuteron, discussed in the last paragraph, are the main theoretical basis for our choice. We note that the NN scattering phase shifts of high angular momentum being essentially determined by the pion, do also provide bounds on the pion coupling constant; however, these bounds are not as precise as those provided by the deuteron. The plain reason for this is that the experimental deuteron data are simply more accurate.

In our fits to the NN data, we keep the tensor to vector ratio of the p-coupling, f_p/g_p , fixed at its empirical value of 6.1; we vary the vector coupling g_p only. Then, on the basis of our model and with

Table 4
Meson parameters applied in our full model and from other sources

Vertex	$J^P(I^G)$ ^a	Meson mass m_a (MeV)	$g_a^2/4\pi$ resp. $f_a^2/4\pi$	$g_a^2/4\pi(k^2=0)$ ^b , [f_a^2/g_a] resp. $f_a^2/4\pi(k^2=0)$	Coupling constants from other sources or comments	Refs.	Cutoff mass Λ_a (GeV)	n_a
NN π	$0^-(1^-)$	138.03	14.4 ^c	14.08	14.28 ± 0.18 πN scattering 14.52 ± 0.40 pp forward dispersion relations πN phase-shift analyses:	Koch [118] Kroll [119]	1.3	1
NN η	$1^-(1^+)$	769	0.84 ^d	0.41; [6.1]	14.25 0.55 ± 0.06; [6.1 ± 0.6] fit to $N\bar{N} \rightarrow \pi\pi$ partial waves	Bugg [96] Arndt [95] Höhler [120]	1.4	1
NN ω	$1^-(0^-)$	782.6	20	10.6; [0.0]	nucleon form factors $24 \pm 5 \pm 7$ nucleon form factors 12.0 NN and $N\bar{N}$ scattering	Pietarinen [121] Grein [122] Höhler [123] Grein [122] Grein + Kroll [124] Hamilton [98]	1.5	1
NN δ	$0^+(1^-)$	983	2.8173	1.62	8.1 ± 1.5 NN forward scattering 5.7 ± 2.0 fixed-s dispersion relation	Dursu [91] and section 5 See eq. (8.2)	2.0 1.7 1.2 1.4	1 1 1 2
NN σ'	$0^+(0^+)$	550	5.6893	4.56	—			
N $\Delta\pi$	$0^-(1^-)$	138.03	0.224	0.218	$\pi\pi$ S-wave interaction quark model			
N $\Delta\rho$	$1^-(1^+)$	769	20.45	4.86				

^a spin J , parity P , isospin I , G-parity G . Nucleon mass $m = 938.926$ MeV, mass of Δ -isobar $m^* = 1232$ MeV.

^b $g_a^2(k^2) = g_a^2[(J_a^2 - m_a^2)/(J_a^2 + k^2)]^{2\alpha_a}$, for $f_a^2(k^2)$ equivalently.

^c $g_{NN\pi}^2 = (2m/m_\pi)^2 f_{NN\pi}^2 / g_{NN\pi}^2 / 4\pi$ is given.

^d $g_{NN\eta}^2 / 4\pi$ is given.

the constraint that the NN data should be reproduced accurately, our value for g_p^2 is determined with high precision (within a few percent). The resulting value for g_p^2 (at the meson pole) is somewhat larger than the value deduced from a dispersion-theoretical analysis of πN scattering [120, 122]. Note, however, that the strength, i.e. the value for the coupling constant at $k^2 = 0$, which is the decisive quantity determining the behaviour in the important low angular-momentum partial waves, has to be compared. Apart from the coupling constant, this strength depends strongly on the pNN form factor, which is a function of the momentum transfer. In ref. [120] the momentum dependence is not the same as in our case. In fact, as a consequence of our form factor (which is supported by current bag model calculations for the pion vertex), the strength of our pNN vertex is not larger than that of ref. [120] in the physical region.

Finally, we mention that the large tensor to vector ratio of the p-coupling found in refs. [120–122] and applied in our work seems to disagree with the vector dominance model for the electromagnetic form factor of the nucleon in its simple interpretation, in which one is led to $f_p/g_p = 3.7$. However, in ref. [125] it is shown how the large value for f_p/g_p can be reconciled with the vector dominance model by assuming that there is also a direct vector coupling of the photon to the nucleon.

Our value for the ω -coupling constant at the meson pole, g_ω^2 , is roughly twice as large as the corresponding strength (i.e. the value at $k^2 = 0$)*. The latter agrees roughly with the dispersion-theoretical analyses done by Grein and Kroll [122, 124] (which do not provide any k^2 -dependence) but is about twice as large as the value preferred by Hamilton and Oades [98], based on SU(3) arguments** and a dispersion-theoretical analysis of KN scattering. The need for the large ω -coupling constant with regard to a quantitative description of the NN data has been discussed at length and was demonstrated in detail in section 6 and fig. 10, to which we refer the interested reader.

The $\delta(983)$ -meson which, because of its relatively small coupling constant in conjunction with its large mass, contributes little, is needed in our model for a simultaneous and precise fit of both S-wave phase shifts and the corresponding low-energy parameters (and the deuteron binding energy).

The physical basis for the $\pi\pi$ S-wave contribution (σ') and its quantitative derivation and description has been given in length in section 5.

Our values for the $N\Delta\pi$ - and $N\Delta\rho$ -coupling constants have been obtained from the quark-model relations

$$\begin{aligned} f_{N\Delta\pi}^2 &= \frac{72}{25} f_{NN\pi}^2, & f_{NN\pi}^2 &= (m_\pi/2m)^2 g_{NN\pi}^2, \\ f_{N\Delta\rho}^2 &= \frac{f_{N\Delta\pi}^2}{f_{NN\pi}^2} g_{NN\rho}^2 \left(\frac{m_\rho}{2m}\right)^2 \left(1 + \frac{f_{NN\rho}}{g_{NN\rho}}\right)^2. \end{aligned} \tag{8.2}$$

(For a derivation of these relations see, e.g. Brown and Weise [126].)

8.2.2. The vertex form factors

To all vertices we apply the factor eq. (3.3) which is characterized by the cutoff mass Λ_α . These cutoff masses are lying in the quite narrow band of 1.2–1.5 GeV. (Note that Λ_σ has no physical meaning since σ' -exchange represents only an effective description of correlated S-wave 2π -exchange; the

* Once we like to note that the reason for the large difference of the coupling constant at the pole compared to $k^2 = 0$ is merely due to the ansatz for the form factor eq. (3.3) which we have chosen simply for convenience. In fact there are form factors which show no such difference, e.g. the eikonal form factor applied in the HM2 potential [53]. Consequently that potential uses (at the pole!) $g_\omega^2/4\pi = 10$ and $g_\rho^2/4\pi = 0.5$. However, the eikonal form factor causes problems in nuclear structure because of its energy dependence.

** The naive quark model suggests $g_\omega^2 = 9g_\rho^2$; see ref. [57], appendix B to chapter X.

δ -meson and its cutoff is of little relevance.) Such values lead to a rather mild suppression of meson exchange in the range of 0.5 to 1.0 fm in a coordinate-space description; they give rise to substantial changes below 0.5 fm.

It is important to note that our value for the $NN\pi$ vertex cutoff, $\Lambda_{NN\pi} = 1.3$ GeV, is a lower limit for that vertex with regard to a quantitative description of the deuteron properties and the NN scattering data, particularly P-phase shifts. In contrast, our cutoff mass for the $N\Delta\pi$ vertex, $\Lambda_{N\Delta\pi} = 1.2$ GeV, is an upper limit. Beyond that value the uncorrelated 2π -exchange in lower partial waves becomes uncontrollably large. We note that in former (static) models including Δ -isobars [70] there used to be a tremendous difference between $\Lambda_{NN\pi}$ and $\Lambda_{N\Delta\pi}$ (of the order of 1 GeV) which is unreasonable. The fact that we obtain very close values for the cutoff masses of both pion vertices is due to our rather large value for $\Lambda_{N\Delta\pi}$ of 1.2 GeV (compared to former models). This value, which is more consistent with $\Lambda_{NN\pi}$, is possible due to the inclusion of ρ -exchange and of meson retardation which both suppress the Δ contributions in a natural and realistic way.

Furthermore, we like to stress that our form factor for the ρNN vertex agrees very well with results obtained from fits to the electromagnetic form factor of the nucleon [125]. Note that for the electromagnetic form factor of the nucleon a dipole is preferred whereas we use a monopole (per vertex). However, the NN problem is rather insensitive to the particular analytic structure of the form factor and could be equally well described in terms of dipole form factors if an equivalent cutoff mass is used. The rule by which the cutoff masses have to be compiled is: $\Lambda_{\text{dipole}} = \sqrt{2}\Lambda_{\text{monopole}}$. In this sense we agree precisely with the findings of ref. [125] for the electromagnetic form factor of the nucleon.

As stated before, the presence of form factors is dictated by the extended quark structure of hadrons and the cutoff masses Λ_α can be directly related to the hadron size. In the Cloudy-Bag Model (CBM) [7], for example, the πNN form factor is given by

$$F_{NN\pi}(k) = 3 \frac{j_1(kR)}{kR}; \quad k = |k|, \quad (8.3)$$

where j_1 is a spherical Bessel function, k the momentum transfer and R the bag radius, which, in that model, is supposed to be between 0.8 and 1 fm. As far as low-energy ($E_{\text{lab}} \lesssim 300$ MeV) NN scattering is concerned, eq. (8.3) can be well approximated [127] by eq. (3.3) (using $n_\alpha = 1$) if the cutoff parameters are related by $\Lambda_\pi = \sqrt{10}/R$. Thus, the CBM radius $R \gtrsim 0.8$ fm corresponds to a cutoff-mass $\Lambda_\pi \lesssim 0.8$ GeV, which leads to a modification of the π -exchange potential at distances of 2 fm, see ref. [127]. A similar, strong suppression is to be expected for the other meson exchanges. It turns out that, in the framework of our meson-exchange model, a quantitative description of the NN data is by no means possible with such small values for Λ_α ; the lower limit for the NN vertex cutoffs in our model is 1.3 GeV, which corresponds to $R \approx 0.5$ fm. Quite interestingly, there is also an upper limit for some NN vertices, particularly the ρ (of about 1.6 GeV), which might indicate that a certain minimal extension of the nucleon ($R \approx 0.4$ fm) has to be implemented at any rate in order to account for the empirical facts of the NN system. As discussed, the cutoff mass for the $N\Delta\pi$ vertex used in our model, $\Lambda_{N\Delta\pi} = 1.2$ GeV, is an *upper* limit, which is even more indicative that the assumption of an extended structure of the hadrons is crucial to our meson exchange model.

8.3. Final remarks concerning the results

In summary we note that not all parameters given in table 4 are varied to obtain a best fit to the NN data. In fact, there are essentially only six fitted parameters in our model, namely $g_{NN\pi}$, $g_{NN\rho}$, $g_{NN\omega}$, $\Lambda_{NN\pi}$, $\Lambda_{N\Delta\pi}$ and $\Lambda_{NN\rho}$.

The high quality of the quantitative description of the NN data by our model can be clearly traced to the inclusion of the crossed-box diagrams for all two-boson-exchange processes considered. When these crossed boxes are omitted the fit of the data deteriorates considerably and, at the same time, the meson–nucleon coupling constants resulting from such a fit assume in part unrealistic values [71].

9. The parametrization of the nuclear force by one-boson-exchange terms

In this section, we parametrize our full model in simple OBE terms (i.e. as one-boson-exchange potential (OBEP)) in q - as well as in r -space. Such a parametrization will allow, for instance, an easy application in nuclear structure calculations.

9.1. A relativistic OBEP in q -space (OBEPQ)

We start with the parametrization in momentum space. First, we omit the 3π and 4π processes discussed in section 7 which have not been crucial, anyhow. Then, motivated by the results obtained at the end of section 6, we replace the 2π (apart from ρ) plus $\pi\rho$ contributions by (scalar iso-scalar) σ -exchange. After this we are left with OBE terms only, which, however, still have the unpleasant feature of being energy-dependent. This complicates applications to nuclear structure physics considerably*. Therefore, in the next step, we neglect the retardation terms in the OBE propagators which cause the energy dependence, by applying the OBE in the framework of the Blankenbecler–Sugar (BbS) reduction [64] of the Bethe–Salpeter equation [63]**. An additional advantage of the BbS equation is that it is very similar (using “minimal relativity” it is, in fact, formally identical) to the (nonrelativistic) Schrödinger equation, in spite of the fact that it is a relativistic equation. This feature makes the application of the potential in usual (nonrelativistic) nuclear structure physics particularly easy. The explicit expressions for this energy-independent momentum space OBEP are derived and given in appendix E.

It is important for us to keep the parameters of the crucial mesons, namely π , ρ and ω , (almost) exactly the same as in our full model (compare tables 5 and 4), since we believe that the full model is a reliable basis for the determination of those parameters. The σ and δ parameters are adjusted such that a quantitative description of the deuteron binding energy and the low-energy scattering parameters is regained (table 6)***. We also add the η -meson, which is not contained in our full model (see section 4) and which typically occurs in OBE potentials. The η is needed for an improvement of the 3P_1 phase shifts which, due to the absence of the $\pi\rho$ contributions, are always too high in OBE approximations, see fig. 17. The η -coupling constant is at the upper limit of SU(3) predictions (see ref. [57], appendix B to chapter X). Note that one essential feature of our model, namely the small tensor force leading to a small deuteron D-state probability, is preserved in our approximation. This is due to a rather tricky cancellation. Although the neglect of meson retardation increases the tensor force, see section 3, this effect is largely cancelled by the omission of the 3π and 4π contributions discussed in section 7. The

* A parametrization of our full model using (energy-dependent) time-ordered OBE terms is given in appendix B.2.

** Alternatively one can also use the relativistic Thompson equation [128]. This equation and the pseudovector coupling of the pion, both being particularly appropriate for relativistic nuclear structure physics, is applied in the OBE parametrization of the Bonn potential given in ref. [129].

*** For the $T=0$ NN states we choose a slightly higher σ mass than in $T=1$ (see table 5). The reason for this is that the shorter ranged crossed 2π and double Δ diagrams prevail in $T=0$. Note, however, that the $T=1$ parameters given in the table also fit the $T=0$ phase shifts and all deuteron parameters. Yet the accurate description of the triplet S low-energy scattering parameters a_t and r_t , require the higher σ mass. This is important for few-body reactions at low energies. For the many-body problem the different σ mass for the $T=0$ states plays essentially no role. This remark applies to all OBEPs presented in this paper.

Table 5
Meson parameters used in the relativistic (energy-independent) momentum space one-boson-exchange potential (OBEPQ)

	$g_a^2/4\pi; [f_a/g_a]$	$g_a^2/4\pi(k^2 = 0)$	m_a [MeV]	Λ_a [GeV]	n_a
π	14.6	14.27	138.03	1.3	1
ρ	0.81; [6.1]	0.43	769	2.0	2
η	5	3.75	548.8	1.5	1
ω	20; [0.0]	10.6	782.6	1.5	1
δ	1.1075	0.64	983	2.0	1
σ	8.2797 ^a	7.07	550 ^a	2.0	1

Nuclear mass: $m = 938.926$ MeV. For notation and empirical values see table 4. Here, there are NN vertices only.

^aThe parameters for the σ -boson given in the table apply only to the $T = 1$ NN potential. For $T = 0$ we have: $m_\sigma = 720$ MeV, $g_\sigma^2/4\pi = 16.9822$ and $\Lambda_\sigma = 2$ GeV. The parameters for the other mesons in the table are the same for $T = 0$ and $T = 1$.

η -exchange then further reduces the tensor force to about the strength found in the full model. The deuteron wave function of this energy-independent model is given in appendix D.3.3.

As is seen from fig. 17, and is of course expected from former OBE calculations, this simple picture is quite successful in describing the NN scattering phase shifts. There are some slight, though characteristic deficiencies at higher energies compared with the predictions of the full model; however, they should in general play no significant role in low-energy nuclear structure calculations.

9.2. A nonrelativistic OBEP in r -space (OBEPR)

For convenience, we also present an OBE parametrization in r -space. This is obtained by also simplifying the vertex functions using so-called nonrelativistic approximations such that an analytic Fourier transformation into r -space can be performed. The resulting local potential expressions are given in appendix F. As before, the parameters have to be slightly readjusted, see appendix F, table 14, in order to obtain realistic predictions for the empirical data, with the constraint to reproduce again one

Table 6
Deuteron and low-energy scattering parameters predicted by the relativistic (energy-independent) momentum space OBEPQ

Theory	Experiment
ϵ_d (MeV)	2.2246
P_D (%)	4.38
Q_d (fm^2)	0.274 ^a
μ_d (μ_N)	0.8548 ^a
A_S ($\text{fm}^{-1/2}$)	0.8862
D/S	0.0262
r_d (fm)	1.9684
a_s (fm)	-23.744
r_s (fm)	2.704
a_t (fm)	5.424
r_t (fm)	1.760

For notation and references for the experimental data see table 3.

^aMeson-exchange-current corrections not included. For Q_d these range between 0.005 and 0.014 fm^2 [116].

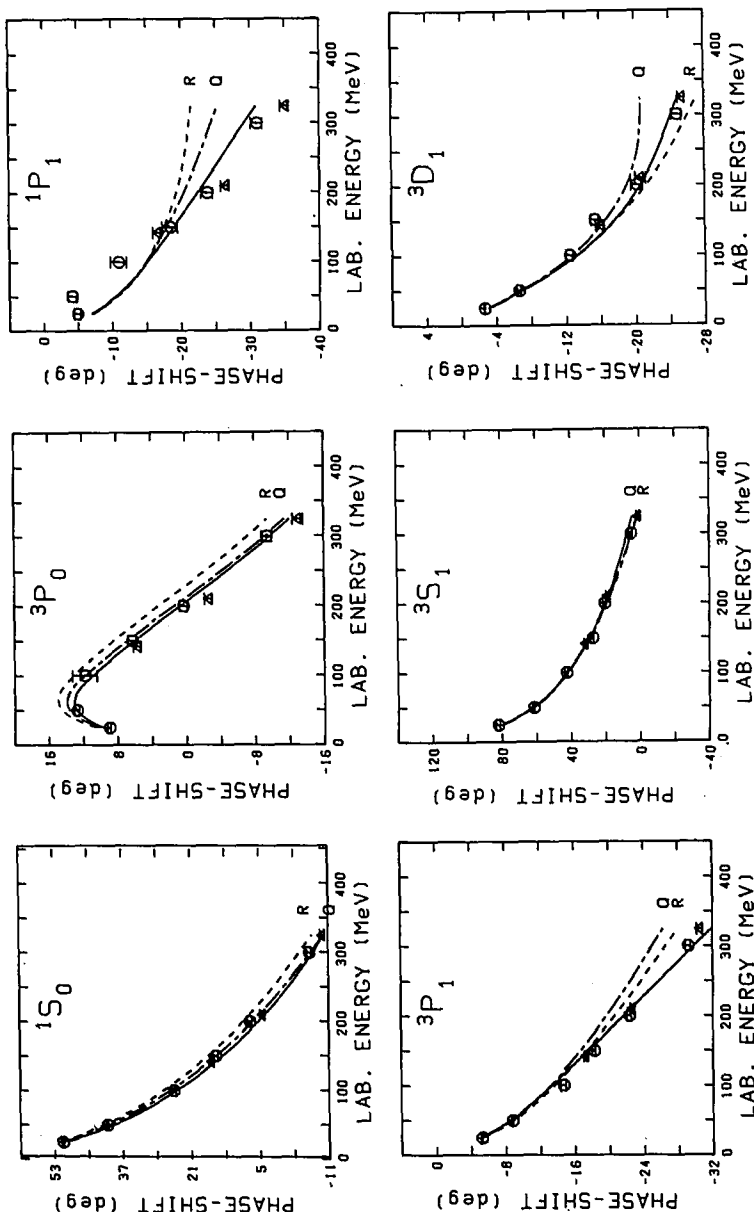


Fig. 17. The description of NN phase shifts by OBEP in comparison to the full model. The solid line represents the result predicted by our full model. The dashed-dotted line refers to the momentum space OBEP(Q) discussed in the section 9.1 with the parameters given in table 5. The dashed line gives the results of the coordinate space OBEP(R) with the parameters given in appendix F, table 14. Error bars as in fig. 15.

essential feature of our model, namely the low deuteron D-state probability (as far as possible in the limited framework of an energy-independent local r -space potential (see table 14)).

Figure 17 demonstrates that small deficiencies occur in the description of the empirical phase shifts at higher energies. Again, however, such discrepancies should not have any large impact on nuclear structure calculations.

9.3. Features of approximate representations of the nuclear force

Approximate representations of the nuclear force are typically energy-independent [49, 50, 52, 60, 86]. A characteristic feature of energy-independent potentials is that it becomes more difficult to combine a weak tensor force (low P_D) with a large Q_d and D/S (compare tables 6 and 3). Though the value for Q_d in table 6 is still compatible with current estimates of meson-current corrections for Q_d [116], it is lower than in our energy-dependent full model. Similar tendencies occur in the ϵ_1 -mixing parameter. While the energy-dependent full model – in spite of its weak tensor force – has no problems in ϵ_1 up to $E_{\text{lab}} = 210$ MeV, the energy-independent models Q (section 9.1) and R (section 9.2) are doing alright only up to $E_{\text{lab}} \approx 100$ –150 MeV (a range which, however, is sufficient for most nuclear structure applications; note again that the Fermi momentum at nuclear matter density is equivalent to $E_{\text{lab}} \approx 125$ MeV).

This problem could be cured by using a larger $NN\pi$ cutoff mass ($\Lambda_{NN\pi} \approx 2.5$ GeV, see e.g. HM1 [52]) which, however, implies a much stronger tensor force ($P_D \approx 5.8\%$). This mechanism is probably responsible for the fact that all conventionally used potentials which are energy-independent have an (almost) point-like $NN\pi$ vertex and consequently predict a large P_D . However, a priori the nuclear force is energy-dependent and has no problems to combine a weak tensor force with an accurate description of ϵ_1 and Q_d . Therefore we will not change the pion form factor determined reliably in our full model, namely $\Lambda_{NN\pi} = 1.3$ GeV, when we construct approximate models. The problems with Q_d and D/S can be partly counterbalanced by an increased pion coupling constant. The features discussed here are summarized in table 7. From that table and fig. 17 it is also apparent that a relativistic nonlocal potential (OBEPQ) is generally doing better in describing the NN data than a nonrelativistic local one (OBEPQ).

Commonly these typical problems of nonrelativistic local r -space potentials are compensated by a wild and uncontrollable expenditure of unphysical parameters [49, 60, 86]. We have reasons not to follow that trend here.

Finally, we show in fig. 18 the half-off-shell R -matrix, eq. (C.2), for the various models in the 1S_0 partial wave and for a fixed energy. It is seen that the off-shell behaviour induced by the simple parametrizations is very different from the original model, in spite of the fact that the on-shell data (phase shifts) are quite the same in all cases. The reasons for the different off-shell behaviour of OBEPQ and OBEPQ, on the one hand, and the full model, on the other hand, are meson retardation and higher-order diagrams which both have about an equally strong effect. Commonly employed NN

Table 7
Some deuteron properties and the pion coupling constant for various meson-exchange models presented in this paper

	P_D	Q_d	D/S	$g_\pi^2/4\pi$
Full model	4.25%	0.281	0.0267	14.4
OBEPQ	4.38%	0.274	0.0262	14.6
OBEPQ	4.81%	0.274	0.0260	14.9

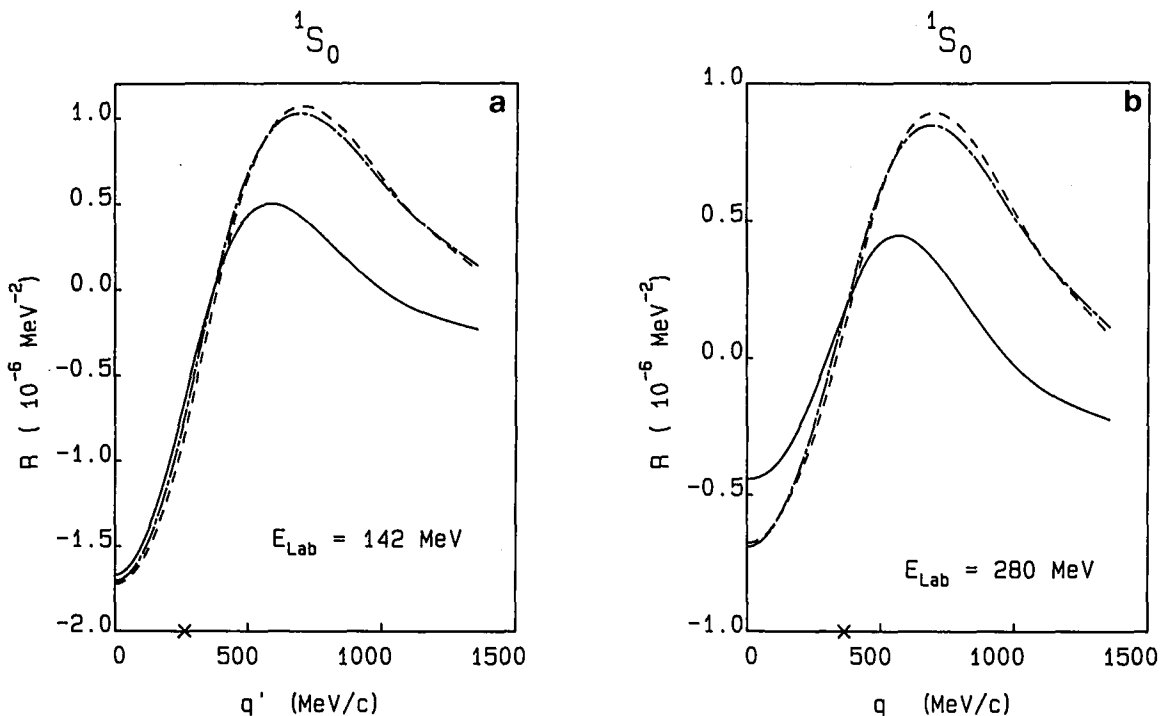


Fig. 18. Half-off-shell R -matrix, $R(q', q; q)$, in the 1S_0 partial wave, for various models of the nuclear force. The results are given for (a) $E_{\text{Lab}} = 142$ MeV ($E_{\text{Lab}} = 2q^2/m$) and (b) $E_{\text{Lab}} = 280$ MeV, as a function of q' . The on-shell value is marked by a cross. The full line stands for the full model; the dashed-dotted for OBEPQ; the dashed for OBEPR.

potentials [60, 86] have a half-off-shell R -matrix very similar to OBEPQ and OBEPR. It would be interesting to see whether this different off-shell behaviour has any impact on observable quantities.

10. Some remarks concerning nuclear structure

A long standing problem in nuclear matter theory is that conventional two-nucleon potentials seem to underbind nuclear matter considerably (by several MeV) at densities below the empirical nuclear matter saturation density (i.e. for $k_F \leq 1.35 \text{ fm}^{-1}$ with k_F the Fermi momentum). On the other hand, these same potentials lead to overbinding for $k_F > 1.35 \text{ fm}^{-1}$ (see refs. [130, 131]). As a consequence of these two deficiencies, saturation is predicted at about twice the empirical saturation density. The results in finite nuclei reflect this deficient feature observed in nuclear matter; namely, light nuclei (e.g. ^3H , ^4He , ^{16}O) are strongly underbound, whereas heavier nuclei are predicted with too small radii [130, 131]. These results have (mis-) led some physicists to the belief that rather elaborate three-nucleon forces must exist in nature with the peculiar feature of being attractive at low nuclear densities and turning repulsive at higher densities. This belief is based on the assumption that *all realistic* two-nucleon potentials lead to nuclear matter results of the deficient kind described above. However, this assumption is wrong. In fact, the two-nucleon interaction presented in this paper has – as pointed out repeatedly – a relatively weak tensor force, which is reflected in a low deuteron D-state probability (P_D). Our model shows that a weak tensor force ($P_D \approx 4.5\%$) is consistent with all known NN data and is strongly suggested by meson theory. In addition, e.g. from forward deuteron photodisintegration [114], there are empirical indications that the percentage D state is low ($\approx 4.5\%$) [115]. The common

prejudice that realistic potentials should predict a high P_D ($\approx 5.5\text{--}6.5\%$) is due to an accident. For plain convenience only the simplest NN interactions have been applied in nuclear structure; simplest meaning an energy-*independent*, local, phenomenological, r -space potential. Due to the (unphysical) assumption of point hadrons and the static approximation inherent to these simplest potentials the tensor force (derived from OPE) must turn out to be strong. However, as pointed out in this work, the extended structure of hadrons and meson retardation have to be taken into account in a consistent and refined meson theory. Both produce sizable effects on the tensor force cutting it down such that the P_D turns out to be about 4.5%. This has important consequences for the nuclear matter binding energy. Namely, a low P_D nuclear potential does not underbind nuclear matter anymore at densities below nuclear matter saturation. In fact, the NN interaction presented in this paper predicts an energy per nucleon of -12.7 MeV at $k_F = 1.1 \text{ fm}^{-1}$ (the average density of ^{16}O) and -15.6 MeV at $k_F = 1.25 \text{ fm}^{-1}$ * in agreement with the empirical nuclear matter curve given in ref. [131]. Of course, there is overbinding at higher densities, $k_F \geq 1.35 \text{ fm}^{-1}$. However, these densities do not occur in realistic nuclei, and therefore are not very relevant for conventional nuclear structure physics, particularly, in the range of light and medium heavy nuclei. Furthermore, at higher densities there are medium effects of various kinds which quench the binding strength of the nuclear force when it is inserted into the nuclear many-body problem. These effects are due to meson and isobar degrees of freedom [70, 133, 135, 136] as well as strongly density-dependent relativistic effects [82, 83, 85, 129]. In fact, when the relativistic medium effects as estimated by Brown et al. [85] and calculated accurately in ref. [129] are added, saturation is obtained at $k_F = 1.36 \text{ fm}^{-1}$ and an energy per nucleon of about -16 MeV which are the empirical values. Due to the strong density dependence of the medium effect, the result at lower densities remains essentially unaltered. Therefore, it is a reasonable approach to nuclear structure physics to consider the light and medium heavy nuclei, first, in the framework of two-body forces only. With regard to the low density of these systems “fancy” corrections, like medium effects and many-body forces, should not play an important role. Therefore, a low P_D nuclear force, as presented in this paper, applied to light and medium heavy nuclei might solve some of the traditional theoretical nuclear structure problems. Also, from empirical deductions of shell-model matrix elements a weak tensor force is indicated [137].

If one wants to include fancier ingredients, like three-body forces, which might be quite appropriate at higher densities, they have to be evaluated in a way consistent with the two-body force applied. For instance, Δ -excitation of the nucleon in the medium gives rise to a three-body force due to π - and p -exchange with different nucleons [138]. For these meson exchanges the same coupling constants and form factors apply as determined and used for the two-body force, i.e. there is no free parameter in the three-body force! Also the same theoretical framework has to be applied for all processes considered. When including Δ -degrees of freedom this framework leads already to medium effects on the two-body force which have to be taken into account simultaneously with the three-body force. There will be partial cancellations between both effects. An isolated consideration of only one of the two effects is therefore meaningless. Only this consistent consideration of many-body effects and many-body forces, for which our model provides the basis, can claim credibility in going beyond the conventional framework of a two-body potential.

* Applying OBEPQ (see section 9.1) in a lowest-order Brueckner calculation using the continuous choice for the single-particle potential in nuclear matter. Note that a lowest-order Brueckner calculation with the continuous choice leads to very much the same results as choosing the “gap” prescription (see ref. [133] for a definition) and including three- and four-body correlations. This is seen clearly when comparing Day’s results [130] for HM1 [52] with those given in ref. [133] (see fig. 3, therein) for that same NN potential using the continuous choice. In fact, in ref. [134] it is explicitly proven that higher correlations in the framework of the continuous choice turn out to be negligibly small.

11. Summary, conclusions and outlook

In this paper, we have presented a comprehensive field-theoretical meson-exchange model for the NN interaction. Our general scheme is to treat nucleons, isobars and mesons on an equal footing. Consequently we start from a field-theoretical Hamiltonian H which in its interaction part consists of NN-meson and $N\Delta$ -meson vertices. H is treated in relativistic time-ordered perturbation theory which allows for a well-defined transition from the two- to the many-body problem. The extended structure of hadrons is taken into account by vertex form factors which are parametrized by the so-called cutoff mass Λ_α . The constraint of a quantitative description of the NN data up to $E_{\text{lab}} \approx 300$ MeV leads to cutoff masses in the range 1.2–1.5 GeV. Our model is considered comprehensive and consistent in the sense that it includes all relevant diagrams with a total exchanged mass up to about the cutoff mass (≈ 1 GeV). The various meson-exchange contributions in that range are introduced step by step proceeding from lowest-order to higher-order processes and from long range to short range.

The well-known one-meson-exchange contributions from π and ω provide the (long-range) tensor and the short-range repulsion and spin-orbit force. Our 2π -exchange model describing the intermediate range of the nuclear force takes nucleon resonances (isobars) and direct $\pi\pi$ interaction into account. The latter contribution is consistent with quantitative results from $\pi\pi$ scattering. For the uncorrelated 2π -exchange, box and crossed-box contributions are included both being about equally large. Higher angular momentum phase shifts of NN scattering reflecting an intermediate internucleonic range are described quantitatively by this model. Within the uncertainties inherent to the dispersion theoretic approach to the 2π -exchange we achieve agreement with results stemming from that theory.

For the description of the low angular momentum phase shifts (particularly P-waves) it turns out to be crucial to include diagrams of combined π - and ρ -exchange. Furthermore, a strong omega-coupling constant is required.

Further diagrams of 3π - and 4π -exchange have little significance due to strong mutual cancellations in between those contributions. In this way a strong convergence in our diagrammatic expansion is clearly established provided that the diagrams are grouped in a suitable way as dictated by the physics of the NN problem.

An excellent quantitative description of the deuteron data, NN scattering phase shifts and observables is achieved. This can clearly be traced to the “completeness” of the set of diagrams we include in our model. Most noticeably, the tensor force turns out to be weak in our model which is seen in a low percentage D state of the deuteron, whereas the quadrupole moment and the asymptotic D/S state of the deuteron are large and in perfect agreement with experiment. The weak tensor force can be attributed to ρ -exchange, a realistic π NN form factor and the inclusion of meson retardation.

The coupling constants obtained from the best fit to the data are in overall agreement with information from other sources (e.g. πN scattering, electromagnetic form factor of the nucleon). Due to the comprehensive character of our model within the framework of meson theory, our parameter values are essentially uniquely determined*. In order to further establish (from the theoretical point of view) the validity of the meson-exchange picture for the (low-energy) NN problem, these values could be compared with reliable determinations from QCD, which, however, do not exist at present.

Our model represents a sound basis for addressing several important issues in nuclear and intermediate-energy physics in the future. First of all, its energy dependence leads automatically to meson production processes at intermediate energies and therefore provides a consistent description of

* If one takes in addition self-energy diagrams explicitly into account (which is necessary for a realistic treatment of the NN problem above pion threshold) the resulting best fit parameters will change only slightly [139].

the NN interaction and the coupling to pion production channels. Moreover, the weak tensor force has strong implications for nuclear structure leading generally to more attraction in the nuclear few and many-body system. This feature may contribute to the solution of some long-standing problems in that field. Furthermore, the comprehensive set of diagrams contributing to the NN interaction, represents a sound basis for a consistent generalization to three-body forces and a “complete” accounting of meson-exchange-current contributions to the electromagnetic properties of nuclei. Medium modifications of the nuclear force, when applied in the many-body problem, due to relativistic effects as well as meson and isobar degrees of freedom are other outstanding problems which can be examined thoroughly on the basis of our model. The issues raised as well as many others are an exciting challenge for the future.

Acknowledgement

The authors acknowledge support by Prof. K. Bleuler. Two of the authors (R.M. and K.H.) would like to thank G.E. Brown for many stimulating discussions and continuous interactions over more than a decade on the topic of this article. These authors also acknowledge the fruitful collaboration with M.R. Anastasio, X. Bagnoud, A. Faessler and H. Müther. The project was finished while one of the authors (R.M.) was visiting TRIUMF/Vancouver (Canada) in the years of 1984 and 1985. Another author (K.H.) was visiting TRIUMF during the summer of 1985. Both these authors would like to thank the staff of TRIUMF, H.W. Fearing, R.W. Woloshyn and B.K. Jennings, for their kind hospitality. All authors enjoyed stimulating discussions with D. Schütte. One of the authors (R.M.) gratefully acknowledges discussions and advice concerning the manuscript from R.A. Arndt, L.N. Chang, H.E. Conzett, H.W. Fearing, T. Mizutani, A. Picklesimer, F. Sammarruca, R.M. Thaler and W. Wilcox. Finally, thanks are due to M. Heese of the Institut für Kernphysik der KFA Jülich for her patience in typing various versions of the manuscript until its final form could be reached.

Appendix A: Field-theoretical framework for mesons and baryons

Our starting point is the field-theoretical Hamiltonian

$$H = H_0 + W \quad (\text{A.1})$$

with the free Hamiltonian

$$H_0 = h_0 + t, \quad (\text{A.2})$$

where

$$h_0 = \sum_{\beta} E_{\beta} b_{\beta}^+ b_{\beta} \quad (\text{A.3})$$

is the kinetic energy operator for baryons and

$$t = \sum_{\alpha} \omega_{\alpha} a_{\alpha}^+ a_{\alpha} \quad (\text{A.4})$$

the corresponding operator for mesons. a_α^+, a_α and b_β^+, b_β are the creation, destruction operators for mesons (bosons) and baryons (fermions) obeying the usual commutator and anticommutator relations. α and β denote all quantum numbers which specify the respective state completely. Note that therefore the sum in eqs. (A.3) and (A.4) also includes the integration over all momenta. ω_α and E_β are the renormalized (physical) relativistic kinetic energies of mesons and baryons, respectively. Thus, we work in a Hilbert space which consists of physical meson and baryon states.

For the meson–baryon interaction term W we assume the general structure

$$W = \sum_{\beta' \beta \alpha} W_{\beta' \beta \alpha} b_\beta^+ b_\beta a_\alpha + \text{h.c.} \quad (\text{A.5})$$

with h.c. denoting the hermitian conjugate.

In this paper we will restrict ourselves to $N(939)$ and $\Delta(1232)$ for the baryons and to the mesons given in table 4. The reasons for this sub-selection are discussed in sections 4 and 5. With these particles we have the interaction terms described pictorially in fig. 1(a) for nucleons and mesons and in fig. 1(b) for nucleons, Δ -isobars and mesons. We omit $\Delta\Delta$ vertices. Note that the Δ is treated in the quark-model sense, i.e. as a new particle distinct from the nucleon. The scheme displayed in eqs. (A.1)–(A.5) is the basis for a field-theoretical description of nuclear physics in terms of nucleons, isobars and mesons. Though, in this paper, we will confine ourselves to the two-nucleon problem below pion-production threshold, we mention that the extension above is straightforward [139] and that, furthermore, important issues of nuclear physics such as the many-body problem, meson-exchange currents and isobar contributions to the electromagnetic properties of nuclei can be treated consistently on the basis of this scheme [68, 140].

The next step is to define a transition matrix T (restricted to the two-nucleon space) by relating it to the standard S -matrix,

$$\langle \beta'_1 \beta'_2 | S | \beta_1 \beta_2 \rangle = \langle \beta'_1 \beta'_2 | \beta_1 \beta_2 \rangle - 2\pi i \delta^{(4)}(P' - P) \langle \beta'_1 \beta'_2 | T | \beta_1 \beta_2 \rangle, \quad (\text{A.6})$$

where P (P') is the total four-momentum in the in (out)-going state, $|\beta_1 \beta_2\rangle = b_{\beta_1}^+ b_{\beta_2}^+ |0\rangle$ and $|0\rangle$ the vacuum state. Treating H in time-ordered perturbation theory [141, 142], $\langle \beta'_1 \beta'_2 | T | \beta_1 \beta_2 \rangle$ can be represented by a series expansion defined by all diagrams containing two ingoing, $\beta_1 \beta_2$, and two outgoing, $\beta'_1 \beta'_2$, nucleon lines. This series can partially be summed by solving a (three-dimensional) integral equation of the Lippmann–Schwinger type

$$T(E) = V(E) + V(E) \frac{1}{E - h_0^{(N)} + i\epsilon} T(E), \quad (\text{A.7})$$

with E the energy of the initial state and $h_0^{(N)}$ the nucleonic part of the baryon kinetic energy operator, eq. (A.3). The energy (E)-dependent quasipotential $V(E)$ (the kernel of this integral equation) consists of the (infinite) sum of all diagrams involving at least one meson or one Δ -isobar in each intermediate state (irreducible diagrams in the NN channel). Diagrams involving at least one intermediate state with nucleons only are generated by the scattering equation. For example, in fig. 19, diagrams (a) and (b) belong to $V(E)$ whereas (c) and (d) are generated by the scattering equation. Note that each time ordering has to be taken into account separately. For example, there are twelve diagrams involving one Δ which contribute to $V(E)$. These diagrams are shown in fig. 20. In this figure, diagrams 1–4, having one intermediate state without a meson, are the iterative diagrams; 5–6 are called stretched-box

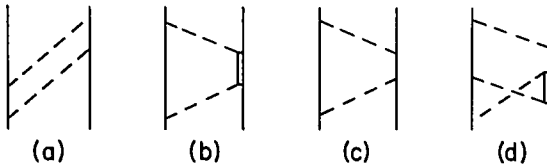


Fig. 19. Diagrams appearing in the perturbation expansion. (a) and (b) belong to $V(E)$ whereas (c) and (d) are generated by the scattering equation (A.7).

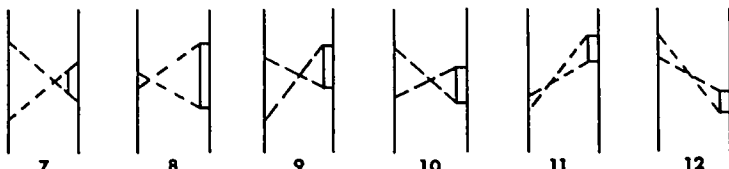
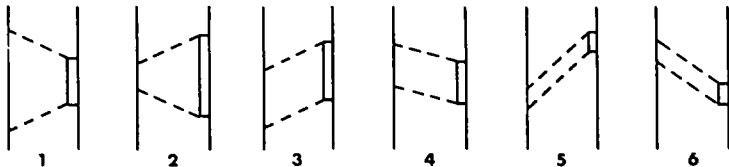


Fig. 20. Time-ordered diagrams with positive-energy $N\Delta$ intermediate states. Diagrams 1–4 are the iterative boxes, 5–6 stretched boxes and 7–12 crossed boxes.

diagrams, whereas 7–12 are the so-called crossed-box diagrams. In order to show all diagrams included in $V(E)$ in a way which is easy to survey, we introduce a short-hand notation (which is applied in sections 4–7): e.g., graphically, we will represent diagrams 1–5 and 7–12 by one diagram each, see fig. 21. Note that the sum of all time-orderings shown corresponds to Feynman diagrams with the exclusion of negative-energy states. Furthermore, in our short notation, the two time-orderings for single-meson exchange will be represented by one diagram. For the case of one-pion exchange this is shown in fig. 22. We account for self-energy contributions by defining the free Hamiltonian with renormalized quantities and using empirical masses in the meson exchange diagrams, which is correct on-shell and should be a good approximation since we stay below pion-production threshold.

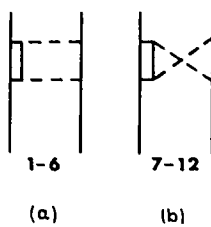


Fig. 21. Graphical short-hand notation for $N\Delta$ processes. Diagram (a) represents the sum of diagrams 1–6 of fig. 20 whereas diagram (b) stands for diagrams 7–12 of that same figure.

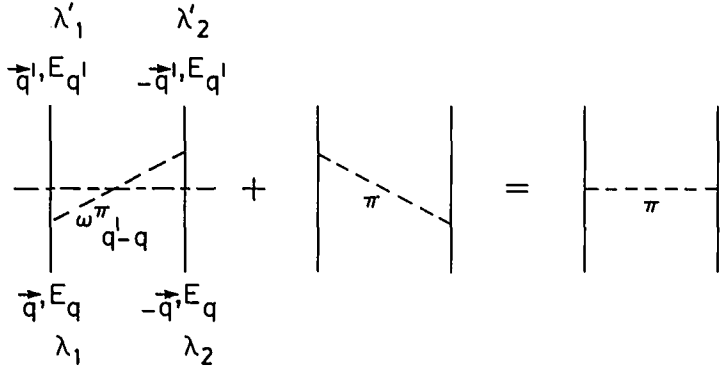


Fig. 22. Graphical short-hand notation for the two time-ordered processes of one-pion exchange.

Appendix B: Meson-exchange contributions in time-ordered perturbation theory

B.1. The fields and the interaction Hamiltonians

We start with the standard representation for the field operators

$$\begin{aligned}
 \psi(x) &= \frac{1}{(2\pi)^{3/2}} \sum_{q,\lambda} u(q, \lambda) \exp(-i q \cdot x) b_{q,\lambda}, \\
 \psi_\mu(x) &= \frac{1}{(2\pi)^{3/2}} \sum_{q,\lambda} u_\mu(q, \lambda) \exp(-i q \cdot x) b_{q,\lambda}, \\
 \phi(x) &= \frac{1}{(2\pi)^{3/2}} \sum_k \frac{1}{\sqrt{2\omega_k}} [\exp(-i k \cdot x) a_k + \exp(i k \cdot x) a_k^+], \\
 \phi_\mu(x) &= \frac{1}{(2\pi)^{3/2}} \sum_{k,s} \frac{1}{\sqrt{2\omega_k}} \epsilon_\mu(k, s) [\exp(-i k \cdot x) a_{k,s} + \exp(i k \cdot x) a_{k,s}^+],
 \end{aligned} \tag{B.1}$$

for nucleons, Δ -isobars, scalar (pseudoscalar) and vector mesons, respectively. (Note that we omit antiparticles from the beginning.) In our notation, the sum Σ over a momentum, e.g. q , stands for the integral $\int d^3q$. Spinors are represented in a helicity state basis, as this is most appropriate and convenient for the evaluation of meson-exchange contributions to the NN interaction. The helicity λ is defined as the eigenvalue of the operator $s \cdot \hat{q}$ with s the spin operator and $\hat{q} = q/|q|$ the unit momentum operator of the baryon. The Dirac spinors, $u(q, \lambda)$, are normalized by

$$u^+(q, \lambda) u(q, \lambda) = 1. \tag{B.2}$$

$u_\mu(q, \lambda)$ is the Rarita–Schwinger spinor [111, 143, 144] representing a Δ -isobar with spin 3/2. $\epsilon_\mu(k, s)$ is the polarization vector describing vector mesons, ω_k denotes the energy of a meson and $k \cdot x$ is the scalar product of the four-momentum k and space-time four-vector x . We follow the conventions and notations of Bjorken and Drell [145], except when stated otherwise. (Note, e.g., that our normalization

of the Dirac spinors eq. (B.2) differs from ref. [145].) The isospin dependence, which can be trivially taken into account, is suppressed, as customary, when formalism is described.

The interaction Hamiltonian is defined by

$$W = - \int d^3x \left[\mathcal{L}_I(x) - \frac{\partial \mathcal{L}_I}{\partial \dot{\varphi}_\alpha^{(\mu)}} \dot{\varphi}_\alpha^{(\mu)} \right]_{x_0=0}, \quad (\text{B.3})$$

where the dot denotes the time derivative. Applying time-ordered perturbation theory [141], we work in the Schrödinger picture, in which the interaction is time-independent. This explains the “condition” $x_0 = 0$ in eq. (B.3). With the definition for W (eq. (B.3)) we derive from the interaction Lagrangian densities, eqs. (3.1) and (3.2), together with the vertex form factor function, eq. (3.3), and the fields, eq. (B.1), the matrix elements $W_{\beta'\beta\alpha}$ defined in eq. (A.5).

$$\begin{aligned} W_{\beta'\beta\alpha}^{(\text{NNps})} &= - \frac{g_{ps}}{[2\omega_k^{ps}(2\pi)^3]^{1/2}} \delta^{(3)}(\mathbf{q}_{\beta'} - \mathbf{q}_\beta - \mathbf{k}) \bar{u}(\mathbf{q}_{\beta'}, \lambda_{\beta'}) i \gamma^5 u(\mathbf{q}_\beta, \lambda_\beta) F_{ps}(k^2), \\ W_{\beta'\beta\alpha}^{(\text{NNs})} &= - \frac{g_s}{[2\omega_k^s(2\pi)^3]^{1/2}} \delta^{(3)}(\mathbf{q}_{\beta'} - \mathbf{q}_\beta - \mathbf{k}) \bar{u}(\mathbf{q}_{\beta'}, \lambda_{\beta'}) u(\mathbf{q}_\beta, \lambda_\beta) F_s(k^2), \end{aligned} \quad (\text{B.4})$$

$$\begin{aligned} W_{\beta'\beta\alpha}^{(\text{NNv})} &= - \frac{\epsilon^\mu(k, s)}{[2\omega_k^v(2\pi)^3]^{1/2}} \delta^{(3)}(\mathbf{q}_{\beta'} - \mathbf{q}_\beta - \mathbf{k}) [(g_v + f_v) \bar{u}(\mathbf{q}_{\beta'}, \lambda_{\beta'}) \gamma_\mu u(\mathbf{q}_\beta, \lambda_\beta) \\ &\quad - \frac{f_v}{2m} \bar{u}(\mathbf{q}_{\beta'}, \lambda_{\beta'}) (\mathbf{q}_{\beta'} + \mathbf{q}_\beta)_\mu u(\mathbf{q}_\beta, \lambda_\beta)] F_v(k^2), \\ W_{\beta'\beta\alpha}^{(\Delta N\pi)} &= + \frac{f_{N\Delta\pi}}{m_\pi} \frac{i}{[2\omega_k^\pi(2\pi)^3]^{1/2}} \delta^{(3)}(\mathbf{q}_{\beta'} - \mathbf{q}_\beta - \mathbf{k}) k^i \bar{u}_i(\mathbf{q}_{\beta'}, \lambda_{\beta'}) u(\mathbf{q}_\beta, \lambda_\beta) F_{N\Delta\pi}(k^2), \\ W_{\beta'\beta\alpha}^{(\Delta N\rho)} &= - \frac{f_{N\Delta\rho}}{m_\rho} \frac{1}{[2\omega_k^\rho(2\pi)^3]^{1/2}} \delta^{(3)}(\mathbf{q}_{\beta'} - \mathbf{q}_\beta - \mathbf{k}) [k^i \epsilon^\nu(k, s) \bar{u}_\nu(\mathbf{q}_{\beta'}, \lambda_{\beta'}) \gamma^5 \gamma_i u(\mathbf{q}_\beta, \lambda_\beta) \\ &\quad - k^i \epsilon^\mu(k, s) \bar{u}_j(\mathbf{q}_{\beta'}, \lambda_{\beta'}) \gamma^5 \gamma_\mu u(\mathbf{q}_\beta, \lambda_\beta)] F_{N\Delta\rho}(k^2). \end{aligned} \quad (\text{B.5})$$

The vertex $W_{\beta'\beta\alpha}^{(\Delta N\alpha)}$ is obtained from $W_{\beta'\beta\alpha}^{(\Delta N\alpha)}$ by taking the complex conjugate and changing \mathbf{k} to $-\mathbf{k}$ in the δ -function. Note that for the quantum numbers of the different particles, we have used the following notation: mesons: $\alpha = (\omega_k^\alpha, \mathbf{k}, s)$, baryons: $\beta = (E_\beta, \mathbf{q}_\beta, \lambda_\beta)$ – (apart from total spin, isospin, parity and others). As seen clearly from eqs. (B.4) and (B.5), in time-ordered perturbation theory there is three-momentum conservation at the vertices. Furthermore, all particles are always on their mass shell. Therefore, energy is not conserved at the vertices.

To obtain the NNps vertex as given in eq. (B.4) we applied the Dirac equation to the original pseudovector coupling. In the case of the NNv vertex we applied the Gordon decomposition [145]. In both cases there is an additional off-shell term which we omit. The effects of these (omitted) off-shell terms are such that a small change in the cutoff parameter of the vertex form factor $F_\alpha(k^2)$ would compensate for them.

B.2. The second-order contributions

The lowest-order diagrams contributing to the NN interaction kernel $V(E)$ are of second order in W and are given by

$$\left\langle \beta'_1 \beta'_2 \left| W \frac{1}{E - h_0 - t} W \right| \beta_1 \beta_2 \right\rangle_{\text{linked}} = \delta^{(3)}(\mathbf{q}_{\beta'_1} + \mathbf{q}_{\beta'_2} - \mathbf{q}_{\beta_1} - \mathbf{q}_{\beta_2}) \langle \beta'_1 \beta'_2 | V^{(2)}(E) | \beta_1 \beta_2 \rangle. \quad (\text{B.6})$$

Explicitly we obtain for the one-pion-exchange potential (fig. 22), in the two-nucleon center of mass (c.m.) system and helicity-state basis,

$$\begin{aligned} \langle q' \lambda'_1 \lambda'_2 | V_\pi^{(2)}(E) | q \lambda_1 \lambda_2 \rangle &= 2 \frac{g_\pi^2}{(2\pi)^3} \tau_1 \cdot \tau_2 \frac{1}{2\omega_k^\pi} \frac{\bar{u}(q', \lambda'_1) i \gamma^5 u(q, \lambda_1) \bar{u}(-q', \lambda'_2) i \gamma^5 u(-q, \lambda_2)}{E - E_{q'} - E_q - \omega_k^\pi} \\ &\times F_\pi^2(k^2). \end{aligned} \quad (\text{B.7})$$

Here, $E = 2E_q$ is the starting energy, λ_i, λ'_i ($i = 1, 2$) are the relevant helicities; $E_q = \sqrt{m^2 + \mathbf{q}^2}$, $E_{q'} = \sqrt{m^2 + \mathbf{q}'^2}$ and $\omega_k^\pi = \sqrt{m_\pi^2 + (q' - q)^2}$. The $\tau_1 \cdot \tau_2$ factor is due to the exchange of an isospin $I = 1$ meson. The denominator is obtained by subtracting the energies involved in the intermediate state (dashed-dotted line in fig. 22) from the starting energy; the factor 2 arises because there are two time orderings, which both give the same contribution. The static approximation for the meson propagator (which we will *not* use) is obtained by setting $E = E_{q'} + E_q$ leading to

$$\frac{-1}{(\omega_k^\pi)^2} = \frac{-1}{(q' - q)^2 + m_\pi^2}. \quad (\text{B.8})$$

Analogously, the OBE contribution due to scalar exchange is given by

$$\langle q' \lambda'_1 \lambda'_2 | V_s^{(2)}(E) | q \lambda_1 \lambda_2 \rangle = \frac{g_s^2}{(2\pi)^3} \frac{1}{\omega_k^s} \frac{\bar{u}(q', \lambda'_1) u(q, \lambda_1) \bar{u}(-q', \lambda'_2) u(-q, \lambda_2)}{E - E_{q'} - E_q - \omega_k^s} \cdot F_s^2(k^2) \quad (\text{B.9})$$

and for the exchange of vector mesons

$$\begin{aligned} \langle q' \lambda'_1 \lambda'_2 | V_v^{(2)}(E) | q \lambda_1 \lambda_2 \rangle &= -\frac{1}{(2\pi)^3} \frac{1}{\omega_k^v} \frac{1}{E - E_{q'} - E_q - \omega_k^v} F_v^2(k^2) \\ &\times \left[(g_v + f_v) \bar{u}(q', \lambda'_1) \gamma^\mu u(q, \lambda_1) - \frac{f_v}{2m} \bar{u}(q', \lambda'_1) (q' + q)^\mu u(q, \lambda_1) \right] \\ &\times \left[(g_v + f_v) \bar{u}(-q', \lambda'_2) \gamma_\mu u(-q, \lambda_2) \right. \\ &\left. - \frac{f_v}{2m} \bar{u}(-q', \lambda'_2) (q' + q)^\mu u(-q, \lambda_2) \right], \end{aligned} \quad (\text{B.10})$$

where

$$\sum_{s=1}^3 \epsilon^\mu(k, s) \epsilon^\nu(k, s) = -g^{\mu\nu} + k^\mu k^\nu / m_v^2 \quad (\text{B.11})$$

has been used with the last term on the r.h.s. being dropped.

This finishes the consideration of one-meson-exchange contributions. For further more detailed evaluations of eqs. (B.7)–(B.10) see appendix E. It is well known that with the OBE contributions derived so far, a quantitative description of the NN data is, indeed, possible. In table 8 we give an

Table 8
Meson and low-energy parameters (LEP) of an (energy-dependent) one-boson-exchange potential based on time-ordered perturbation theory (OBEPT)

	$g_a^2/4\pi; [f_a/g_a]$	m_a (MeV)	Λ_a (GeV)	LEP	Theory
π	14.6	138.03	1.75	ϵ_d (MeV)	2.2245
ρ	0.92; [6.1]	769.0	1.5	P_D (%)	4.27
η	5.0	548.8	1.5	Q_d (fm ²)	0.278
ω	20.0; [0.0]	782.6	1.5	D/S	0.0267
δ	1.1585	983.0	2.0	a_s (fm)	-23.748
σ	8.8543 ^a	550.0 ^a	2.0	r_s (fm)	2.759
				a_t (fm)	5.426
				r_t (fm)	1.755

Nucleon mass: $m = 938.926$ MeV. For notation and experimental data see tables 3 and 4, $n_a = 1$.

^a The parameters for the σ -boson given in the table apply only to the $T = 1$ NN potential. For $T = 0$ we have: $m_\sigma = 615$ MeV, $g_\sigma^2/4\pi = 11.7027$ and $\Lambda_\sigma = 2.0$ GeV. The parameters for the other mesons are the same for $T = 0$ and $T = 1$.

example. Note that π and η are pseudoscalar, σ and δ scalar and ω and ρ vector mesons. The expressions for the exchange of the isospin $I = 1$ mesons π , δ and ρ get an additional factor $\tau_1 \cdot \tau_2$. The NN potential is defined as the sum of the OBE contributions of these six mesons.

B.3. Fourth-order contributions

Now let us turn to the fourth-order diagrams in W which are given by

$$\begin{aligned} & \left\langle \beta'_1 \beta'_2 \left| W \frac{1}{E - h_0 - t} W \frac{1}{E - h_0 - t} W \frac{1}{E - h_0 - t} W \right| \beta_1 \beta_2 \right\rangle_{\text{linked}} \\ &= \delta^{(3)}(\mathbf{q}_{\beta'_1} + \mathbf{q}_{\beta'_2} - \mathbf{q}_{\beta_1} - \mathbf{q}_{\beta_2}) \langle \beta'_1 \beta'_2 | V^{(4)}(E) | \beta_1 \beta_2 \rangle. \end{aligned} \quad (\text{B.12})$$

This expression contains iterative plus noniterative diagrams with nucleons as well as Δ -isobars in intermediate states, involving all possible two-meson exchanges. Note that the one-meson-exchange contributions are iterated in the scattering equation (A.7). Therefore we have to remove all iterative diagrams involving two-nucleon intermediate states from eq. (B.12).

In order to elucidate the structure of eq. (B.12) we will, as an example, consider the processes with $N\Delta$ intermediate states and involving 2π -exchange. For notation, see fig. 23. We start with the iterative contributions represented by diagrams 1–4 of fig. 20,

$$\begin{aligned} \langle \mathbf{q}' \lambda'_1 \lambda'_2 | M^{\text{it}} | \mathbf{q} \lambda_1 \lambda_2 \rangle &= \frac{g_\pi^2}{(2\pi)^6} \frac{f_{N\Delta\pi}^2}{m_\pi^2} (2 + \frac{2}{3} \tau_1 \cdot \tau_2) \int d^3 k \frac{1}{4\omega_{q'-k}^\pi \omega_{q-k}^\pi D^\pi} \\ &\times \bar{u}(\mathbf{q}', \lambda'_1) i(k - q')_i P_+^{ij}(k) i(k - q)_j u(\mathbf{q}, \lambda_1) F_{N\Delta\pi}[(q' - k)^2] F_{N\Delta\pi}[(q - k)^2] \\ &\times \bar{u}(-\mathbf{q}', \lambda'_2) i\gamma^5 \Lambda_+(-k) i\gamma^5 u(-\mathbf{q}, \lambda_2) F_{NN\pi}[(q' - k)^2] F_{NN\pi}[(q - k)^2], \end{aligned} \quad (\text{B.13})$$

where $\Lambda_+(-k)$ is the projection operator for positive-energy nucleon states

$$\Lambda_+(k) = \frac{1}{2E_k} (\gamma^0 E_k - \boldsymbol{\gamma} \cdot \mathbf{k} + m) \quad (\text{B.14})$$

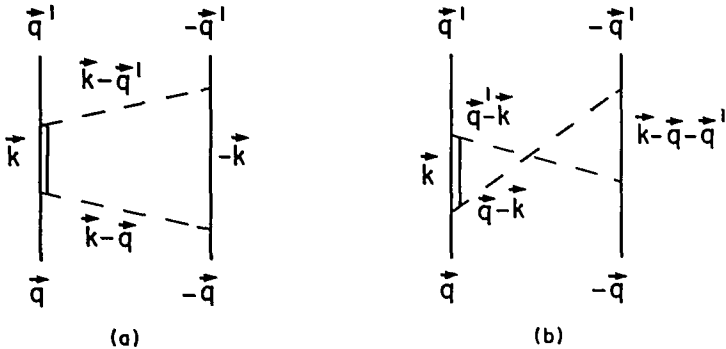


Fig. 23. Selected-box (a) and crossed-box (b) diagram displaying the notation used in the text.

and $P_+^{\mu\nu}(k)$ the corresponding operator for the Δ -isobar [111, 143, 144]

$$P_+^{\mu\nu}(k) = \Lambda_+^*(k) \left[-g^{\mu\nu} + \frac{1}{3}\gamma^\mu\gamma^\nu + \frac{2}{3}\frac{k^\mu k^\nu}{m^{*2}} + \frac{1}{3}\frac{\gamma^\mu k^\nu - \gamma^\nu k^\mu}{m^*} \right], \quad (\text{B.15})$$

where we have used m^* for the mass and $E_q^* = (q^2 + m^{*2})^{1/2}$ for the energy of the Δ -isobar, and

$$\Lambda_+^*(k) = \frac{1}{2E_k^*} (\gamma^0 E_k^* - \dot{\gamma} \cdot k + m^*) . \quad (\text{B.16})$$

For the derivation of the isospin factor $(2 + \frac{2}{3}\tau_1 \cdot \tau_2)$ see ref. [126]. Furthermore,

$$\begin{aligned}
& \frac{1}{D^{\text{it}}} = \sum_{j=1}^4 \frac{1}{D_j^{\text{it}}} , \\
& D_1^{\text{it}} = (E - E_{q'} - E_k - \omega_{q'-k}^\pi)(E - E_k - E_k^*)(E - E_q - E_k - \omega_{q-k}^\pi) , \\
& D_2^{\text{it}} = (E - E_{q'} - E_k^* - \omega_{q'-k}^\pi)(E - E_k - E_k^*)(E - E_q - E_k^* - \omega_{q-k}^\pi) , \\
& D_3^{\text{it}} = (E - E_{q'} - E_k^* - \omega_{q'-k}^\pi)(E - E_k - E_k^*)(E - E_q - E_k - \omega_{q-k}^\pi) , \\
& D_4^{\text{it}} = (E - E_{q'} - E_k - \omega_{q'-k}^\pi)(E - E_k - E_k^*)(E - E_q - E_k^* - \omega_{q-k}^\pi) .
\end{aligned} \tag{B.17}$$

Again the precise structure of the denominators is obtained by the general rule that, in each intermediate state, the involved energies have to be subtracted from the starting energy. In order to obtain the stretched-box diagrams (5 and 6 of fig. 20) one simply has to replace D^{II} by D^{s} where

$$\begin{aligned} \frac{1}{D^s} &= \frac{1}{D_1^s} + \frac{1}{D_2^s}, \\ D_1^s &= (E - E_{q'} - E_k^* - \omega_{q'-k}^\pi)(E - E_{q'} - E_q - \omega_{q'-k}^\pi - \omega_{q-k}^\pi)(E - E_q - E_k - \omega_{q-k}^\pi), \\ D_2^s &= (E - E_{q'} - E_k - \omega_{q'-k}^\pi)(E - E_{q'} - E_q - \omega_{q'-k}^\pi - \omega_{q-k}^\pi)(E - E_q - E_k^* - \omega_{q-k}^\pi). \end{aligned} \quad (\text{B.18})$$

For the crossed-box diagrams (diagrams 7–12 of fig. 20, see also fig. 23(b)) we get

$$\begin{aligned} \langle q' \lambda'_1 \lambda'_2 | M^c | q \lambda_1 \lambda_2 \rangle &= \frac{g_\pi^2}{(2\pi)^6} \frac{f_{N\Delta\pi}^2}{m_\pi^2} (2 - \frac{2}{3}\tau_1 \cdot \tau_2) \int d^3k \frac{1}{4\omega_{q'-k}^\pi \omega_{q-k}^\pi D^c} \\ &\times \bar{u}(q', \lambda'_1) i(q' - k)_i P_+^{ij}(k) i(q - k)_j u(q, \lambda_1) F_{N\Delta\pi}[(q' - k)^2] F_{N\Delta\pi}[(q - k)^2] \\ &\times \bar{u}(-q', \lambda'_2) i\gamma^5 \Lambda_+(k - q - q') i\gamma^5 u(-q, \lambda_2) F_{NN\pi}[(q' - k)^2] F_{NN\pi}[(q - k)^2], \end{aligned} \quad (\text{B.19})$$

with

$$\frac{1}{D^c} = \sum_{j=1}^6 \frac{1}{D_j^c},$$

$$\begin{aligned} D_1^c &= (E - E_{q'} - E_k^* - \omega_{q'-k}^\pi)(E - E_{k-q-q'} - E_k^* - \omega_{q'-k}^\pi - \omega_{q-k}^\pi)(E - E_q - E_k^* - \omega_{q-k}^\pi), \\ D_2^c &= (E - E_{k-q-q'} - E_{q'} - \omega_{q-k}^\pi)(E - E_k^* - E_{k-q-q'} - \omega_{q'-k}^\pi - \omega_{q-k}^\pi) \\ &\times (E - E_{k-q-q'} - E_q - \omega_{q'-k}^\pi), \\ D_3^c &= (E - E_{k-q-q'} - E_{q'} - \omega_{q'-k}^\pi)(E - E_k^* - E_{k-q-q'} - \omega_{q'-k}^\pi - \omega_{q-k}^\pi)(E - E_k^* - E_q - \omega_{q-k}^\pi), \\ D_4^c &= (E - E_k^* - E_{q'} - \omega_{q'-k}^\pi)(E - E_k^* - E_{k-q-q'} - \omega_{q'-k}^\pi - \omega_{q-k}^\pi)(E - E_q - E_{k-q-q'} - \omega_{q'-k}^\pi), \\ D_5^c &= (E - E_{q'} - E_{k-q-q'} - \omega_{q-k}^\pi)(E - E_{q'} - E_q - \omega_{q'-k}^\pi - \omega_{q-k}^\pi)(E - E_q - E_k^* - \omega_{q-k}^\pi), \\ D_6^c &= (E - E_{q'} - E_k^* - \omega_{q'-k}^\pi)(E - E_{q'} - E_q - \omega_{q'-k}^\pi - \omega_{q-k}^\pi)(E - E_q - E_{k-q-q'} - \omega_{q'-k}^\pi). \end{aligned} \quad (\text{B.20})$$

Based on the vertex functions, eqs. (B.4), (B.5), it is straightforward to write down the corresponding expressions for all the other diagrams considered in this paper. The evaluation of these expressions is, however, quite involved. Therefore, we refer the interested reader to the literature for further details. For the diagrams of 2π -exchange see refs. [70, 72–74]. The πp contributions can be found in refs. [71] and [75] (the latter reference contains also the noniterative $\pi\sigma$ and $\pi\omega$ diagrams).

For the noniterative πp diagrams with one or two Δ -isobars in the intermediate states, the evaluation of which is extremely involved (see ref. [76]), we use an approximation. This approximation is suggested by the special isospin structure of box and crossed-box diagrams. Namely, for $N\Delta$ processes, the sum of all time orderings is given by

$$A_{N\Delta} = (2 + \frac{2}{3}\tau_1 \cdot \tau_2)B_{N\Delta} + (2 - \frac{2}{3}\tau_1 \cdot \tau_2)C_{N\Delta}. \quad (\text{B.21})$$

Here, $(2 + \frac{2}{3}\tau_1 \cdot \tau_2)B_{N\Delta}$ denotes the contribution from all box diagrams (1–6 of fig. 20), whereas $(2 - \frac{2}{3}\tau_1 \cdot \tau_2)C_{N\Delta}$ stands for the contribution of all crossed-box contributions (7–12 of fig. 20). Equation (B.21) can be rewritten as

$$A_{N\Delta} = 2(B_{N\Delta} + C_{N\Delta}) + \frac{2}{3}\tau_1 \cdot \tau_2(B_{N\Delta} - C_{N\Delta}). \quad (\text{B.22})$$

Assuming $B_{N\Delta} \approx C_{N\Delta}$, one obtains

$$A_{N\Delta} \approx 4B_{N\Delta}, \quad (\text{B.23})$$

$B_{N\Delta}$ consists of the four iterative diagrams (1–4 of fig. 20), which can be calculated easily with the help of transition potentials (see ref. [71]), furthermore, two stretched-box diagrams (5–6 of fig. 20) are contained in $B_{N\Delta}$. The evaluation of these stretched-box diagrams is as involved as for the crossed-box diagrams. Since, however, these are known to be small compared to the iterative diagrams, we are ultimately led to the approximation

$$A_{N\Delta} \approx 4B'_{N\Delta}, \quad (\text{B.24})$$

where $B'_{N\Delta}$ denotes the contribution from the iterative box diagrams only. Thus, eq. (B.24) replaces the exact result by twice the isoscalar part of the iterative contributions. The quality of this approximation has been found to be very good for isospin $T = 1$ NN states, whereas it seems to overestimate the contributions in isospin $T = 0$ states [76]. It turned out that this overestimation is extremely strong in the ${}^3(\text{SD})_1$ states. Since the unapproximated result is quite small in this partial wave [76], we drop the contribution due to eq. (B.24) in the ${}^3(\text{SD})_1$ states.

The noniterative πp contributions with $\Delta\Delta$ intermediate states are treated in analogy to the $N\Delta$ case just discussed. We have in obvious notation:

$$A_{\Delta\Delta} = \left(\frac{4}{3} - \frac{2}{9}\boldsymbol{\tau}_1 \cdot \boldsymbol{\tau}_2 \right) B_{\Delta\Delta} + \left(\frac{4}{3} + \frac{2}{9}\boldsymbol{\tau}_1 \cdot \boldsymbol{\tau} \right) C_{\Delta\Delta}, \quad (\text{B.25})$$

leading to

$$A_{\Delta\Delta} \approx \frac{8}{3}B'_{\Delta\Delta}. \quad (\text{B.26})$$

The fourth-order contributions of 2π - and $\pi\rho$ -exchange, which are derived in part in this appendix and discussed with regard to their mathematical structure, allow for a quantitative description of the NN data when complemented by OBE. Such a model is discussed in section 6. The parameters of this model are given here in table 9. Note that this is not our final “full model” of sections 7 and 8.

Table 9
Meson and low-energy parameters (LEP) of a model discussed in section 6

	$g_a^2/4\pi; [f_a/g_a]$ resp. $f_a^2/4\pi$	m_a	Λ_a	n_a	LEP	Theory
NN π	14.4	138.03	1.5	1	ϵ_a (MeV)	2.2245
NN ρ	0.84; [6.1]	769	1.4	1	P_D (%)	4.17
NN ω	20; [0.0]	782.6	1.5	1	Q_d (fm 2)	0.276
NN δ	2.6653	983	2.0	1	D/S	0.0262
NN σ'	5.723	550	1.9	1	a_s (fm)	-23.749
					r_s (fm)	2.798
N $\Delta\pi$	0.224	138.03	1.1	1	a_t (fm)	5.436
N $\Delta\rho$	20.45	769	1.4	2	r_t (fm)	1.768

For notation and experimental data see tables 3 and 4.

Appendix C: NN scattering

C.1. The R-matrix equation

For the evaluation of NN scattering phase shifts it is convenient to work with the R -matrix*, which is related to the T -matrix, eq. (A.7), by

$$T(E) = R(E) - i\pi R(E) \delta(E - h_0^{(N)}) T(E). \quad (\text{C.1})$$

Thus, for $R(E)$ we obtain from eq. (A.7)

$$R(E) = V(E) + V(E) \frac{\mathcal{P}}{E - h_0^{(N)}} R(E), \quad (\text{C.2})$$

where \mathcal{P} denotes the principal value to be applied when the integration over the continuous spectrum of $h_0^{(N)}$ is carried out.

As meson-exchange contributions to $V(E)$ are most conveniently represented in the helicity formalism, we will consider eq. (C.2) in a plane wave helicity state basis in the two-nucleon c.m. system. (We closely follow the presentation given in ref. [51].)

$$\begin{aligned} \langle q'\lambda'_1\lambda'_2 | R(E) | q\lambda_1\lambda_2 \rangle &= \langle q'\lambda'_1\lambda'_2 | V(E) | q\lambda_1\lambda_2 \rangle \\ &\quad + \sum_{h_1,h_2} \mathcal{P} \int \frac{d^3k}{E - 2E_k} \langle q'\lambda'_1\lambda'_2 | V(E) | kh_1h_2 \rangle \langle kh_1h_2 | R(E) | q\lambda_1\lambda_2 \rangle. \end{aligned} \quad (\text{C.3})$$

Here, q , q' and k are the relative momenta for the initial, final and intermediate states, respectively; λ_i , λ'_i , and h_i ($i = 1, 2$) denote the corresponding helicities for nucleon 1 and 2. For example, for nucleon 1 in the initial state the helicity λ_1 is defined as the eigenvalue of the helicity operator $(\frac{1}{2}\sigma_1 \cdot q)/|q|$, with $\frac{1}{2}\sigma_1$ the spin operator for nucleon 1; the eigenvalues are $\pm\frac{1}{2}$. The summation in eq. (C.3) extends over positive energy intermediate-state helicities, $h_i = \pm\frac{1}{2}$. $E_k = \sqrt{m^2 + k^2}$ and m denotes the nucleon mass. Part of the notation is displayed in fig. 22.

As phase shifts are only defined in terms of partial waves, it is desirable to have eq. (C.3) in partial wave decomposition.

Introducing the two-nucleon state basis $|JM\lambda_1\lambda_2\rangle$, with J the total angular momentum and M its z-component, and assuming rotational invariance, we have the following expansion for $R(E)$:

$$\langle q'\lambda'_1\lambda'_2 | R(E) | q\lambda_1\lambda_2 \rangle = \sum_{JM} \langle \hat{q}'\lambda'_1\lambda'_2 | JM\lambda_1\lambda_2 \rangle \langle \lambda'_1\lambda'_2 | R'(q', q; E) | \lambda_1\lambda_2 \rangle \langle JM\lambda_1\lambda_2 | \hat{q}\lambda_1\lambda_2 \rangle, \quad (\text{C.4})$$

where $q \equiv |q|$, $q' \equiv |q'|$, $\hat{q} = q/q$ and $\hat{q}' = q'/q'$. An equivalent decomposition can be done for $V(E)$. The matrix elements of the transformation from a plane wave helicity basis to angular momentum helicity states are [147, 57]

$$\langle JM\lambda_1\lambda_2 | \hat{q}\lambda_1\lambda_2 \rangle = \left(\frac{2J+1}{4\pi}\right)^{1/2} D_{M\lambda}^{(J)}(\varphi, \vartheta, -\varphi) \delta_{\lambda_1,\lambda'_1} \delta_{\lambda_2,\lambda'_2}, \quad (\text{C.5})$$

* Also referred to as the K -matrix in the literature (see e.g. ref. [146]).

where ϑ and φ are polar and azimuthal angles defining the direction of q with respect to the z -axis; $D_{MM}^{(J)}$ is the conventional irreducible rotation matrix and $\lambda = \lambda_1 - \lambda_2$. These matrix elements satisfy the normalization condition

$$\int d\Omega \langle JM\lambda_1\lambda_2 | \hat{q}\lambda_1\lambda_2 \rangle \langle \hat{q}\lambda_1\lambda_2 | J'M'\lambda_1\lambda_2 \rangle = \delta_{JJ'}\delta_{MM'} , \quad (\text{C.6})$$

with $d\Omega = d\cos\vartheta d\varphi$. With the help of eqs. (C.4) and (C.6) we can derive now the desired partial wave decomposition of eq. (C.3)

$$\begin{aligned} \langle \lambda'_1\lambda'_2 | R^J(q', q; E) | \lambda_1\lambda_2 \rangle &= \langle \lambda'_1\lambda'_2 | V^J(q', q; E) | \lambda_1\lambda_2 \rangle \\ &\quad + \sum_{h_1, h_2} P \int_0^\infty \frac{dk k^2}{E - 2E_k} \langle \lambda'_1\lambda'_2 | V^J(q', k; E) | h_1 h_2 \rangle \\ &\quad \times \langle h_1 h_2 | R^J(k, q; E) | \lambda_1\lambda_2 \rangle . \end{aligned} \quad (\text{C.7})$$

As, for simplicity, we neglected the isospin dependence so far, we mention now that, assuming charge independence, there are two separate equations for isospin $T=0$ and $T=1$. Equation (C.7) represents a coupled system of integral equations to be solved for R^J .

The solution of eq. (C.7) is considerably facilitated by the following considerations. As there are two eigenvalues for each helicity, there are in general 16 helicity amplitudes $\langle \lambda'_1\lambda'_2 | R^J(q', q; E) | \lambda_1\lambda_2 \rangle$ which are coupled. Fortunately, only six are independent. This is due to the special invariance properties of the NN interaction. Namely, parity conservation (invariance with regard to space reflections) implies

$$\langle \lambda'_1\lambda'_2 | R^J(q', q; E) | \lambda_1\lambda_2 \rangle = \langle -\lambda'_1, -\lambda'_2 | R^J(q', q; E) | -\lambda_1, -\lambda_2 \rangle . \quad (\text{C.8})$$

Conservation of total spin (which is a consequence of isospin and parity conservation in conjunction with the antisymmetry requirement for two-nucleon states) leads to

$$\langle \lambda'_1\lambda'_2 | R^J(q', q; E) | \lambda_1\lambda_2 \rangle = \langle \lambda'_2\lambda'_1 | R^J(q', q; E) | \lambda_2\lambda_1 \rangle . \quad (\text{C.9})$$

For the six independent amplitudes we choose the following set [51]:

$$\begin{aligned} R_1^J(q', q; E) &\equiv \langle ++ | R^J(q', q; E) | ++ \rangle , & R_2^J(q', q; E) &\equiv \langle ++ | R^J(q', q; E) | -- \rangle , \\ R_3^J(q', q; E) &\equiv \langle +- | R^J(q', q; E) | +- \rangle , & R_4^J(q', q; E) &\equiv \langle +- | R^J(q', q; E) | -+ \rangle , \\ R_5^J(q', q; E) &\equiv \langle ++ | R^J(q', q; E) | +- \rangle , & R_6^J(q', q; E) &\equiv \langle +- | R^J(q', q; E) | ++ \rangle , \end{aligned} \quad (\text{C.10})$$

where $\lambda_i = \pm \frac{1}{2}$ is denoted by \pm . Note that time-reversal implies

$$R_5^J(q', q) = R_6^J(q, q') . \quad (\text{C.11})$$

To further simplify the on-coming calculations and, in fact, to partly decouple eq. (C.7), we introduce the following linear combinations of helicity amplitudes:

$$\begin{aligned} {}^0R^J &\equiv R_1^J - R_2^J, & {}^1R^J &\equiv R_3^J - R_4^J, & {}^{12}R^J &\equiv R_1^J + R_2^J, \\ {}^{34}R^J &\equiv R_3^J + R_4^J, & {}^{55}R^J &\equiv 2R_5^J, & {}^{66}R^J &\equiv 2R_6^J, \end{aligned} \quad (\text{C.12})$$

where the usual arguments have been suppressed. Note that ${}^0R^J$ and ${}^1R^J$ are identical to the spin singlet and uncoupled spin triplet matrix elements, respectively, of the conventional LSJ representation. For V^J we introduce the analogous definitions*. With these definitions we obtain now for eq. (C.7) the following set of integral equations

$${}^0R^J(q', q; E) = {}^0V^J(q', q; E) + P \int_0^\infty \frac{dk k^2}{E - 2E_k} {}^0V^J(q', k; E) {}^0R^J(k, q; E), \quad (\text{C.13a})$$

$${}^1R^J(q', q; E) = {}^1V^J(q', q; E) + P \int_0^\infty \frac{dk k^2}{E - 2E_k} {}^1V^J(q', k; E) {}^1R^J(k, q; E), \quad (\text{C.13b})$$

$$\begin{aligned} {}^{12}R^J(q', q; E) &= {}^{12}V^J(q', q; E) + P \int_0^\infty \frac{dk k^2}{E - 2E_k} [{}^{12}V^J(q', k; E) {}^{12}R^J(k, q; E) \\ &\quad + {}^{55}V^J(q', k; E) {}^{66}R^J(k, q; E)], \\ {}^{34}R^J(q', q; E) &= {}^{34}V^J(q', q; E) + P \int_0^\infty \frac{dk k^2}{E - 2E_k} [{}^{34}V^J(q', k; E) {}^{34}R^J(k, q; E) \\ &\quad + {}^{66}V^J(q', k; E) {}^{55}R^J(k, q; E)], \end{aligned} \quad (\text{C.13c})$$

$$\begin{aligned} {}^{55}R^J(q', q; E) &= {}^{55}V^J(q', q; E) + P \int_0^\infty \frac{dk k^2}{E - 2E_k} [{}^{12}V^J(q', k; E) {}^{55}R^J(k, q; E) \\ &\quad + {}^{55}V^J(q', k; E) {}^{34}R^J(k, q; E)], \end{aligned}$$

$$\begin{aligned} {}^{66}R^J(q', q; E) &= {}^{66}V^J(q', q; E) + P \int_0^\infty \frac{dk k^2}{E - 2E_k} [{}^{34}V^J(q', k; E) {}^{66}R^J(k, q; E) \\ &\quad + {}^{66}V^J(q', k; E) {}^{12}R^J(k, q; E)]. \end{aligned}$$

Note that only the four equations (C.13c) are coupled. The solution of eq. (C.13) is most conveniently done by the matrix inversion method [67, 148].

2.2. The phase-shift relations

The on-shell R -matrix elements are related to the Blatt-Biedenharn [149] phase shifts as follows. Spin singlet states ($L = J$)

* How to obtain the meson-exchange contributions in the representation used here for R and V is shown explicitly in appendix E.

$$\operatorname{tg}^0 \delta^J(E_{\text{lab}}) = -\frac{1}{2} \pi q E_q^0 R^J(q, q; E). \quad (\text{C.14a})$$

Uncoupled spin triplet states ($L = J$)

$$\operatorname{tg}^1 \delta^J(E_{\text{lab}}) = -\frac{1}{2} \pi q E_q^1 R^J(q, q; E). \quad (\text{C.14b})$$

Coupled states

$$\begin{aligned} \operatorname{tg} \delta_{\mp}^J(E_{\text{lab}}) &= -\frac{1}{4} \pi q E_q \left[{}^{12}R^J + {}^{34}R^J \mp \frac{{}^{12}R^J - {}^{34}R^J - 4\sqrt{J(J+1)} {}^{55}R^J}{(2J+1) \cos 2\varepsilon_J} \right], \\ \operatorname{tg} 2\varepsilon_J(E_{\text{lab}}) &= -2 \frac{\sqrt{J(J+1)}({}^{12}R^J - {}^{34}R^J) + {}^{55}R^J}{{}^{12}R^J - {}^{34}R^J - 4\sqrt{J(J+1)} {}^{55}R^J}, \end{aligned} \quad (\text{C.14c})$$

where in eq. (C.14c) the on-shell arguments ($q, q; E$) have been suppressed for the R -matrix elements, and the lower index \mp stands for $L = J \mp 1$. Note that the on-shell momentum in the c.m. system, q , is related to the laboratory energy, E_{lab} , by

$$E_{\text{lab}} = 2q^2/m. \quad (\text{C.15})$$

For the energy of the initial state in the c.m. system, E , we have

$$E = 2E_q, \quad (\text{C.16})$$

with $E_q = \sqrt{m^2 + q^2}$. (We use units such that $\hbar = c = 1$; conversion factor: $\hbar c = 197.3286 \text{ MeV}\cdot\text{fm}$.)^{*} For all phase shifts published in this work we use the so-called bar convention introduced by Stapp et al. [97]. These are related to the Blatt–Biedenharn phase shifts by

$$\bar{\delta}_+^J + \bar{\delta}_-^J = \delta_+^J + \delta_-^J, \quad \sin(\bar{\delta}_-^J - \bar{\delta}_+^J) = \operatorname{tg} 2\bar{\varepsilon}_J / \operatorname{tg} 2\varepsilon_J, \quad \sin(\delta_-^J - \delta_+^J) = \sin 2\bar{\varepsilon}_J / \sin 2\varepsilon_J. \quad (\text{C.17})$$

C.3. Relating to LSJ basis

Work in nuclear physics uses prevailingly a $|JMLS\rangle$ basis for two-nucleon states, with L the orbital angular momentum and S the total spin. The matrix elements for the transformation from this conventional basis to the $|JM\lambda_1\lambda_2\rangle$ basis, which we use here, are [147, 57]

$$\langle JMLS | JM\lambda_1\lambda_2 \rangle = \left(\frac{2L+1}{2J+1} \right)^{1/2} \langle LS0\lambda | J\lambda \rangle \langle \frac{11}{22}, \lambda_1, -\lambda_2 | S\lambda \rangle, \quad (\text{C.18})$$

with $\lambda = \lambda_1 - \lambda_2$ (for the Clebsch–Gordon coefficients we use the notation of Messiah [150], i.e. $\langle j_1 j_2 m_1 m_2 | j_1 j_2 JM \rangle = \langle j_1 j_2 m_1 m_2 | JM \rangle$).

^{*} For practical calculations we recommend to use units of MeV for energies, masses and momenta.

The formal transformation of $R(E)$ is

$$\begin{aligned} \langle JML'S|R(q', q; E)|JMLS\rangle &= \sum_{\lambda_1\lambda_2\lambda'_1\lambda'_2} \langle JML'S|JML\lambda'_1\lambda'_2\rangle \langle \lambda'_1\lambda'_2|R^J(q', q; E)|\lambda_1\lambda_2\rangle \\ &\times \langle JML\lambda_1\lambda_2|JMLS\rangle. \end{aligned} \quad (\text{C.19})$$

Note that due to rotational invariance $R(E)$ does not depend on M . Defining the R -matrix elements in LJS basis by

$$i^{L'-L} R_{L'L}^{JS}(q', q; E) \equiv \langle JML'S|R(q', q; E)|JMLS\rangle, \quad (\text{C.20})$$

and applying eqs. (C.18) and (C.19) we obtain for the cases of particular interest:
spin singlet

$$R_{J,J}^{J0} = {}^0R^J \quad (\text{C.21a})$$

uncoupled spin triplet

$$R_{J,J}^{J1} = {}^1R^J \quad (\text{C.21b})$$

coupled states

$$\begin{aligned} R_{J-1,J-1}^{J1} &= \frac{1}{2J+1} [J^{12}R^J + (J+1)^{34}R^J + \sqrt{J(J+1)} {}^aR^J], \\ R_{J+1,J+1}^{J1} &= \frac{1}{2J+1} [(J+1)^{12}R^J + J^{34}R^J - \sqrt{J(J+1)} {}^aR^J], \\ R_{J-1,J+1}^{J1} &= \frac{1}{2J+1} [\sqrt{J(J+1)} {}^bR^J - J^{55}R^J + (J+1)^{66}R^J], \\ R_{J+1,J-1}^{J1} &= \frac{1}{2J+1} [\sqrt{J(J+1)} {}^bR^J + (J+1)^{55}R^J - J^{66}R^J], \end{aligned} \quad (\text{C.21c})$$

where we use the abbreviation

$${}^aR^J \equiv {}^{55}R^J + {}^{66}R^J, \quad {}^bR^J \equiv {}^{12}R^J - {}^{34}R^J.$$

The arguments of $R(q', q; E)$ are suppressed in eq. (C.21).

For the coupled states the (real, on-shell) R -matrix elements are conventionally parametrized in terms of Blatt–Biedenharn [149] phase shifts δ'_+ , δ'_- and the mixing parameter ε_J . This is achieved with the help of a unitary transformation U .

$$U \begin{pmatrix} R_{J-1,J-1}^J & R_{J-1,J+1}^J \\ R_{J+1,J-1}^J & R_{J+1,J+1}^J \end{pmatrix} U^T = \begin{pmatrix} R'_- & 0 \\ 0 & R'_+ \end{pmatrix}, \quad (\text{C.22})$$

with

$$U = \begin{pmatrix} \cos \varepsilon_j & \sin \varepsilon_j \\ -\sin \varepsilon_j & \cos \varepsilon_j \end{pmatrix}. \quad (\text{C.23})$$

The diagonal R -matrix elements obtained in eq. (C.22) are related to the phase shifts by

$$\operatorname{tg} \delta_{\mp}^J = -\frac{1}{2} \pi q E_q R_{\mp}^J. \quad (\text{C.24})$$

From eqs. (C.22)–(C.24) one derives the phase shifts in terms of the R -matrix in conventional LSJ basis (compare e.g. refs. [67] and [148]).

$$\begin{aligned} \operatorname{tg} \delta_{\mp}^J &= -\frac{\pi}{4} q E_q \left[R_{J-1,J-1}^J + R_{J+1,J+1}^J \pm \frac{R_{J-1,J-1}^J - R_{J+1,J+1}^J}{\cos 2\varepsilon_J} \right], \\ \operatorname{tg} 2\varepsilon_J &= \frac{2R_{J+1,J-1}^J}{R_{J-1,J-1}^J - R_{J+1,J+1}^J}. \end{aligned} \quad (\text{C.25})$$

Our phase shift relations, eq. (C.14), are obtained by applying the transformation, eq. (C.21) to eq. (C.25).

Appendix D: The deuteron

D.1. The deuteron equation

In order to derive the equation for the deuteron bound state, we make use of the fact that $V(E)$ is related to effective potentials introduced in the Bloch–Horowitz scheme [151]. The total Hilbert space of nucleon, isobar and meson states, \mathcal{H} , is first decomposed into two subspaces: the nucleonic Fock space \mathcal{H}_N and the rest \mathcal{H}_R ; $\mathcal{H} = \mathcal{H}_N + \mathcal{H}_R$. We introduce projection operators:

$$P: \mathcal{H} \rightarrow \mathcal{H}_N, \quad Q: \mathcal{H} \rightarrow \mathcal{H}_R, \quad \text{with} \quad P = 1 - Q. \quad (\text{D.1})$$

H is the Hamiltonian of the system under consideration with

$$H: \mathcal{H} \rightarrow \mathcal{H}, \quad \text{and} \quad H\phi = E\phi. \quad (\text{D.2})$$

In the next step we define an effective operator

$$H_{\text{eff}}(E)P\phi = EP\phi \quad (\text{D.3})$$

by

$$H_{\text{eff}}(E) = PHP + PHQ \frac{1}{E - QHQ} QHP. \quad (\text{D.4})$$

Setting $H = H_0 + W$ ($[H_0, P] = 0$) we may expand the denominator of eq. (D.4) in terms of W . This

expansion for $H_{\text{eff}}(E)$ can be represented by a set of diagrams which, for the two-nucleon problem, are precisely the irreducible diagrams represented by $V(E)$ and occurring in the expansion for the scattering amplitude $T(E)$, i.e.,

$$H_{\text{eff}}(E) = H_0 + V(E). \quad (\text{D.5})$$

The Schrödinger equation

$$H_{\text{eff}}(E)\psi = E\psi \quad (\text{D.6})$$

(with $\psi \equiv P\phi$) is for unbound states equivalent to the scattering equation (A.7). For bound states it yields the eigenvalue equation for the deuteron with $E = E_d = 2m - \varepsilon_d$ where ε_d is the binding energy of the deuteron and m the nucleon mass. It reads explicitly, in a helicity-state basis

$$\langle q\lambda_1\lambda_2 | \psi \rangle = \frac{1}{E - 2E_q} \sum_{h_1, h_2} \int_0^\infty d^3k \langle q\lambda_1\lambda_2 | V(E) | kh_1h_2 \rangle \langle kh_1h_2 | \psi \rangle, \quad (\text{D.7})$$

with $E_q = \sqrt{m^2 + q^2}$. After a partial-wave decomposition (compare appendix C, eqs. (C.3)–(C.7)) we obtain

$$\psi^J(q, \lambda_1\lambda_2) = \frac{1}{E - 2E_q} \sum_{h_1, h_2} \int_0^\infty dk k^2 \langle \lambda_1\lambda_2 | V^J(q, k; E) | h_1h_2 \rangle \psi^J(k, h_1h_2), \quad (\text{D.8})$$

where we define $\psi^J(q, \lambda_1\lambda_2) \equiv \langle JM\lambda_1\lambda_2 | \psi(q) \rangle$. Similar to eq. (C.7) for the NN scattering problem, eq. (D.8) represents a coupled system of integral equations to be solved (numerically) for ψ^J . Proceeding in analogy to eqs. (C.7)–(C.13) of appendix C we deduce the following set of only partially coupled equations (cf. also ref. [51]):

$${}^0\psi^J(q) = \frac{1}{E - 2E_q} \int_0^\infty dk k^2 {}^0V^J(q, k; E) {}^0\psi^J(k), \quad (\text{D.9a})$$

$${}^1\psi^J(q) = \frac{1}{E - 2E_q} \int_0^\infty dk k^2 {}^1V^J(q, k; E) {}^1\psi^J(k), \quad (\text{D.9b})$$

$${}^{12}\psi^J(q) = \frac{1}{E - 2E_q} \int_0^\infty dk k^2 [{}^{12}V^J(q, k; E) {}^{12}\psi^J(k) + {}^{55}V^J(q, k; E) {}^{34}\psi^J(k)], \quad (\text{D.9c})$$

$${}^{34}\psi^J(q) = \frac{1}{E - 2E_q} \int_0^\infty dk k^2 [{}^{66}V^J(q, k; E) {}^{12}\psi^J(q, k) + {}^{34}V^J(q, k; E) {}^{34}\psi^J(k)],$$

where for $V^J(E)$ we apply the notation introduced in eqs. (C.10) and (C.12) and where for the wave functions we use the following definitions:

Spin singlet

$${}^0\psi^J(q) = \frac{1}{\sqrt{2}} [\psi^J(q, ++) - \psi^J(q, --)] . \quad (\text{D.10a})$$

Uncoupled spin triplet

$${}^1\psi^J(q) = -\frac{1}{\sqrt{2}} [\psi^J(q, +-) - \psi^J(q, -+)] . \quad (\text{D.10b})$$

Coupled triplet cases

$${}^{12}\psi^J(q) \equiv \psi^J(q, ++) + \psi^J(q, --) , \quad {}^{34}\psi^J(q) \equiv \psi^J(q, +-) + \psi^J(q, -+) . \quad (\text{D.10c})$$

The two coupled equations (D.9c) represent for $J = 1$ the deuteron problem. The two wave functions resulting from a solution can be represented in LSJ basis by

$$\psi_{J-1}^J(q) = \frac{i^{(-J+1)}}{[2(2J+1)]^{1/2}} [\sqrt{J} {}^{12}\psi^J(q) + \sqrt{J+1} {}^{34}\psi^J(q)] , \quad (\text{D.11a})$$

$$\psi_{J+1}^J(q) = \frac{i^{(-J-1)}}{[2(2J+1)]^{1/2}} [-\sqrt{J+1} {}^{12}\psi^J(q) + \sqrt{J} {}^{34}\psi^J(q)] , \quad (\text{D.11b})$$

where we used eq. (C.18) and the definition $i^L \psi_L^J(q) \equiv \langle JMLS | \psi(q) \rangle$. For the deuteron ($J = 1$) eq. (D.11a) represents the S-wave and eq. (D.11b) the D-wave.

D.2. Deuteron properties

In terms of the momentum space S- and D-waves from eq. (D.11), now denoted by $\psi_0(q)$ and $\psi_2(q)$, respectively, the deuteron properties are (note that throughout this work we use units such that $\hbar = c = 1$; conversion factor: $\hbar c = 197.3286 \text{ MeV} \cdot \text{fm}$):

Normalization

$$\int_0^\infty dq q^2 [(\psi_0(q))^2 + (\psi_2(q))^2] = 1 , \quad (\text{D.12})$$

D-state probability

$$P_D = \int_0^\infty dq q^2 (\psi_2(q))^2 . \quad (\text{D.13})$$

The probability for non (-pure) nucleonic components in the deuteron wave function, P_α , is evaluated by [152]

$$P_a = -\frac{\partial}{\partial E} \langle \psi_d | V(E) | \psi_d \rangle|_{E=E_d} = -\frac{\partial}{\partial E} e(E)|_{E=E_d}, \quad (\text{D.14})$$

with ψ_d the deuteron wave function, $E_d = 2m - \varepsilon_d$ and $e(E_d) = E_d$.

Magnetic moment

$$\mu_d = \mu_p + \mu_n - \frac{3}{2}[\mu_p + \mu_n - \frac{1}{2}]P_D, \quad (\text{D.15})$$

with

$$\mu_p = 2.79290, \quad \mu_n = -1.91315, \quad (\text{D.16})$$

the magnetic moments of proton and neutron, respectively, in units of nuclear magnetons [108].

The quadrupole moment operator for the deuteron is expressed in terms of the relative distance r between proton and neutron and its third component z

$$\hat{Q}_d = \frac{1}{4}(3z^2 - r^2) = \frac{1}{2}r^2 P_2(\cos \vartheta) = (\pi/5)^{1/2}r^2 Y_2^0(\vartheta, \varphi). \quad (\text{D.17})$$

Using the conventional configuration space wave functions one obtains

$$Q_d = \frac{1}{20} \int_0^\infty dr r^2 w(r)[\sqrt{8}u(r) - w(r)], \quad (\text{D.18})$$

with $u(r)$ and $w(r)$ the wave functions for $l=0$ and $l=2$, respectively, normalized according to

$$\int_0^\infty dr[(u(r))^2 + (w(r))^2] = 1. \quad (\text{D.19})$$

By Fourier transformation of the r -space wave functions and with the help of the spherical Bessel equation, Q_d is expressed in terms of the momentum space wave functions

$$Q_d = -\frac{1}{20} \int_0^\infty dq \left\{ \sqrt{8} \left[q^2 \frac{d\psi_0(q)}{dq} \frac{d\psi_2(q)}{dq} + 3q\psi_2(q) \frac{d\psi_0(q)}{dq} \right] + q^2 \left(\frac{d\psi_2(q)}{dq} \right)^2 + 6(\psi_2(q))^2 \right\}. \quad (\text{D.20})$$

To avoid ambiguities in formula (D.20) and in the following considerations, we have fixed the sign of the wave functions arbitrarily such that they are always positive for low momenta.

For some deuteron properties the r -space wave functions are required. Therefore we Fourier-transform $\psi_0(q)$ and $\psi_2(q)$ into r -space by performing the following numerical integration

$$\frac{\varphi_L(r)}{r} = \sqrt{\frac{2}{\pi}} \int_0^\infty q^2 dq j_L(qr) \psi_L(q), \quad (\text{D.21})$$

with j_L the spherical Bessel function, $L = 0$ or 2 and

$$\varphi_0(r) \equiv u(r), \quad \varphi_2(r) \equiv w(r).$$

The normalization is given in eq. (D.19). In terms of these configuration space wave functions the asymptotic S-state, A_s , is

$$u(r) \xrightarrow[r \rightarrow \infty]{} A_s e^{-\alpha r} \quad (\text{D.22})$$

and the asymptotic D/S state, η (denoted by D/S in our tables),

$$w(r) \xrightarrow[r \rightarrow \infty]{} \eta A_s \left(1 + \frac{3}{\alpha r} + \frac{3}{(\alpha r)^2}\right) e^{-\alpha r}, \quad (\text{D.23})$$

with $\alpha = (m \varepsilon_d)^{1/2} = 0.231609 \text{ fm}^{-1}$. The root-mean-square radius for the deuteron is

$$r_d = \left[\int_0^\infty dr r^2 ((u(r))^2 + (w(r))^2) \right]^{1/2}. \quad (\text{D.24})$$

D.3. The deuteron wave functions

D.3.1. The ansatz for the parametrization

In some applications it is useful to have the deuteron wave functions in analytic form. Therefore, we present a parametrization of the deuteron wave functions of our full model (section 8) as well as of the energy-independent OBEP (section 9.1). We use a discrete superposition of Yukawa-type functions, similar to ref. [153]. The ansatz for the analytic versions of the r -space wave functions, denoted by $u_a(r)$ and $w_a(r)$, is

$$u_a(r) = \sum_{j=1}^{n_u} C_j \exp(-m_j r), \quad w_a(r) = \sum_{j=1}^{n_w} D_j \exp(-m_j r) \left(1 + \frac{3}{m_j r} + \frac{3}{(m_j r)^2}\right). \quad (\text{D.25})$$

The normalization is given in eq. (D.19).

The corresponding momentum space wave functions are

$$\psi_0^a(q) = \left(\frac{2}{\pi}\right)^{1/2} \sum_{j=1}^{n_u} \frac{C_j}{q^2 + m_j^2}, \quad \psi_2^a(q) = \left(\frac{2}{\pi}\right)^{1/2} \sum_{j=1}^{n_w} \frac{D_j}{q^2 + m_j^2}, \quad (\text{D.26})$$

which is the analytic result of the Fourier integration

$$\sqrt{\frac{2}{\pi}} \int_0^\infty dr r j_L(qr) \varphi_L^a(r), \quad (\text{D.27})$$

with $\varphi_0^a(r) = u_a(r)$ and $\varphi_2^a(r) = w_a(r)$ for $L = 0$ and 2 , respectively. The momentum space wave functions eq. (D.26) are the analytic versions of eq. (D.11) with the normalization eq. (D.12). The

Table 10

Coordinate-space deuteron wave functions $u(r)$ and $w(r)$ obtained from our (energy-dependent) full model;
 $\int_0^\infty dr[u^2(r) + w^2(r)] = 1$

r (fm)	$u(r)$	$w(r)$	r (fm)	$u(r)$	$w(r)$
0.10000 - 01	0.16321 - 01	-0.47979 - 03	0.27000 + 01	0.46411 + 00	0.10571 + 00
0.20000 - 01	0.26634 - 01	-0.64419 - 03	0.28000 + 01	0.45556 + 00	0.10167 + 00
0.30000 - 01	0.37144 - 01	-0.81153 - 03	0.29000 + 01	0.44691 + 00	0.97690 - 01
0.40000 - 01	0.45513 - 01	-0.12124 - 02	0.30000 + 01	0.43820 + 00	0.93798 - 01
0.50000 - 01	0.52425 - 01	-0.17530 - 02	0.32000 + 01	0.42079 + 00	0.86330 - 01
0.60000 - 01	0.58495 - 01	-0.22129 - 02	0.34000 + 01	0.40358 + 00	0.79344 - 01
0.70000 - 01	0.63775 - 01	-0.26426 - 02	0.36000 + 01	0.38670 + 00	0.72867 - 01
0.80000 - 01	0.68237 - 01	-0.30763 - 02	0.38000 + 01	0.37024 + 00	0.66894 - 01
0.90000 - 01	0.71943 - 01	-0.35476 - 02	0.40000 + 01	0.35429 + 00	0.61417 - 01
0.10000 + 00	0.75085 - 01	-0.40330 - 02	0.42000 + 01	0.33887 + 00	0.56411 - 01
0.20000 + 00	0.92615 - 01	-0.71908 - 02	0.44000 + 01	0.32401 + 00	0.51836 - 01
0.30000 + 00	0.10844 + 00	-0.50743 - 02	0.46000 + 01	0.30970 + 00	0.47658 - 01
0.40000 + 00	0.13541 + 00	0.28432 - 02	0.48000 + 01	0.29597 + 00	0.43853 - 01
0.50000 + 00	0.17394 + 00	0.15617 - 01	0.50000 + 01	0.28282 + 00	0.40389 - 01
0.60000 + 00	0.22117 + 00	0.31737 - 01	0.52000 + 01	0.27020 + 00	0.37228 - 01
0.70000 + 00	0.27189 + 00	0.49471 - 01	0.54000 + 01	0.25811 + 00	0.34339 - 01
0.80000 + 00	0.32159 + 00	0.67297 - 01	0.56000 + 01	0.24654 + 00	0.31707 - 01
0.90000 + 00	0.36694 + 00	0.83924 - 01	0.58000 + 01	0.23548 + 00	0.29311 - 01
0.10000 + 01	0.40633 + 00	0.98583 - 01	0.60000 + 01	0.22490 + 00	0.27120 - 01
0.11000 + 01	0.43907 + 00	0.11083 + 00	0.65000 + 01	0.20043 + 00	0.22410 - 01
0.12000 + 01	0.46521 + 00	0.12056 + 00	0.70000 + 01	0.17859 + 00	0.18635 - 01
0.13000 + 01	0.48526 + 00	0.12787 + 00	0.75000 + 01	0.15910 + 00	0.15565 - 01
0.14000 + 01	0.49983 + 00	0.13296 + 00	0.80000 + 01	0.14174 + 00	0.13077 - 01
0.15000 + 01	0.50967 + 00	0.13611 + 00	0.85000 + 01	0.12626 + 00	0.11028 - 01
0.16000 + 01	0.51560 + 00	0.13760 + 00	0.90000 + 01	0.11247 + 00	0.93422 - 02
0.17000 + 01	0.51834 + 00	0.13772 + 00	0.95000 + 01	0.10018 + 00	0.79457 - 02
0.18000 + 01	0.51851 + 00	0.13671 + 00	0.10000 + 02	0.89232 - 01	0.67748 - 02
0.19000 + 01	0.51660 + 00	0.13481 + 00	0.10500 + 02	0.79478 - 01	0.58021 - 02
0.20000 + 01	0.51305 + 00	0.13222 + 00	0.11000 + 02	0.70792 - 01	0.49785 - 02
0.21000 + 01	0.50821 + 00	0.12911 + 00	0.11500 + 02	0.63055 - 01	0.42813 - 02
0.22000 + 01	0.50235 + 00	0.12562 + 00	0.12000 + 02	0.56158 - 01	0.36950 - 02
0.23000 + 01	0.49569 + 00	0.12185 + 00	0.12500 + 02	0.50020 - 01	0.31932 - 02
0.24000 + 01	0.48340 + 00	0.11791 + 00	0.13000 + 02	0.44553 - 01	0.27623 - 02
0.25000 + 01	0.48062 + 00	0.11387 + 00	0.13500 + 02	0.39679 - 01	0.23981 - 02
0.26000 + 01	0.47249 + 00	0.10979 + 00	0.14000 + 02	0.35339 - 01	0.20841 - 02

Data files for these wave functions in r - as well as in q -space are available from the authors.

Table 11

Coefficients for the parametrized deuteron wave functions of the (energy-dependent) full model. The last C_j and the last three D_j are to be computed from eq. (D.28) ($n_u = n_w = 11$)

C_j (fm $^{-1/2}$)	D_j (fm $^{-1/2}$)
0.90457337 + 00	0.24133026 - 01
-0.35058661 + 00	-0.64430531 + 00
-0.17635927 + 00	0.51093352 + 00
-0.10418261 + 02	-0.54419065 + 01
0.45089439 + 02	0.15872034 + 02
-0.14861947 + 03	-0.14742981 + 02
0.31779642 + 03	0.44956539 + 01
-0.37496518 + 03	-0.71152863 - 01
0.22560032 + 03	eq. (D.28)
-0.54858290 + 02	eq. (D.28)
eq. (D.28)	eq. (D.28)

boundary conditions $u_a(r) \rightarrow r$ and $w_a(r) \rightarrow r^3$ as $r \rightarrow 0$ lead to one constraint for C_j and three constraints for D_j , namely

$$C_{n_w} = - \sum_{j=1}^{n_w-1} C_j ,$$

$$D_{n_w-2} = \frac{m_{n_w-2}^2}{(m_{n_w}^2 - m_{n_w-2}^2)(m_{n_w-1}^2 - m_{n_w-2}^2)} \left(-m_{n_w-1}^2 m_{n_w}^2 \sum_{j=1}^{n_w-3} \frac{D_j}{m_j^2} \right.$$

$$\left. + (m_{n_w-1}^2 + m_{n_w}^2) \sum_{j=1}^{n_w-3} D_j - \sum_{j=1}^{n_w-3} D_j m_j^2 \right) , \quad (\text{D.28})$$

Table 12
Coordinate-space deuteron wave functions $u(r)$ and $w(r)$ obtained from the (energy-independent) relativistic momentum space OBEPQ (see section 9.1); $\int_0^\infty dr [u^2(r) + w^2(r)] = 1$

r (fm)	$u(r)$	$w(r)$	r (fm)	$u(r)$	$w(r)$
0.10000 - 01	0.28698 - 02	0.76083 - 05	0.27000 + 01	0.45772 + 00	0.10780 + 00
0.20000 - 01	0.57125 - 02	0.36385 - 04	0.28000 + 01	0.44902 + 00	0.10331 + 00
0.30000 - 01	0.85499 - 02	0.42535 - 04	0.29000 + 01	0.44026 + 00	0.98942 - 01
0.40000 - 01	0.11414 - 01	-0.40792 - 05	0.30000 + 01	0.43148 + 00	0.94715 - 01
0.50000 - 01	0.14295 - 01	-0.50366 - 04	0.32000 + 01	0.41401 + 00	0.86710 - 01
0.60000 - 01	0.17162 - 01	-0.42507 - 04	0.34000 + 01	0.39682 + 00	0.79302 - 01
0.70000 - 01	0.20020 - 01	-0.10325 - 04	0.36000 + 01	0.38002 + 00	0.72515 - 01
0.80000 - 01	0.22890 - 01	-0.76468 - 05	0.38000 + 01	0.36370 + 00	0.66333 - 01
0.90000 - 01	0.25778 - 01	-0.33183 - 04	0.40000 + 01	0.34792 + 00	0.60700 - 01
0.10000 + 00	0.28679 - 01	-0.59642 - 05	0.42000 + 01	0.33268 + 00	0.55581 - 01
0.20000 + 00	0.58968 - 01	-0.50538 - 03	0.44000 + 01	0.31802 + 00	0.50942 - 01
0.30000 + 00	0.94182 - 01	-0.13195 - 02	0.46000 + 01	0.30393 + 00	0.46735 - 01
0.40000 + 00	0.13752 + 00	-0.14398 - 02	0.48000 + 01	0.29042 + 00	0.42917 - 01
0.50000 + 00	0.18942 + 00	0.14858 - 02	0.50000 + 01	0.27746 + 00	0.39448 - 01
0.60000 + 00	0.24647 + 00	0.10337 - 01	0.52000 + 01	0.26504 + 00	0.36302 - 01
0.70000 + 00	0.30335 + 00	0.26043 - 01	0.54000 + 01	0.25316 + 00	0.33446 - 01
0.80000 + 00	0.35552 + 00	0.46762 - 01	0.56000 + 01	0.24180 + 00	0.30848 - 01
0.90000 + 00	0.40042 + 00	0.69199 - 01	0.58000 + 01	0.23092 + 00	0.28478 - 01
0.10000 + 01	0.43751 + 00	0.90401 - 01	0.60000 + 01	0.22052 + 00	0.26317 - 01
0.11000 + 01	0.46591 + 00	0.10857 + 00	0.65000 + 01	0.19650 + 00	0.21716 - 01
0.12000 + 01	0.48747 + 00	0.12295 + 00	0.70000 + 01	0.17506 + 00	0.18019 - 01
0.13000 + 01	0.50286 + 00	0.13348 + 00	0.75000 + 01	0.15595 + 00	0.15046 - 01
0.14000 + 01	0.51313 + 00	0.14053 + 00	0.80000 + 01	0.13891 + 00	0.12621 - 01
0.15000 + 01	0.51919 + 00	0.14468 + 00	0.85000 + 01	0.12373 + 00	0.10645 - 01
0.16000 + 01	0.52190 + 00	0.14646 + 00	0.90000 + 01	0.11021 + 00	0.90087 - 02
0.17000 + 01	0.52194 + 00	0.14636 + 00	0.95000 + 01	0.98161 - 01	0.76615 - 02
0.18000 + 01	0.51988 + 00	0.14484 + 00	0.10000 + 02	0.87430 - 01	0.65320 - 02
0.19000 + 01	0.51614 + 00	0.14226 + 00	0.10500 + 02	0.77870 - 01	0.55910 - 02
0.20000 + 01	0.51111 + 00	0.13892 + 00	0.11000 + 02	0.69356 - 01	0.47980 - 02
0.21000 + 01	0.50508 + 00	0.15031 + 00	0.11500 + 02	0.61773 - 01	0.41263 - 02
0.22000 + 01	0.49826 + 00	0.13077 + 00	0.12000 + 02	0.55017 - 01	0.35606 - 02
0.23000 + 01	0.49085 + 00	0.12627 + 00	0.12500 + 02	0.49002 - 01	0.30758 - 02
0.24000 + 01	0.48298 + 00	0.12166 + 00	0.13000 + 02	0.43644 - 01	0.26628 - 02
0.25000 + 01	0.47477 + 00	0.11701 + 00	0.13500 + 02	0.38870 - 01	0.23112 - 02
0.26000 + 01	0.46633 + 00	0.11238 + 00	0.14000 + 02	0.34621 - 01	0.20065 - 02

Data files for these wave functions in r - as well as in q -space are available from the authors.

Table 13
Coefficients for the parametrized deuteron wave functions
of the (energy-independent) relativistic momentum space
OBEPQ. The last C_i and the last three D_j are to be
computed from eq. (D.28) ($n_u = n_w = 11$)

C_i (fm $^{-1/2}$)	D_j (fm $^{-1/2}$)
0.88628672 + 00	0.23237078 - 01
-0.27591814 + 00	-0.52115578 + 00
-0.11610727 + 00	-0.57197401 + 00
-0.12975243 + 02	0.27570246 + 01
0.77490155 + 02	-0.26157324 + 02
-0.27298039 + 03	0.84419883 + 02
0.53402693 + 03	-0.98308997 + 02
-0.56328069 + 03	0.38498490 + 02
0.30214616 + 03	eq. (D.28)
-0.64920925 + 02	eq. (D.28)
eq. (D.28)	eq. (D.28)

and two other relations deduced by circular permutation of $n_w - 2$, $n_w - 1$, n_w . The masses m_j are then chosen to be $m_j = \alpha + (j - 1)m_0$, with $m_0 = 0.9 \text{ fm}^{-1}$ and $\alpha = (m\epsilon_d)^{1/2} = 0.231609 \text{ fm}^{-1}$. This choice ensures the correct asymptotic behaviour. We use $n_u = n_w = 11$.

D.3.2. The wave functions for the full model

The r -space wave functions for our full (energy-dependent) model for the NN interaction (section 8) are tabulated in table 10. The coefficients of the parametrization defined in appendix D.3.1 are given in table 11. The accuracy of our parametrization is characterized by

$$I_S = \left(\int_0^\infty dr [u(r) - u_a(r)]^2 \right)^{1/2} = 9.5 \times 10^{-4}, \quad I_D = \left(\int_0^\infty dr [w(r) - w_a(r)]^2 \right)^{1/2} = 23.6 \times 10^{-4} \quad (\text{D.29})$$

This parametrization reproduces well the theoretical deuteron properties listed in table 3. Note that the wave function as given in tables 10 and 11 is normalized to unity. The probability for the non (-pure) nucleonic components is 3.79%. For some applications it may appear appropriate to “renormalize” the wave function accordingly. This is intimately related to the energy-dependence of the potential (see also footnote to table 3 and eq. (D.14)).

D.3.3. The wave functions for the energy-independent OBEPQ

Alternatively we list in table 12 the r -space wave functions from the (energy-independent) relativistic momentum space OBEPQ presented in section 9.1, with the deuteron properties given in table 6. The coefficients for the parametrization explained in appendix D.3.1 are presented in table 13. The accuracy is similar to eq. (D.29). The original deuteron properties predicted by this OBEP are well reproduced by the analytic wave functions. (Note that in this case we have $\alpha = (m\epsilon_\alpha)^{1/2} = 0.231607 \text{ fm}^{-1}$.)

Appendix E: Relativistic momentum space OBEP (OBEPQ)

The momentum space OBEP presented in this appendix will be constructed in the framework of the relativistic three-dimensional Blankenbecler–Sugar (BbS) [64] reduction of the Bethe–Salpeter (BS) [63] equation. First, we shall briefly sketch the scheme of that reduction (more can be found in refs. [51] and [154]) and then we will present the explicit momentum space expressions defining that potential.

E.1. The BbS equation

E.1.1. The derivation

The full BS equation may be written in operator form by

$$\hat{M} = \hat{V} + \hat{V}G\hat{M} \quad (\text{E.1})$$

with \hat{M} the invariant amplitude for the two-nucleon scattering process, \hat{V} the sum of all connected two-particle irreducible diagrams and G the relativistic two-nucleon propagator. Relativistic three-dimensional equations are typically derived by replacing eq. (E.1) by the following equivalent set of equations

$$\hat{M} = \hat{W} + \hat{W}g\hat{M}, \quad (\text{E.2a})$$

$$\hat{W} = \hat{V} + \hat{V}(G - g)\hat{W}, \quad (\text{E.2b})$$

where g is a covariant three-dimensional propagator. In general, the second term on the r.h.s. of eq. (E.2b) is left out to obtain a true simplification of the original equation (E.1). Many different choices for g have been proposed [154].

To demonstrate the BbS suggestion [64] more clearly we write out the BS equation (E.1) in the c.m. frame

$$\hat{M}(q'; q | P) = \hat{V}(q'; q | P) + \int d^4k \hat{V}(q'; k | P) G(k | P) \hat{M}(k; q | P), \quad (\text{E.3})$$

with

$$G(k | P) = \frac{i}{(2\pi)^4} \frac{1}{[\frac{1}{2}\not{P} + \not{k} - m + i\varepsilon]^{(1)} [\frac{1}{2}\not{P} - \not{k} - m + i\varepsilon]^{(2)}},$$

where q , k and q' are the initial, intermediate and final *relative* four-momenta, respectively, and P is the total four-momentum in the c.m. frame; $P = (\sqrt{s}, \mathbf{0})$ with \sqrt{s} the total energy. The superscripts refer to particle (1) and (2). The notation is as in Bjorken and Drell [145]. The *individual* four-momenta of the two particles in the c.m. frame are $\frac{1}{2}\not{P} \pm q$, $\frac{1}{2}\not{P} \pm k$ and $\frac{1}{2}\not{P} + q'$ for the initial, intermediate and final state, respectively. Note that \hat{V} and \hat{M} are 16×16 matrices in spinor space which, when sandwiched between Dirac spinors, give the corresponding matrix elements.

The BbS choice for the covariant three-dimensional propagator is

$$g(k, s) = \delta(k_0) \tilde{g}(k, s), \quad (\text{E.4a})$$

with

$$\tilde{g}(k, s) = \frac{1}{(2\pi)^3} \frac{m^2}{E_k} \frac{\Lambda_+^{(1)}(k)\Lambda_+^{(2)}(-k)}{\frac{1}{4}s - E_k^2 + i\epsilon}, \quad (\text{E.4b})$$

where $\Lambda_+^{(i)}$ ($i = 1, 2$) are the covariant positive energy projection operators for the two nucleons in intermediate states and $E_k \equiv \sqrt{m^2 + k^2}$. Replacing G in eq. (E.3) by the expression eq. (E.4a) we obtain the BbS equation

$$\hat{M}(0, q'; 0, q | \sqrt{s}) = \hat{V}(0, q'; 0, q) + \int d^3k \hat{V}(0, q'; 0, k) \tilde{g}(k, s) \hat{M}(0, k; 0, q | \sqrt{s}), \quad (\text{E.5})$$

in which the two nucleons are equally off their mass shell. The total c.m. energy is

$$\sqrt{s} = 2E_q, \quad (\text{E.6})$$

with $E_q \equiv \sqrt{m^2 + q^2}$. Inserting this in the propagator \tilde{g} and omitting unnecessary arguments, we obtain for eq. (E.5)

$$\hat{M}(q', q) = \hat{V}(q', q) + \int d^3k \frac{m^2}{E_k} \frac{\hat{V}(q', k) \Lambda_+^{(1)}(k) \Lambda_+^{(2)}(-k)}{q^2 - k^2 + i\epsilon} \hat{M}(k, q). \quad (\text{E.7})$$

Defining

$$\bar{M}(q', q) = \sqrt{m/E_{q'}} \hat{M}(q', q) \sqrt{m/E_q}, \quad \bar{V}(q', q) = \sqrt{m/E_{q'}} \hat{V}(q', q) \sqrt{m/E_q}, \quad (\text{E.8})$$

which has become known by “minimal relativity”, eq. (E.7) can be cast into the form

$$\bar{M}(q', q) = \bar{V}(q', q) + m \int d^3k \bar{V}(q', k) \frac{\Lambda_+^{(1)}(k) \Lambda_+^{(2)}(-k)}{q^2 - k^2 + i\epsilon} \bar{M}(k, q). \quad (\text{E.9})$$

Taking matrix elements of eq. (E.9), we obtain an equation for the scattering amplitude T . Its form is identical to the familiar nonrelativistic Lippmann–Schwinger equation, in spite of the fact that we do have a relativistic, covariant equation. Using eq. (C.1) we obtain the R -matrix equation

$$R(q', q) = V(q', q) + mP \int d^3k \frac{V(q', k) R(k, q)}{q^2 - k^2}, \quad (\text{E.10})$$

where spin and isospin dependences are suppressed, as before.

E.1.2. The particular features of the BbS equation

The similarity of the BbS equation to the nonrelativistic Lippmann–Schwinger equation is one of its great virtues. This allows to apply a potential, which is derived from relativistic meson theory, in conventional nonrelativistic nuclear structure physics without any technical problems.

Another point to be discussed is meson retardation. Due to eq. (E.5) BbS ignores meson retardation completely, i.e., the meson propagator (for a scalar meson) in the framework of the BbS equation is

$$\frac{-1}{(q' - q)^2 + m_\alpha^2}. \quad (\text{E.11})$$

As explained in section 3 and appendix B.2 this neglect of retardation enhances the meson propagator, particularly in the case of pion exchange. A correct treatment of meson retardation, as done in time-ordered perturbation theory, leads to the meson propagator

$$\frac{1}{\omega_k(E_q - E_{q'} - \omega_k)}, \quad (\text{E.12})$$

with $\omega_k = \sqrt{(q' - q)^2 + m_\alpha^2}$.

However, all other known three-dimensional reductions of the BS equation enhance the pion contribution even more than BbS. For example the meson propagator

$$\frac{1}{(E_{q'} - E_q)^2 - (q' - q)^2 - m_\alpha^2} \quad (\text{E.13})$$

used by Schierholz [155], Gross [156] and also in part of our former work [51] increases the tensor force due to the pion even more strongly than BbS. In fact, the additional term in eq. (E.13) has an effect which is exactly opposite to that of the correct retardation. (Note, that $E_{q'} = \sqrt{m^2 + q'^2}$ and $E_q = \sqrt{m^2 + q^2}$ are on-mass-shell energies which are untypical for intermediate states.) This is also evident from ref. [154] (see fig. 5, therein: the curves closest to BS, namely E and F , denote the results for BbS and Thompson [128], respectively, both having the meson propagator eq. (E.11)). The conclusion is: if a simplification concerning the meson propagator has to be done anyhow (to achieve energy independence), to simply ignore the retardation à la eq. (E.11) is probably the best choice.

E.1.3. R-matrix and deuteron equation

Equation (E.10) represented in a helicity state basis reads

$$\begin{aligned} \langle q'\lambda'_1\lambda'_2|R(E)|q\lambda_1\lambda_2\rangle &= \langle q'\lambda'_1\lambda'_2|V|q\lambda_1\lambda_2\rangle \\ &+ m \sum_{h_1, h_2} P \int \frac{d^3k}{q^2 - k^2} \langle q'\lambda'_1\lambda'_2|V|kh_1h_2\rangle \langle kh_1h_2|R(E)|q\lambda_1\lambda_2\rangle. \end{aligned} \quad (\text{E.14})$$

The further partial wave decomposition proceeds exactly as in appendix C.1 except that the two-nucleon propagator used there, namely $1/(E - 2E_k)$, has to be replaced by $m/(q^2 - k^2)$. The phase-shift relations, appendix C.2 eq. (C.14), are now (for the case of spin singlet)

$$\operatorname{tg} {}^0\delta^J(E_{\text{lab}}) = -\frac{1}{2}\pi q m {}^0R^J(q, q; E) \quad (\text{E.15})$$

(with $q \equiv |q|$) and analogously for the other cases; i.e. in eq. (C.14) E_q has to be replaced by m . This is the nonrelativistic phase-shift relation. The fact that seemingly a nonrelativistic relation applies here is due to the factors of “minimal relativity”, see eq. (E.8). Recalling that

$$R(q, q; E) = \frac{m}{E_q} \hat{R}(q, q; E) \quad (\text{E.16})$$

with \hat{R} an invariant matrix element we can rewrite eq. (E.15) by

$$\operatorname{tg} {}^0\delta'(E_{\text{lab}}) = -\frac{1}{2}\pi q \frac{m^2}{E_q} {}^0\hat{R}'(q, q; E) \quad (\text{E.17})$$

which is the relation required for relativistic elastic unitarity.

Note that in time-ordered perturbation theory (appendix B and C) we have for the relationship between the R -matrix and the invariant matrix element

$$R(q, q; E) = \frac{m^2}{E_q^2} \hat{R}(q, q; E). \quad (\text{E.18})$$

Together with the phase shift relation eq. (C.14) one again obtains eq. (E.17). The difference between eqs. (E.16) and (E.18) is due to a different normalization of the Dirac spinors (compare eq. (B.2) and eq. (E.25) below) and “minimal relativity”. This difference should be kept in mind when the expressions following in appendix E.2 are used for an OBEP in time-ordered perturbation theory (e.g. that given in appendix B.2, table 8).

The deuteron equation is

$$\langle q\lambda_1\lambda_2 | \phi \rangle = \frac{-m}{q_d^2 + q^2} \sum_{h_1, h_2} \int d^3k \langle q\lambda_1\lambda_2 | V | kh_1 h_2 \rangle \langle kh_1 h_2 | \phi \rangle, \quad (\text{E.19})$$

with $q_d^2 \equiv m\varepsilon_d$, where ε_d is the binding energy. Again, the partial wave decomposition proceeds analogously to appendix D.1 replacing $1/(E - 2E_q)$ by $-m/(q_d^2 + q^2)$. All formulae of the appendices D.2 and D.3 apply unaltered.

E.2. The relativistic momentum space OBE contributions

The potential V to be applied in eqs. (E.14) and (E.19) is defined as the sum of one-boson-exchange contributions

$$V \equiv \sum_{\alpha=\pi, \rho, \eta, \omega, \delta, \sigma} V_{\alpha}^{\text{OBE}}, \quad (\text{E.20})$$

which we will give now explicitly.

The vertices have been given in appendix B, eq. (B.4) (conventions and notations of Bjorken–Drell [145]). (A relativistic momentum space OBEP using the pseudo-vector coupling consistently for π and η , which is important for relativistic nuclear structure physics, is published in ref. [129].)

E.2.1. The OBE amplitudes in plane wave helicity states

The Lagrangians mentioned, lead to the following one-boson-exchange contributions (notation as in fig. 22) in plane wave helicity states*:

* Note that according to canonical Feynman rules there is an additional factor of i for each vertex and each propagator; furthermore, the potential is defined as i times the amplitude. As $i^4 = 1$ we do not bother with factors of i from the beginning.

$$\begin{aligned} \langle q' \lambda'_1 \lambda'_2 | V_{ps}^{\text{OBE}} | q \lambda_1 \lambda_2 \rangle = & -\frac{g_{ps}^2}{(2\pi)^3} \sqrt{\frac{m}{E_{q'}}} \sqrt{\frac{m}{E_q}} \frac{F_{ps}^2[(q' - q)^2]}{(q' - q)^2 + m_{ps}^2} \\ & \times \bar{u}(q', \lambda'_1) i \gamma^5 u(q, \lambda_1) \bar{u}(-q', \lambda'_2) i \gamma^5 u(-q, \lambda_2), \end{aligned} \quad (\text{E.21})$$

$$\begin{aligned} \langle q' \lambda'_1 \lambda'_2 | V_s^{\text{OBE}} | q \lambda_1 \lambda_2 \rangle = & -\frac{g_s^2}{(2\pi)^3} \sqrt{\frac{m}{E_{q'}}} \sqrt{\frac{m}{E_q}} \frac{F_s^2[(q' - q)^2]}{(q' - q)^2 + m_s^2} \\ & \times \bar{u}(q', \lambda'_1) u(q, \lambda_1) \bar{u}(-q', \lambda'_2) u(-q, \lambda_2), \end{aligned} \quad (\text{E.22})$$

$$\begin{aligned} \langle q' \lambda'_1 \lambda'_2 | V_v^{\text{OBE}} | q \lambda_1 \lambda_2 \rangle = & \frac{1}{(2\pi)^3} \sqrt{\frac{m}{E_{q'}}} \sqrt{\frac{m}{E_q}} \frac{F_v^2[(q' - q)^2]}{(q' - q)^2 + m_v^2} \left\{ (g_v + f_v) \bar{u}(q', \lambda'_1) \gamma_\mu u(q, \lambda_1) \right. \\ & - \frac{f_v}{2m} \bar{u}(q', \lambda'_1) [(q' + q)_\mu + (E_{q'} - E_q)(g_\mu^0 - \gamma_\mu \gamma^0)] u(q, \lambda_1) \Big\} \\ & \times \left\{ (g_v + f_v) \bar{u}(-q', \lambda'_2) \gamma^\mu u(-q, \lambda_2) \right. \\ & \left. - \frac{f_v}{2m} \bar{u}(-q', \lambda'_2) [(q' + q)_\mu + (E_{q'} - E_q)(g^{\mu 0} - \gamma^\mu \gamma^0)] u(-q, \lambda_2) \right\}. \end{aligned} \quad (\text{E.23})$$

The form factor applied to each vertex is

$$F_\alpha[(q' - q)^2] = \left(\frac{\Lambda_\alpha^2 - m_\alpha^2}{\Lambda_\alpha^2 + (q' - q)^2} \right)^{n_\alpha}. \quad (\text{E.24})$$

Note that in this appendix dealing with covariant perturbation theory, we normalize the Dirac spinors by

$$\bar{u}(q, \lambda) u(q, \lambda) = 1. \quad (\text{E.25})$$

(This is in contrast to appendix B.) In the case of the vector bosons, the Gordon decomposition has been used [145]; off-shell terms are not dropped in eq. (E.23).

In the propagator for vector bosons

$$\frac{-g_{\mu\nu} + k_\mu k_\nu / m_v^2}{-(q' - q)^2 - m_v^2}, \quad (\text{E.26})$$

the $k_\mu k_\nu$ term which vanishes on-shell anyhow, is omitted. The off-shell effect of that term was examined in ref. [52] and found to be unimportant.

The final goal is to have the V_α^{OBE} represented in partial waves, since NN phase shifts are only defined in such terms and nuclear structure calculations are conventionally done in an *LSJ* basis. However, before this partial wave decomposition can be done we need the V_α^{OBE} in a more explicit form, particularly with regard to their angular dependence.

The Dirac spinors in helicity representation are (cf. ref. [51])

$$\begin{aligned} u(q, \lambda_1) &= \sqrt{\frac{E_q + m}{2m}} \left(\frac{1}{2\lambda_1 q / (E_q + m)} \right) |\lambda_1\rangle, \\ u(-q, \lambda_2) &= \sqrt{\frac{E_q + m}{2m}} \left(\frac{1}{2\lambda_2 q / (E_q + m)} \right) |\lambda_2\rangle, \end{aligned} \quad (\text{E.27})$$

($q \equiv |q|$, $E_q \equiv \sqrt{m^2 + q^2}$) and correspondingly for the primed arguments. Choosing q along the z -axis and q' in the xz -plane we have

$$|\lambda_1\rangle = \chi_{\lambda_1}, \quad |\lambda_2\rangle = \chi_{-\lambda_2}, \quad (\text{E.28})$$

$$|\lambda'_1\rangle = \exp\left(-\frac{i}{2} \sigma_y \vartheta\right) \chi_{\lambda_1}, \quad |\lambda'_2\rangle = \exp\left(-\frac{i}{2} \sigma_y \vartheta\right) \chi_{-\lambda_2}, \quad (\text{E.29})$$

with ϑ the scattering angle. $|\lambda_i^{(\prime)}\rangle$ ($i = 1, 2$) is the eigenstate of the helicity operator for the i th particle with unit momentum \hat{p}_i ,

$$\frac{1}{2} \boldsymbol{\sigma}_i \cdot \hat{p}_i |\lambda_i^{(\prime)}\rangle = \lambda_i^{(\prime)} |\lambda_i^{(\prime)}\rangle, \quad (\text{E.30})$$

and χ_κ is the conventional Pauli spinor

$$\frac{1}{2} \sigma_z \chi_\kappa = \kappa \chi_\kappa. \quad (\text{E.31})$$

With the Dirac spinors eq. (E.27) and the representation of the γ -matrices as given by Bjorken–Drell [145], we obtain V_a^{OBE} more explicitly:

$$\begin{aligned} \langle q' \lambda'_1 \lambda'_2 | V_{ps}^{\text{OBE}} | q \lambda_1 \lambda_2 \rangle &= \frac{g_{ps}^2}{(2\pi)^3} \sqrt{\frac{m}{E_{q'}}} \sqrt{\frac{m}{E_q}} \frac{F_{ps}^2[(q' - q)^2]}{(q' - q)^2 + m_{ps}^2} \\ &\times \frac{W'W}{4m^2} \left(\frac{2\lambda_1 q}{W} - \frac{2\lambda'_1 q'}{W'} \right) \left(\frac{2\lambda_2 q}{W} - \frac{2\lambda'_2 q'}{W'} \right) \langle \lambda'_1 \lambda'_2 | \lambda_1 \lambda_2 \rangle, \end{aligned} \quad (\text{E.32})$$

$$\begin{aligned} \langle q' \lambda'_1 \lambda'_2 | V_s^{\text{OBE}} | q \lambda_1 \lambda_2 \rangle &= -\frac{g_s^2}{(2\pi)^3} \sqrt{\frac{m}{E_{q'}}} \sqrt{\frac{m}{E_q}} \frac{F_s^2[(q' - q)^2]}{(q' - q)^2 + m_s^2} \\ &\times \frac{W'W}{4m^2} \left(1 - \frac{4q' q \lambda'_1 \lambda_1}{W'W} \right) \left(1 - \frac{4q' q \lambda'_2 \lambda_2}{W'W} \right) \langle \lambda'_1 \lambda'_2 | \lambda_1 \lambda_2 \rangle. \end{aligned} \quad (\text{E.33})$$

For vector boson exchange the potential is the sum of three terms ($V_v^{\text{OBE}} = V_{vv}^{\text{OBE}} + V_{v\bar{v}}^{\text{OBE}} + V_{v\bar{v}}^{\text{OBE}}$):

$$\begin{aligned} \langle q' \lambda'_1 \lambda'_2 | V_{vv}^{\text{OBE}} | q \lambda_1 \lambda_2 \rangle &= \frac{g_v^2}{(2\pi)^3} \sqrt{\frac{m}{E_{q'}}} \sqrt{\frac{m}{E_q}} \frac{F_v^2[(q' - q)^2]}{(q' - q)^2 + m_v^2} \\ &\times \frac{W'W}{4m^2} \left[\left(1 + \frac{4qq' \lambda_1 \lambda'_1}{WW'} \right) \left(1 + \frac{4qq' \lambda_2 \lambda'_2}{WW'} \right) \langle \lambda'_1 \lambda'_2 | \lambda_1 \lambda_2 \rangle \right. \\ &\left. - 4 \left(\frac{q \lambda_1}{W} + \frac{q' \lambda'_1}{W'} \right) \left(\frac{q \lambda_2}{W} + \frac{q' \lambda'_2}{W'} \right) \langle \lambda'_1 \lambda'_2 | \boldsymbol{\sigma}_1 \cdot \boldsymbol{\sigma}_2 | \lambda_1 \lambda_2 \rangle \right], \end{aligned} \quad (\text{E.34a})$$

$$\begin{aligned}
\langle \mathbf{q}' \lambda'_1 \lambda'_2 | V_{tt}^{\text{OBE}} | \mathbf{q} \lambda_1 \lambda_2 \rangle = & \frac{f_v^2}{(2\pi)^3} \sqrt{\frac{m}{E_{q'}}} \sqrt{\frac{m}{E_q}} \frac{F_v^2[(\mathbf{q}' - \mathbf{q})^2]}{(\mathbf{q}' - \mathbf{q})^2 + m_v^2} \\
& \times \frac{W'W}{4m^2} \left\{ \left[\left(1 + \frac{4q'q\lambda'_1\lambda_1}{W'W} \right) \left(1 + \frac{4q'q\lambda'_2\lambda_2}{W'W} \right) \right. \right. \\
& - 2 \frac{E_{q'} + E_q}{m} \left(1 - \frac{16q'^2 q^2 \lambda'_1 \lambda_1 \lambda'_2 \lambda_2}{W'^2 W^2} \right) \\
& + \left(1 - \frac{4q'q\lambda'_1\lambda_1}{W'W} \right) \left(1 - \frac{4q'q\lambda'_2\lambda_2}{W'W} \right) \frac{3(E_{q'}E_q + M^2) + q'q \cos \vartheta}{2m^2} \Big] \langle \lambda'_1 \lambda'_2 | \lambda_1 \lambda_2 \rangle \\
& - \left[\left(\frac{2q'\lambda'_1}{W'} + \frac{2q\lambda_1}{W} \right) \left(\frac{2q'\lambda'_2}{W'} + \frac{2q\lambda_2}{W} \right) + \frac{E_{q'} - E_q}{m} \left(\frac{4q'^2 \lambda'_1 \lambda'_2}{W'^2} - \frac{4q^2 \lambda_1 \lambda_2}{W^2} \right) \right. \\
& \left. \left. + \frac{(E_{q'} - E_q)^2}{4m^2} \left(\frac{2q'\lambda'_1}{W'} - \frac{2q\lambda_1}{W} \right) \left(\frac{2q'\lambda'_2}{W'} - \frac{2q\lambda_2}{W} \right) \right] \langle \lambda'_1 \lambda'_2 | \boldsymbol{\sigma}_1 \cdot \boldsymbol{\sigma}_2 | \lambda_1 \lambda_2 \rangle \right\}, \tag{E.34b}
\end{aligned}$$

$$\begin{aligned}
\langle \mathbf{q}' \lambda'_1 \lambda'_2 | V_{vt}^{\text{OBE}} | \mathbf{q} \lambda_1 \lambda_2 \rangle = & \frac{2g_v f_v}{(2\pi)^3} \sqrt{\frac{m}{E_{q'}}} \sqrt{\frac{m}{E_q}} \frac{F_v^2[(\mathbf{q}' - \mathbf{q})^2]}{(\mathbf{q}' - \mathbf{q})^2 + m_v^2} \\
& \times \frac{W'W}{4m^2} \left\{ \left[\frac{W' + W}{M} \frac{16q'^2 q^2 \lambda'_1 \lambda'_2 \lambda_1 \lambda_2}{W'^2 W^2} - \frac{E_{q'} + E_q - 2m}{m} \right] \langle \lambda'_1 \lambda'_2 | \lambda_1 \lambda_2 \rangle \right. \\
& - \left[\left(\frac{2q'\lambda'_1}{W'} + \frac{2q\lambda_1}{W} \right) \left(\frac{2q'\lambda'_2}{W'} + \frac{2q\lambda_2}{W} \right) + \frac{E_{q'} - E_q}{2m} \left(\frac{4q'^2 \lambda'_1 \lambda'_2}{W'^2} - \frac{4q^2 \lambda_1 \lambda_2}{W^2} \right) \right] \\
& \left. \times \langle \lambda'_1 \lambda'_2 | \boldsymbol{\sigma}_1 \cdot \boldsymbol{\sigma}_2 | \lambda_1 \lambda_2 \rangle \right\}. \tag{E.34c}
\end{aligned}$$

In eqs. (E.32)–(E.34) the abbreviations $W = E_q + m$, $W' = E_{q'} + m$ are used. Denoting the angle between \mathbf{q} and \mathbf{q}' by ϑ , the helicity state matrix elements needed are:

$$\langle \lambda'_1 \lambda'_2 | \lambda_1 \lambda_2 \rangle = \{ |\lambda'_1 + \lambda_1| \cos \frac{1}{2} \vartheta + (\lambda'_1 - \lambda_1) \sin \frac{1}{2} \vartheta \} \{ |\lambda'_2 + \lambda_2| \cos \frac{1}{2} \vartheta - (\lambda'_2 - \lambda_2) \sin \frac{1}{2} \vartheta \}, \tag{E.35}$$

$$\begin{aligned}
\langle \lambda'_1 \lambda'_2 | \boldsymbol{\sigma}_1 \cdot \boldsymbol{\sigma}_2 | \lambda_1 \lambda_2 \rangle = & - \{ (\lambda'_1 + \lambda_1) \sin \frac{1}{2} \vartheta + |\lambda'_1 - \lambda_1| \cos \frac{1}{2} \vartheta \} \{ (\lambda'_2 + \lambda_2) \sin \frac{1}{2} \vartheta - |\lambda'_2 - \lambda_2| \cos \frac{1}{2} \vartheta \} \\
& - \{ |\lambda'_1 + \lambda_1| \sin \frac{1}{2} \vartheta - (\lambda'_1 - \lambda_1) \cos \frac{1}{2} \vartheta \} \{ |\lambda'_2 + \lambda_2| \sin \frac{1}{2} \vartheta + (\lambda'_2 - \lambda_2) \cos \frac{1}{2} \vartheta \} \\
& - \{ (\lambda'_1 + \lambda_1) \cos \frac{1}{2} \vartheta - |\lambda'_1 - \lambda_1| \sin \frac{1}{2} \vartheta \} \{ (\lambda'_2 + \lambda_2) \cos \frac{1}{2} \vartheta + |\lambda'_2 - \lambda_2| \sin \frac{1}{2} \vartheta \}. \tag{E.36}
\end{aligned}$$

Equations (E.35) and (E.36) are easily verified by using eqs. (E.28) and (E.29)

E.2.2. Partial wave decomposition

The partial wave expansion of V is

$$\langle \mathbf{q}'\lambda'_1\lambda'_2|V|\mathbf{q}\lambda_1\lambda_2\rangle = \sum_{JM} \langle \hat{\mathbf{q}}'\lambda'_1\lambda'_2|JM\lambda'_1\lambda'_2\rangle \langle \lambda'_1\lambda'_2|V^J(q', q)|\lambda_1\lambda_2\rangle \langle JM\lambda_1\lambda_2|\hat{\mathbf{q}}\lambda_1\lambda_2\rangle, \quad (\text{E.37})$$

with the transformation matrix elements given in eq. (C.5). The transformation coefficients are considerably simplified by using the addition theorem for rotation matrices and by choosing \mathbf{q} along the z -axis and \mathbf{q}' in the xz -plane:

$$\langle \mathbf{q}'\lambda'_1\lambda'_2|V|\mathbf{q}\lambda_1\lambda_2\rangle = \frac{1}{4\pi} \sum_J (2J+1) d_{\lambda\lambda'}^J(\vartheta) \langle \lambda'_1\lambda'_2|V^J(q', q)|\lambda_1\lambda_2\rangle, \quad (\text{E.38})$$

with $\lambda = \lambda_1 - \lambda_2$, $\lambda' = \lambda'_1 - \lambda'_2$ and $d_{\lambda\lambda'}^J(\vartheta)$ the reduced rotation matrices (Jacobi polynomials). They satisfy

$$d_{\lambda\lambda'}^J(\vartheta) = d_{-\lambda', -\lambda}^J(\vartheta) = (-)^{\lambda - \lambda'} d_{\lambda'\lambda}^J(\vartheta) \quad (\text{E.39})$$

and the orthogonality relation

$$\int_{-1}^{+1} d(\cos \vartheta) d_{\lambda\lambda'}^J(\vartheta) d_{\lambda\lambda'}^{J'}(\vartheta) = \delta_{JJ'} \frac{2}{2J+1}. \quad (\text{E.40})$$

Using (E.40), (E.38) can be inverted to obtain

$$\langle \lambda'_1\lambda'_2|V^J(q', q)|\lambda_1\lambda_2\rangle = 2\pi \int_{-1}^{+1} d(\cos \vartheta) d_{\lambda\lambda'}^J(\vartheta) \langle \mathbf{q}'\lambda'_1\lambda'_2|V|\mathbf{q}\lambda_1\lambda_2\rangle. \quad (\text{E.41})$$

This is the basic formula for the representation of the V_a^{OBE} in partial wave helicity states.

As discussed in appendix C.1, due to the special symmetry properties of the nuclear force, only six helicity amplitudes are independent. Furthermore, six linear combinations of these amplitudes are of particular practical interest, see eqs. (C.10) and (C.12) (with R to be replaced by V).

When evaluating these six partial wave amplitudes for the OBE potentials eqs. (E.32)–(E.34) by applying eq. (E.41) one obtains products of reduced rotation matrices and trigonometrical functions. These can be expressed in terms of the more convenient Legendre polynomials, $P_J(\cos \vartheta)$, namely

$$d_{00}^J(\vartheta) = P_J(\cos \vartheta),$$

$$\begin{aligned} (1 + \cos \vartheta) d_{11}^J(\vartheta) &= P_J + \frac{J+1}{2J+1} P_{J-1} + \frac{J}{2J+1} P_{J+1} \\ &= P_J + \frac{J}{J+1} \cos \vartheta P_J + \frac{1}{J+1} P_{J-1}, \end{aligned}$$

$$\begin{aligned}
(1 - \cos \vartheta) d_{-11}(\vartheta) &= -P_J + \frac{J+1}{2J+1} P_{J-1} + \frac{J}{2J+1} P_{J+1} \\
&= -P_J + \frac{J}{J+1} \cos \vartheta P_J + \frac{1}{J+1} P_{J-1}, \\
\sin \vartheta d_{10}^J(\vartheta) &= -\sin \vartheta d_{01}^J(\vartheta) = \frac{\sqrt{J(J+1)}}{2J+1} (P_{J+1} - P_{J-1}) \\
&= \sqrt{\frac{J}{J+1}} (\cos \vartheta P_J - P_{J-1}),
\end{aligned} \tag{E.42}$$

where the argument of $P_J(\cos \vartheta)$ is mostly suppressed. These expressions in conjunction with eq. (E.41) give rise to the following integrals:

$$I_J^{(0)}(m_\alpha) \equiv \int_{-1}^{+1} dt \frac{P_J(t)}{(q' - q)^2 + m_\alpha^2} = \frac{1}{q'q} Q_J(z_\alpha), \tag{E.43}$$

with $t = \cos \vartheta$, $z_\alpha = (q'^2 + q^2 + m_\alpha^2)/2q'q$ and $Q_J(z_\alpha)$ the Legendre functions of the second kind [157] ($Q_0(z_\alpha) = \frac{1}{2} \ln[(z_\alpha + 1)/(z_\alpha - 1)]$). And furthermore

$$\begin{aligned}
I_J^{(1)}(m_\alpha) &\equiv \int_{-1}^{+1} dt \frac{tP_J(t)}{(q' - q)^2 + m_\alpha^2} = \frac{Q_J^{(1)}(z_\alpha)}{q'q}, \\
I_J^{(2)}(m_\alpha) &\equiv \frac{1}{J+1} \int_{-1}^{+1} dt \frac{JtP_J(t) + P_{J-1}(t)}{(q' - q)^2 + m_\alpha^2} = \frac{Q_J^{(2)}(z_\alpha)}{q'q}, \\
I_J^{(3)}(m_\alpha) &\equiv \sqrt{\frac{J}{J+1}} \int_{-1}^{+1} dt \frac{tP_J(t) - P_{J-1}(t)}{(q' - q)^2 + m_\alpha^2} = \frac{Q_J^{(3)}(z_\alpha)}{q'q}, \\
I_J^{(4)}(m_\alpha) &\equiv \int_{-1}^{+1} dt \frac{t^2 P_J(t)}{(q' - q)^2 + m_\alpha^2} = \frac{Q_J^{(4)}(z_\alpha)}{q'q}, \\
I_J^{(5)}(m_\alpha) &\equiv \frac{1}{J+1} \int_{-1}^{+1} dt \frac{Jt^2 P_J(t) + tP_{J-1}(t)}{(q' - q)^2 + m_\alpha^2} = \frac{Q_J^{(5)}(z_\alpha)}{q'q}, \\
I_J^{(6)}(m_\alpha) &\equiv \sqrt{\frac{J}{J+1}} \int_{-1}^{+1} dt \frac{t^2 P_J(t) - tP_{J-1}(t)}{(q' - q)^2 + m_\alpha^2} = \frac{Q_J^{(6)}(z_\alpha)}{q'q},
\end{aligned} \tag{E.44}$$

with

$$\begin{aligned}
Q_J^{(1)}(z_\alpha) &\equiv z_\alpha Q_J(z_\alpha) - \delta_{J0}, & Q_J^{(2)}(z_\alpha) &\equiv \frac{1}{J+1} (J z_\alpha Q_J(z_\alpha) + Q_{J-1}(z_\alpha)), \\
Q_J^{(3)}(z_\alpha) &\equiv \sqrt{\frac{J}{J+1}} (z_\alpha Q_J(z_\alpha) - Q_{J-1}(z_\alpha)), & Q_J^{(4)}(z_\alpha) &\equiv z_\alpha Q_J^{(1)}(z_\alpha) - \frac{1}{3}\delta_{J1}, \\
Q_J^{(5)}(z_\alpha) &\equiv z_\alpha Q_J^{(2)}(z_\alpha) - \frac{2}{3}\delta_{J1}, & Q_J^{(6)}(z_\alpha) &\equiv z_\alpha Q_J^{(3)}(z_\alpha) + \frac{1}{3}\sqrt{2}\delta_{J1}.
\end{aligned} \tag{E.45}$$

Note that the dependence of the $I_J^{(i)}$ on (q', q) is suppressed in our notation. Equations (E.44)–(E.45) can be verified with the help of the recurrence relations

$$tP_J(t) = \frac{J+1}{2J+1} P_{J+1}(t) + \frac{J}{2J+1} P_{J-1}(t) \tag{E.46}$$

and

$$z_\alpha Q_J(z_\alpha) = \frac{J+1}{2J+1} Q_{J+1}(z_\alpha) + \frac{J}{2J+1} Q_{J-1}(z_\alpha) + \delta_{J0}. \tag{E.47}$$

In numerical calculations there is actually no need to use the Legendre functions of the second kind. The integrals, eqs. (E.43), (E.44), can be computed numerically fast and accurately. This has the advantage that the cutoffs can be included in the integrand, namely by replacing

$$\frac{1}{(q'-q)^2 + m_\alpha^2} \rightarrow \frac{1}{(q'-q)^2 + m_\alpha^2} \left(\frac{\Lambda_\alpha^2 - m_\alpha^2}{(q'-q)^2 + \Lambda_\alpha^2} \right)^{2n_\alpha}. \tag{E.48}$$

When using the Legendre functions of the second kind the product of propagator and cutoffs (r.h.s. of (E.48) for the case of $n_\alpha = 1$) has to be decomposed as

$$\frac{1}{(q'-q)^2 + m_\alpha^2} - \frac{\Lambda_{\alpha,2}^2 - m_\alpha^2}{\Lambda_{\alpha,2}^2 - \Lambda_{\alpha,1}^2} \frac{1}{(q'-q)^2 + \Lambda_{\alpha,1}^2} + \frac{\Lambda_{\alpha,1}^2 - m_\alpha^2}{\Lambda_{\alpha,2}^2 - \Lambda_{\alpha,1}^2} \frac{1}{(q'-q)^2 + \Lambda_{\alpha,2}^2}, \tag{E.49}$$

with

$$\Lambda_{\alpha,1} = \Lambda_\alpha + \varepsilon, \quad \Lambda_{\alpha,2} = \Lambda_\alpha - \varepsilon \quad \text{and} \quad \varepsilon \ll \Lambda_\alpha$$

($\varepsilon \approx 10$ MeV is an appropriate choice) before the (analytic) integration over $\cos \vartheta$ is done. (For the meson propagator of the time-ordered theory, $[\omega_k(E - E_{q'} - E_q - \omega_k)]^{-1}$ (compare appendix B), the integrals eqs. (E.43)–(E.44) can only be solved numerically.)

E.2.3. The final OBE expressions

Inserting eqs. (E.32)–(E.34) into eq. (E.41) and using eqs. (E.35), (E.36), (E.42)–(E.44) we obtain the final expressions for the OBE amplitudes in partial wave decomposition. We present these final results in terms of the linear combinations of helicity amplitudes which are most relevant to practical calculations (for definitions see appendix C, eqs. (C.10) and (C.12)). Only here we abbreviate $E' \equiv E_{q'}$, $E \equiv E_q$.

Pseudo-scalar coupling (ps) (η - and π -meson; for π multiply with $\tau_1 \cdot \tau_2$):

$$\begin{aligned} {}^0V_{\text{ps}}^J &= C_{\text{ps}}(F_{\text{ps}}^{(0)} I_J^{(0)}(m_{\text{ps}}) + F_{\text{ps}}^{(1)} I_J^{(1)}(m_{\text{ps}})) , \\ {}^1V_{\text{ps}}^J &= C_{\text{ps}}(-F_{\text{ps}}^{(0)} I_J^{(0)}(m_{\text{ps}}) - F_{\text{ps}}^{(1)} I_J^{(2)}(m_{\text{ps}})) , \\ {}^{12}V_{\text{ps}}^J &= C_{\text{ps}}(F_{\text{ps}}^{(1)} I_J^{(0)}(m_{\text{ps}}) + F_{\text{ps}}^{(0)} I_J^{(1)}(m_{\text{ps}})) , \\ {}^{34}V_{\text{ps}}^J &= C_{\text{ps}}(-F_{\text{ps}}^{(1)} I_J^{(0)}(m_{\text{ps}}) - F_{\text{ps}}^{(0)} I_J^{(2)}(m_{\text{ps}})) , \\ {}^{55}V_{\text{ps}}^J &= C_{\text{ps}} F_{\text{ps}}^{(2)} I_J^{(3)}(m_{\text{ps}}) , \\ {}^{66}V_{\text{ps}}^J &= -C_{\text{ps}} F_{\text{ps}}^{(2)} I_J^{(3)}(m_{\text{ps}}) , \end{aligned} \tag{E.50}$$

with

$$C_{\text{ps}} = \frac{g_{\text{ps}}^2}{4\pi} \frac{1}{2\pi m^2} \sqrt{\frac{m}{E'}} \sqrt{\frac{m}{E}} ,$$

and

$$F_{\text{ps}}^{(0)} = E'E - m^2 , \quad F_{\text{ps}}^{(1)} = -q'q , \quad F_{\text{ps}}^{(2)} = -m(E' - E) .$$

Scalar coupling (s) (σ - and δ -boson; for δ multiply with $\tau_1 \cdot \tau_2$):

$$\begin{aligned} {}^0V_{\text{s}}^J &= C_{\text{s}}(F_{\text{s}}^{(0)} I_J^{(0)}(m_{\text{s}}) + F_{\text{s}}^{(1)} I_J^{(1)}(m_{\text{s}})) , \\ {}^1V_{\text{s}}^J &= C_{\text{s}}(F_{\text{s}}^{(0)} I_J^{(0)}(m_{\text{s}}) + F_{\text{s}}^{(1)} I_J^{(2)}(m_{\text{s}})) , \\ {}^{12}V_{\text{s}}^J &= C_{\text{s}}(F_{\text{s}}^{(1)} I_J^{(0)}(m_{\text{s}}) + F_{\text{s}}^{(0)} I_J^{(1)}(m_{\text{s}})) , \\ {}^{34}V_{\text{s}}^J &= C_{\text{s}}(F_{\text{s}}^{(1)} I_J^{(0)}(m_{\text{s}}) + F_{\text{s}}^{(0)} I_J^{(2)}(m_{\text{s}})) , \\ {}^{55}V_{\text{s}}^J &= C_{\text{s}} F_{\text{s}}^{(2)} I_J^{(3)}(m_{\text{s}}) , \\ {}^{66}V_{\text{s}}^J &= C_{\text{s}} F_{\text{s}}^{(2)} I_J^{(3)}(m_{\text{s}}) , \end{aligned} \tag{E.51}$$

with

$$C_{\text{s}} = \frac{g_{\text{s}}^2}{4\pi} \frac{1}{2\pi m^2} \sqrt{\frac{m}{E'}} \sqrt{\frac{m}{E}} ,$$

and

$$F_{\text{s}}^{(0)} = -(E'E + m^2) , \quad F_{\text{s}}^{(1)} = q'q , \quad F_{\text{s}}^{(2)} = m(E' + E) .$$

Vector bosons (v) (ω - and ρ -meson; for ρ multiply with $\tau_1 \cdot \tau_2$):
Vector–vector coupling:

$$\begin{aligned} {}^0V_{vv}^J &= C_{vv}(2E'E - m^2)I_J^{(0)}(m_v), \\ {}^1V_{vv}^J &= C_{vv}(E'EI_J^{(0)}(m_v) + q'qI_J^{(2)}(m_v)), \\ {}^{12}V_{vv}^J &= C_{vv}(2q'qI_J^{(0)}(m_v) + m^2I_J^{(1)}(m_v)), \\ {}^{34}V_{vv}^J &= C_{vv}(q'qI_J^{(0)}(m_v) + E'EI_J^{(2)}(m_v)), \\ {}^{55}V_{vv}^J &= -C_{vv}mEI_J^{(3)}(m_v), \\ {}^{66}V_{vv}^J &= -C_{vv}mE'I_J^{(3)}(m_v), \end{aligned} \quad (\text{E.52a})$$

with

$$C_{vv} = \frac{g_v^2}{4\pi} \frac{1}{\pi m^2} \sqrt{\frac{m}{E'}} \sqrt{\frac{m}{E}}.$$

Tensor–tensor:

$$\begin{aligned} {}^0V_{tt}^J &= C_{tt}\{(q'^2 + q^2)(3E'E + m^2)I_J^{(0)}(m_v) \\ &\quad + [q'^2 + q^2 - 2(3E'E + m^2)]q'qI_J^{(1)}(m_v) - 2q'^2q^2I_J^{(4)}(m_v)\}, \\ {}^1V_{tt}^J &= C_{tt}\{[4q'^2q^2 + (q'^2 + q^2)(E'E - m^2)]I_J^{(0)}(m_v) + 2(E'E + m^2)q'qI_J^{(1)}(m_v) \\ &\quad - (q'^2 + q^2 + 4E'E)q'qI_J^{(2)}(m_v) - 2q'^2q^2I_J^{(5)}(m_v)\}, \\ {}^{12}V_{tt}^J &= C_{tt}\{[4m^2 - 3(q'^2 + q^2)]q'qI_J^{(0)}(m_v) \\ &\quad + [6q'^2q^2 - (q'^2 + q^2)(E'E + 3m^2)]I_J^{(1)}(m_v) + 2(E'E + m^2)q'qI_J^{(4)}(m_v)\}, \\ {}^{34}V_{tt}^J &= C_{tt}\{-[q'^2 + q^2 + 4E'E]I_J^{(0)}(m_v) - 2q'^2q^2I_J^{(1)}(m_v) \\ &\quad + [4q'^2q^2 + (q'^2 + q^2)(E'E - m^2)]I_J^{(2)}(m_v) + 2(E'E + m^2)q'qI_J^{(5)}(m_v)\}, \\ {}^{55}V_{tt}^J &= C_{tt}m\{[E'(q'^2 + q^2) + E(3q'^2 - q^2)]I_J^{(3)}(m_v) - 2(E' + E)q'qI_J^{(6)}(m_v)\} \\ {}^{66}V_{tt}^J &= C_{tt}m\{[E(q'^2 + q^2) + E'(3q^2 - q'^2)]I_J^{(3)}(m_v) - 2(E' + E)q'qI_J^{(6)}(m_v)\}, \end{aligned} \quad (\text{E.52b})$$

with

$$C_{tt} = \frac{f_v^2}{4\pi} \frac{1}{8\pi m^4} \cdot \frac{\sqrt{m}}{E'} \sqrt{\frac{m}{E}}.$$

Vector–tensor coupling:

$$\begin{aligned} {}^0V_{vt}^J &= C_{vt}m((q'^2 + q^2)I_J^{(0)}(m_v) - 2q'qI_J^{(1)}(m_v)), \\ {}^1V_{vt}^J &= C_{vt}m(-(q'^2 + q^2)I_J^{(0)}(m_v) + 2q'qI_J^{(2)}(m_v)), \end{aligned}$$

$$\begin{aligned}
 {}^{12}V_{vt}^J &= C_{vt} m (6q' q I_J^{(0)}(m_v) - 3(q'^2 + q^2) I_J^{(1)}(m_v)), \\
 {}^{34}V_{vt}^J &= C_{vt} m (2q' q I_J^{(0)}(m_v) - (q'^2 + q^2) I_J^{(2)}(m_v)), \\
 {}^{55}V_{vt}^J &= C_{vt} (E' q^2 + 3Eq'^2) I_J^{(3)}(m_v), \\
 {}^{66}V_{vt}^J &= C_{vt} (Eq'^2 + 3E' q^2) I_J^{(3)}(m_v),
 \end{aligned} \tag{E.52c}$$

with

$$C_{vt} = \frac{g_v f_v}{4\pi} \frac{1}{2\pi m^3} \sqrt{\frac{m}{E'}} \sqrt{\frac{m}{E}}.$$

E.3. Some final remarks

The potential OBEPQ is defined by eq. (E.20) with the explicit expressions given in appendix E.2.3 and the parameters of table 5*. The OBE expressions eqs. (E.50)–(E.52) are represented such that they can be applied directly in eqs. (C.13) and (D.9) (with the necessary replacement of the two-nucleon propagator according to eqs. (E.14), (E.19)). Alternatively one can also first apply eq. (C.21) to the OBE amplitudes and then perform all calculations in the conventional *LSJ* basis, see e.g. ref. [148]. The deuteron wave functions from OBEPQ are given in appendix D.3.3.

For comparison and adjustment of our conventions and units (as stated before, we use units $\hbar = c = 1$ and recommend units of MeV for energies, masses and momenta in practical calculations; conversion factor: $\hbar c = 197.3286$ MeV fm) to those used in the work of other authors, we recommend to compare the different phase shift relations (ours is given in eq. (E.15)). Also, the partial wave integral equations should be compared with regard to all kinds of factors (see ours in eqs. (C.13) and (D.9)).

If one wants to use the OBE amplitudes presented in this appendix in time-ordered perturbation theory (e.g. for the OBEP presented in appendix B.2 and table 8) one has to do the following changes: Due to the normalization of the Dirac spinors eq. (B.2) and no factor of “minimal relativity” one has to replace

$$\sqrt{\frac{M}{E_{q'}}} \sqrt{\frac{M}{E_q}} \rightarrow \frac{M}{E_{q'}} \frac{M}{E_q}.$$

The off-shell term

$$(E_{q'} - E_q)(g_\mu^0 - \gamma_\mu \gamma^0)$$

in the ρ -exchange (compare eq. (E.23)) is dropped by us in time-ordered perturbation theory. Therefore the expressions for tensor-tensor and vector-tensor coupling are changed. The corresponding expressions are published in ref. [52] (appendix A, case 1, therein).

Appendix F: Coordinate space OBEP (OBEPR)

The meson exchange contributions given in appendix E depend on two momentum variables, namely the incoming and outgoing relative momenta q and q' . A direct Fourier transformation of these

* A computer code for OBEPQ is available from one of the authors (R.M.).

expressions would yield a function of the (relative) in- and outgoing two-nucleon distances r and r' , i.e. a strongly nonlocal expression; moreover, the transformation cannot be done analytically. Thus, an analytic form in r -space can only be obtained after some characteristic approximations in the expressions of appendix E.

We start from eqs. (E.21)–(E.23), but replace the helicity spinors (eq. (E.27)) by spinors

$$u(q, s) = \sqrt{\frac{E_q + m}{2m}} \left(\begin{array}{c} 1 \\ (\sigma \cdot q)/(E_q + m) \end{array} \right) |s\rangle, \quad (\text{F.1})$$

containing the spin operator σ and the Pauli spinor $|s\rangle$. Leaving out the states $|s\rangle$ in the resulting expressions we have a potential operator with spin operators σ_i ($i = 1, 2$) for nucleon i . We then introduce new variables

$$k = q' - q, \quad p = \frac{1}{2}(q' + q), \quad (\text{F.2})$$

expand the relativistic energies in powers of k^2 and p^2 and keep only the lowest order. We then arrive at the following formulas:

pseudoscalar mesons (π, η):

$$V_{\text{ps}}(k, p) = -\frac{g_{\text{ps}}^2}{4m^2} \frac{(\sigma_1 \cdot k)(\sigma_2 \cdot k)}{k^2 + m_{\text{ps}}^2}; \quad (\text{F.3})$$

scalar mesons (σ, δ):

$$V_s(k, p) = -\frac{g_s^2}{k^2 + m_s^2} \left[1 - \frac{p^2}{2m^2} + \frac{k^2}{8m^2} - \frac{i}{2m^2} S \cdot (k \times p) \right], \quad (\text{F.4})$$

where $S = \frac{1}{2}(\sigma_1 + \sigma_2)$;

vector mesons (ω, ρ):

$$\begin{aligned} V_v(k, p) = & \frac{1}{k^2 + m_v^2} \left\{ g_v^2 \left[1 + \frac{3p^2}{2m^2} - \frac{k^2}{8m^2} + \frac{3i}{2m^2} S \cdot (k \times p) - \sigma_1 \cdot \sigma_2 \frac{k^2}{4m^2} + \frac{1}{4m^2} (\sigma_1 \cdot k)(\sigma_2 \cdot k) \right] \right. \\ & + \frac{g_v f_v}{2m} \left[-\frac{k^2}{m} + \frac{4i}{m} S \cdot (k \times p) - \sigma_1 \cdot \sigma_2 \frac{k^2}{m} + \frac{1}{m} (\sigma_1 \cdot k)(\sigma_1 \cdot k) \right] \\ & \left. + \frac{f_v^2}{4m^2} [-\sigma_1 \cdot \sigma_2 k^2 + (\sigma_1 \cdot k)(\sigma_2 \cdot k)] \right\}. \end{aligned} \quad (\text{F.5})$$

The resulting expressions still contain nonlocalities due to p^2 as well as $k \times p$ terms. The latter leads to the angular momentum operator $L = -ir \times \nabla$ in r -space, whereas the former provides ∇^2 terms. An analytic Fourier transformation can now be performed and yields:

pseudoscalar mesons:

$$V_{\text{ps}}(m_{\text{ps}}, r) = \frac{1}{12} \frac{g_{\text{ps}}^2}{4\pi} m_{\text{ps}} \left[\left(\frac{m_{\text{ps}}}{m} \right)^2 Y(m_{\text{ps}}r) \sigma_1 \cdot \sigma_2 + Z(m_{\text{ps}}r) S_{12} \right]; \quad (\text{F.6})$$

scalar mesons:

$$V_s(m_s, r) = -\frac{g_s^2}{4\pi} m_s \left\{ \left[1 - \frac{1}{4} \left(\frac{m_s}{m} \right)^2 \right] Y(m_s r) + \frac{1}{4m^2} [\nabla^2 Y(m_s r) + Y(m_s r) \nabla^2] + \frac{1}{2} Z_1(m_s r) \mathbf{L} \cdot \mathbf{S} \right\}; \quad (\text{F.7})$$

vector mesons:

$$\begin{aligned} V_v(m_v, r) = & \frac{g_v^2}{4\pi} m_v \left\{ \left[1 + \frac{1}{2} \left(\frac{m_v}{m} \right)^2 \right] Y(m_v r) - \frac{3}{4m^2} [\nabla^2 Y(m_v r) + Y(m_v r) \nabla^2] \right. \\ & + \frac{1}{6} \left(\frac{m_v}{m} \right)^2 Y(m_v r) \boldsymbol{\sigma}_1 \cdot \boldsymbol{\sigma}_2 - \frac{3}{2} Z_1(m_v r) \mathbf{L} \cdot \mathbf{S} - \frac{1}{12} Z(m_v r) S_{12} \Big\} \\ & + \frac{1}{2} \frac{g_v f_v}{4\pi} m_v \left\{ (m_v/m)^2 Y(m_v r) + \frac{2}{3} (m_v/m)^2 Y(m_v r) \boldsymbol{\sigma}_1 \cdot \boldsymbol{\sigma}_2 \right. \\ & \left. - 4 Z_1(m_v r) \mathbf{L} \cdot \mathbf{S} - \frac{1}{3} Z(m_v r) S_{12} \right\} \\ & + \frac{f_v^2}{4\pi} m_v \left\{ \frac{1}{6} (m_v/m)^2 Y(m_v r) \boldsymbol{\sigma}_1 \cdot \boldsymbol{\sigma}_2 - \frac{1}{12} Z(m_v r) S_{12} \right\}, \end{aligned}$$

with

$$\begin{aligned} Y(x) &= e^{-x/x}, \quad Z(x) = (m_\alpha/m)^2 (1 + 3/x + 3/x^2) Y(x), \\ Z_1(x) &= \left(\frac{m_\alpha}{m} \right)^2 (1/x + 1/x^2) Y(x), \quad S_{12} = 3 \frac{(\boldsymbol{\sigma}_1 \cdot \mathbf{r})(\boldsymbol{\sigma}_2 \cdot \mathbf{r})}{r^2} - \boldsymbol{\sigma}_1 \cdot \boldsymbol{\sigma}_2, \end{aligned} \quad (\text{F.8})$$

and

$$\nabla^2 = +\frac{1}{r} \frac{d^2}{dr^2} r - \frac{L^2}{r^2}.$$

We use units such that $\hbar = c = 1$ ($\hbar c = 197.3286$ MeV fm). The use of the form factor, eq. (3.3), at each vertex (with $n_\alpha = 1$) leads to the following extended expressions:

$$V_\alpha(r) = V_\alpha(m_\alpha, r) - \frac{\Lambda_{\alpha,2}^2 - m_\alpha^2}{\Lambda_{\alpha,2}^2 - \Lambda_{\alpha,1}^2} V_\alpha(\Lambda_{\alpha,1}, r) + \frac{\Lambda_{\alpha,1}^2 - m_\alpha^2}{\Lambda_{\alpha,2}^2 - \Lambda_{\alpha,1}^2} V_\alpha(\Lambda_{\alpha,2}, r), \quad (\text{F.9})$$

where $\Lambda_{\alpha,1} = \Lambda_\alpha + \varepsilon$, $\Lambda_{\alpha,2} = \Lambda_\alpha - \varepsilon$, $\varepsilon/\Lambda_\alpha \ll 1$. $\varepsilon = 10$ MeV is an appropriate choice.

The full NN potential is the sum of the contributions from six mesons:

$$V(r) = \sum_{\alpha=\pi,\rho,\eta,\omega,\delta,\sigma} V_\alpha(r)$$

Table 14
Meson and low-energy parameters (LEP) for the configuration space one-boson-exchange potential (OBEPR)

	$g_a^2/4\pi; [f_a/g_a]$	m_a (MeV)	Λ_a (GeV)	LEP	Theory
π	14.9	138.03	1.3	ϵ_d (MeV)	2.2246
ρ	0.95; [6.1]	769	1.3	P_D (%)	4.81
η	3	548.8	1.5	Q_d (fm^2)	0.274
ω	20; [0.0]	782.6	1.5	μ_d (μ_N)	0.8524
δ	2.6713	983	2.0	A_s ($\text{fm}^{-1/2}$)	0.8860
σ	7.7823 *	550 *	2.0	D/S	0.0260
				r_d (fm)	1.9691
				a_s (fm)	-23.751
				r_s (fm)	2.662
				a_t (fm)	5.423
				r_t (fm)	1.759

For notation and experimental values see tables 3 and 4. $n_a = 1$ for all mesons.

* The parameters for the σ -boson given in the table apply for the $T=1$ NN potential. For $T=0$ we have: $m_\sigma = 715$ MeV, $g_\sigma^2/4\pi = 16.2061$ and $\Lambda_\sigma = 2.0$ GeV; the parameters for the other mesons are the same for $T=0$ and $T=1$.

where π and η are pseudoscalar (ps), σ and δ scalar (s) and ω and ρ vector (v) mesons. The meson parameters are given in table 14*. Note that for the isovector mesons π , ρ and δ , $V_\alpha(r)$ has to be multiplied by $\tau_1 \cdot \tau_2$ leading to a factor (-3) for $T=0$ NN states.

References

- [1] For an introduction into QCD see, e.g., F.J. Ynduráin, Quantum Chromodynamics (Springer, New York, 1983).
- [2] For a recent review of lattice gauge theories see M. Creutz, L. Jacobs and C. Rebbi, Phys. Rep. 95 (1983) 201.
- [3] G.E. Brown and M. Rho, Phys. Lett. B 82 (1979) 177;
G.E. Brown, M. Rho and V. Vento, Phys. Lett. B 84 (1979) 383.
- [4] A. Mittal and A.N. Mitra, Phys. Rev. D 29 (1984) 1408.
- [5] Yu You-Wen and Zhang Zong-Ye, Nucl. Phys. A 426 (1984) 557;
Y. Fujiwara and K.T. Hecht, preprint, to be published.
- [6] T. DeGrand, R.L. Jaffe, K. Johnson and J. Kiskis, Phys. Rev. D 12 (1975) 2060.
- [7] A.W. Thomas, S. Théberge and G.A. Miller, Phys. Rev. D 24 (1981) 216;
A.W. Thomas, Advances in Nucl. Phys. 13 (1983) 1.
- [8] M. Harvey, Nucl. Phys. A 352 (1981) 301, 326.
M. Harvey, J. LeTourneau and B. Lorazo, Nucl. Phys. A 424 (1984) 428.
- [9] A. Faessler, F. Fernandez, G. Lübeck and K. Shimizu, Phys. Lett. B 112 (1982) 201; Nucl. Phys. A 402 (1983) 555.
- [10] M. Oka and K. Yazaki, Prog. Theor. Phys. 66 (1981) 556, 572;
O. Morimatsu, K. Yazaki and M. Oka, Nucl. Phys. A 424 (1984) 412.
- [11] M. Cvetic, G. Golli, N. Mankoc-Borštnik and M. Rosina, Nucl. Phys. A395 (1983) 349.
- [12] K. Maltman and N. Isgur, Phys. Rev. D 29 (1984) 952.
- [13] Y. Suzuki and K.T. Hecht, Nucl. Phys. A 420 (1984) 525.
- [14] J. Burger and M. Hofmann, Phys. Lett. B 148 (1984) 25; and preprint, Erlangen, 1985.
- [15] F. Wang and C.W. Wong, Nucl. Phys. A 438 (1985) 620.
- [16] K. Holinde, Nucl. Phys. A 415 (1984) 477;
Ch. Elster and K. Holinde, Phys. Lett. B 136 (1984) 135;
K. Holinde, Phys. Lett. B 157 (1985) 123.

* A computer code for OBEPR is available from one of the authors (Ch.E.).

- [17] R.H. Dalitz, *Prog. Part. Nucl. Phys.* 8 (1982) 7;
N. Isgur and G. Karl, *Phys. Rev. D* 18 (1978) 4187;
but see also: H.R. Fiebig and B. Schwesinger, *Nucl. Phys. A* 393 (1983) 349.
- [18] G. 't Hooft, *Nucl. Phys. B* 72 (1974) 461; *B* 75 (1974) 461.
- [19] N.K. Pak and H.C. Tze, *Ann. Phys. (N.Y.)* 117 (1979) 164;
E. Witten, *Nucl. Phys. B* 160 (1979) 57;
J.M. Gipson and H.C. Tze, *Nucl. Phys. B* 183 (1981) 524.
- [20] T.H.R. Skyrme, *Proc. Roy. Soc. A* 260 (1961) 127; *Nucl. Phys.* 31 (1962) 556.
- [21] V. Vento, M. Rho, E. Nyman, J.H. Jun and G.E. Brown, *Nucl. Phys. A* 345 (1980) 413;
G.E. Brown, A.D. Jackson, M. Rho and V. Vento, *Phys. Lett. B* 140 (1984) 285.
- [22] L. Carroll, *Alice's Adventures in Wonderland* (Macmillan, London, 1865).
- [23] S. Nadkarin, H.B. Nielsen and I. Zahed, *Nucl. Phys. B* 253 (1985) 308.
- [24] G. Adkins and C.R. Nappi, *Phys. Lett. B* 137 (1984) 251;
M. Rho, Proc. Int. School of Physics "Enrico Fermi", 18–23 June 1984 (Varenna, Italy);
K. Ikebani, *Kyushu University Preprint*, 1984.
- [25] G.E. Brown and I. Zahed, *Phys. Rep.* 142 (1986) 1.
- [26] Mesons in Nuclei, eds. M. Rho and D.H. Wilkinson (North-Holland, Amsterdam, 1979).
- [27] T.E.O. Ericson and M. Rosa-Clot, *Nucl. Phys. A* 405 (1983) 497;
T.E.O. Ericson, *Nucl. Phys. A* 416 (1984) 281c.
- [28] R. Machleidt, The Meson Theory of Nuclear Forces and Nuclear Matter, in: *Relativistic Dynamics and Quark–Nuclear Physics: Proc. Los Alamos Workshop*, eds. M.B. Johnson and A. Picklesimer (Wiley, New York, 1986) p. 71.
- [29] H. Yukawa, *Proc. Phys. Math. Soc. Japan* 17 (1935) 48.
- [30] G. Wick, *Nature* 142 (1938) 993.
- [31] A. Proca, *J. Phys. Radium* 7 (1936) 347.
- [32] N. Kemmer, *Proc. Roy. Soc. (London) A* 166 (1938) 127.
- [33] C. Møller and L. Rosenfeld, *Kgl. Danske Vid. Selskab, Math.-Fys. Medd.* 17 (1940) No. 8.
- [34] J. Schwinger, *Phys. Rev.* 61 (1942) 387.
- [35] J. Kellogg, I. Rabi, N.F. Ramsey and J. Zacharias, *Phys. Rev.* 56 (1939) 728; 57 (1940) 677.
- [36] W. Pauli, *Meson Theory of Nuclear Forces* (Interscience, New York, 1946).
- [37] For more details about the early period of meson theory see G. Wentzel, *Quantum Theory of Fields* (Interscience, New York, 1949);
L. Rosenfeld, *Nuclear Forces* (North-Holland, Amsterdam, 1948); *Prog. Theor. Phys. (Kyoto)*, Suppl. 1 and 2 (1955).
- [38] C.M.G. Lattes, G.P.S. Occhiadini and C.F. Powell, *Nature* 160 (1947) 453, 486;
E. Gardner and C.M. Lattes, *Science* 107 (1948) 270.
- [39] M. Taketani, S. Nakamura and M. Sasaki, *Prog. Theor. Phys. (Kyoto)* 6 (1951) 581.
- [40] P. Cziffra, M.H. MacGregor, M.J. Moravcsik and H.P. Stapp, *Phys. Rev.* 114 (1959) 880.
G. Breit, M.H. Hull, K.E. Lassila and K.D. Pyatt, *Phys. Rev.* 120 (1960) 2227;
G. Breit, *Rev. Mod. Phys.* 34 (1962) 766.
- [41] J. Iwadare, S. Otsuki, R. Tamagaki and W. Watari, *Prog. Theor. Phys. (Kyoto)* 15 (1956) 86; 16 (1956) 455;
D.Y. Wong, *Phys. Rev. Lett.* 2 (1959) 406;
N.K. Glendenning and G. Kramer, *Phys. Rev.* 126 (1962) 2159.
- [42] M. Taketani, S. Machida and S. Onuma, *Prog. Theor. Phys. (Kyoto)* 7 (1952) 45.
- [43] K.A. Brueckner and K.M. Watson, *Phys. Rev.* 90 (1953) 699; 92 (1953) 1023.
- [44] N. Hoshizaki and S. Machida, *Prog. Theor. Phys. (Kyoto)* 27 (1962) 288.
- [45] The developments in the 1950s are well reviewed in:
Prog. Theor. Phys. (Kyoto), Suppl. 3 (1956);
R.J.N. Phillips, *Rep. Prog. Phys.* 22 (1959) 562;
M.J. Moravcsik, *The Two-Nucleon Interaction* (Clarendon Press, Oxford, 1963).
- [46] J.L. Gammel and R.M. Thaler, *Phys. Rev.* 107 (1957) 291, 1337;
G. Breit, *Proc. Natl. Acad. Sci. (U.S.)* 46 (1960) 746; *Phys. Rev.* 120 (1960) 287;
Y. Nambu, *Phys. Rev.* 106 (1957) 1366;
W.R. Frazer and J.R. Fulco, *Phys. Rev. Lett.* 2 (1959) 365;
J.J. Sakurai, *Ann. Phys. (N.Y.)* 11 (1960) 1; *Phys. Rev.* 119 (1960) 1784.
- [47] *Rev. Mod. Phys.* 39 (1967) 495;
Prog. Theor. Phys. (Kyoto), Suppl. 39 (1967);
P. Signell, *Advances in Nucl. Phys.* 2 (1969) 223.
- [48] Particle Data Group, *Rev. Mod. Phys.* 48 (1976) S116.
- [49] R. de Tourreil, B. Rouben and D.W.L. Sprung, *Nucl. Phys. A* 242 (1975) 445.

- [50] M.M. Nagels, T.A. Rijken and J.D. de Swart, Phys. Rev. D 17 (1978) 768; D 20 (1979) 1633.
- [51] K. Erkelenz, Phys. Rep. 13C (1974) 191.
- [52] K. Holinde and R. Machleidt, Nucl. Phys. A 247 (1975) 495; for a short review of HM1 see also the HM2 paper, next reference.
- [53] K. Holinde and R. Machleidt, Nucl. Phys. A 256 (1976) 479, 497.
- [54] J. Fleischer and J.A. Tjon, Phys. Rev. D 21 (1980) 87;
M.J. Zuilhof and J.A. Tjon, Phys. Rev. C 22 (1980) 2369.
- [55] M.J. Moravcsik, Rep. Prog. Phys. 35 (1972) 587.
- [56] A.D. Jackson, D.O. Riska and B. Verwest, Nucl. Phys. A 249 (1975) 397.
- [57] G.E. Brown and A.D. Jackson, The Nucleon-Nucleon Interaction (North-Holland, Amsterdam, 1976).
- [58] M. Lacombe et al., Phys. Rev. D 12 (1975) 1495.
- [59] R. Vinh Mau, in: Mesons in Nuclei, Vol. I, eds. M. Rho and D.H. Wilkinson (North-Holland, Amsterdam, 1979) p. 151.
- [60] M. Lacombe et al., Phys. Rev. C 21 (1980) 861.
- [61] M.H. Partovi and E.L. Lomon, Phys. Rev. D 2 (1970) 1999.
- [62] F. Partovi and E.L. Lomon, Phys. Rev. D 5 (1972) 1192;
E.L. Lomon, Phys. Rev. D 14 (1976) 2402; D 22 (1980) 229.
- [63] E.E. Salpeter and H.A. Bethe, Phys. Rev. 84 (1951) 1232.
- [64] R. Blankenbecler and R. Sugar, Phys. Rev. 142 (1966) 1051.
- [65] W.T. Nutt and L. Wilets, Phys. Rev. D 1 (1973) 2303; D 7 (1975) 110;
W.T. Nutt, Ann. Phys. (N.Y.) 100 (1976) 490.
- [66] H. Sugawara and F. von Hippel, Phys. Rev. 172 (1968) 1764.
- [67] G.E. Brown, A.D. Jackson and T.T.S. Kuo, Nucl. Phys. A 133 (1969) 481.
- [68] D. Schütte, Nucl. Phys. A 221 (1974) 450.
- [69] K. Kotthoff, K. Holinde, R. Machleidt and D. Schütte, Nucl. Phys. A 242 (1975) 429;
K. Kotthoff, R. Machleidt and D. Schütte, Nucl. Phys. A 264 (1976) 484.
- [70] K. Holinde and R. Machleidt, Nucl. Phys. A 280 (1977) 429.
- [71] K. Holinde, R. Machleidt, M.R. Anastasio, A. Faessler and H. Müther, Phys. Rev. C 18 (1978) 870.
- [72] K. Holinde, R. Machleidt, M.R. Anastasio, A. Faessler and H. Müther, Phys. Rev. C 19 (1979) 948.
- [73] K. Holinde, R. Machleidt, A. Faessler, H. Müther and M.R. Anastasio, Phys. Rev. C 24 (1981) 1159.
- [74] X. Bagnoud, K. Holinde and R. Machleidt, Phys. Rev. C 24 (1981) 1143.
- [75] K. Holinde and R. Machleidt, Nucl. Phys. A 372 (1981) 349.
- [76] X. Bagnoud, K. Holinde and R. Machleidt, Phys. Rev. C 29 (1984) 1792.
- [77] M.J. Zuilhof and J.A. Tjon, Phys. Rev. C 24 (1981) 736.
- [78] S. Weinberg, Phys. Rev. Lett. 18 (1967) 188.
- [79] S.J. Brodsky, Comments Nucl. Part. Phys. 12 (1984) 213.
- [80] E.E. van Faassen and J.A. Tjon, Phys. Rev. C 28 (1983) 2354; C 30 (1984) 285.
- [81] L.G. Arnold, B.C. Clark and R.L. Mercer, Phys. Rev. C 19 (1979) 917;
J.A. McNeil, J.R. Shepard and S.J. Wallace, Phys. Rev. Lett. 50 (1983) 1439;
J.A. Tjon and S.J. Wallace, Phys. Rev. Lett. 54 (1985) 1357.
- [82] M.R. Anastasio, L.S. Celenza, W.S. Pong and C.M. Shakin, Phys. Rep. 100 (1983) 327.
- [83] R. Brockmann and R. Machleidt, Phys. Lett. B 149 (1984) 283;
R. Machleidt and R. Brockmann, Phys. Lett. B 160 (1985) 364.
- [84] M.V. Hynes, A. Picklesimer, P.C. Tandy and R.M. Thaler, Phys. Rev. C 31 (1985) 1438.
- [85] G.E. Brown, W. Weise, G. Baym and J. Speth, Comments Nucl. Part. Phys.
- [86] R.V. Reid, Ann. Phys. (N.Y.) 50 (1968) 411.
- [87] W. Grein and P. Kroll, Nucl. Phys. A 338 (1980) 332.
- [88] F. Close, Introduction to Quarks and Partons (Academic Press, London, 1979).
- [89] Particle Data Group, Rev. Mod. Phys. 56 (1984) S1.
- [90] J.W. Durso, G.E. Brown and M. Saarela, Nucl. Phys. A 430 (1984) 653.
- [91] J.W. Durso, A.D. Jackson and B.J. Verwest, Nucl. Phys. A 345 (1980) 471.
- [92] K. Shimizu, A. Polls, H. Müther and A. Faessler, Nucl. Phys. A 364 (1981) 461.
- [93] Q. Ho-Kim and D. Turcot, Phys. Rev. C 22 (1980) 1352.
- [94] J.W. Durso, M. Saarela, G.E. Brown and A.D. Jackson, Nucl. Phys. A 278 (1977) 445.
- [95] R.A. Arndt et al., Phys. Rev. D 28 (1983) 97.
- [96] R. Dubois et al., Nucl. Phys. A 377 (1982) 554.
- [97] H. Stapp et al., Phys. Rev. 105 (1957) 302.
- [98] J. Hamilton and G.C. Oades, Nucl. Phys. A 424 (1984) 447.
- [99] R. Vinh Mau et al., Phys. Lett. B 44 (1973) 1.

- [100] R. Vinh Mau, private communication.
- [101] C.Y. Cheung and R. Machleidt, Proc. PANIC X, Heidelberg (W. Germany) 1984, Vol. I, p. C13;
C.Y. Cheung and R. Machleidt, Phys. Rev. C 34 (1986) 1181.
- [102] J. Bystricky and F. Lehar, Nucleon-Nucleon Scattering Data, Physics Data 11-3 (1982) (Fachinformationszentrum, Karlsruhe, 1982).
- [103] N. Hoshizaki, Prog. Theor. Phys., Suppl. 42 (1968) 107.
- [104] T.L. Houk, Phys. Rev. C 3 (1971) 1886.
- [105] C. van der Leun and C. Alderliesten, Nucl. Phys. A 380 (1982) 261.
- [106] R.V. Reid and M.L. Vaida, Phys. Rev. Lett. 34 (1975) 1064.
- [107] D.M. Bishop and L.M. Cheung, Phys. Rev. A 20 (1979) 381.
- [108] I. Lindgren, in: Alpha-, Beta-, Gamma-Spectroscopy, ed. K. Siegbahn (North-Holland, Amsterdam, 1965) Vol. II, p. 1623.
- [109] R.W. Bérard et al., Phys. Lett. B 47 (1973) 355.
- [110] G.G. Simon, Ch. Schmitt and V.H. Walther, Nucl. Phys. A 364 (1981) 285.
- [111] O. Dumbrăjs et al., Nucl. Phys. B 216 (1983) 277.
- [112] S. Klarsfeld, J. Martorell and D.W.L. Sprung, J. Phys. G 10 (1984) 165.
- [113] R.B. Wiringa, R.A. Smith and T.L. Ainsworth, Phys. Rev. C 29 (1984) 1207.
- [114] H. Arenhövel and W. Fabian, Nucl. Phys. A 282 (1977) 397;
E.L. Lomon, Phys. Lett. B 68 (1977) 419.
- [115] E.L. Lomon, Ann. Phys. (N.Y.) 125 (1980) 309.
- [116] E. Hadjimichael, Nucl. Phys. A 312 (1978) 341.
M. Kohno, J. Phys. G: Nucl. Phys. 9 (1983) L85.
- [117] R. de Tourreil and D.W.L. Sprung, Nucl. Phys. A 201 (1973) 193.
- [118] R. Koch and E. Pietarinen, Nucl. Phys. A 336 (1980) 331.
- [119] P. Kroll, Physics Data 22-1 (1981) (Fachinformationszentrum, Karlsruhe, 1981).
- [120] G. Höhler and E. Pietarinen, Nucl. Phys. B 95 (1975) 210.
- [121] E. Pietarinen, Helsinki, Univ. HU-/TFT-17-17.
- [122] W. Grein, Nucl. Phys. B 131 (1977) 255.
- [123] G. Höhler et al., Nucl. Phys. B 114 (1976) 505.
- [124] W. Grein and P. Kroll, Nucl. Phys. A 338 (1980) 332.
- [125] F. Iachello, A.D. Jackson and A. Landé, Phys. Lett. B 43 (1973) 191.
- [126] G.E. Brown and W. Weise, Phys. Rep. C 22 (1975) 281.
- [127] K. Holinde, in: Quarks and Nuclear Structure, ed. K. Bleuler, Lecture Notes in Physics (Springer Verlag, Heidelberg, 1984) Vol. 197.
- [128] R.H. Thompson, Phys. Rev. D 1 (1970) 110.
- [129] R. Machleidt and R. Brockmann, Proc. LAMPF Workshop on Dirac Approaches to Nuclear Physics, Los Alamos, NM, 11985, eds. J.R. Shepard, C.Y. Cheung and R.L. Boudrie (Los Alamos Conference LA-10438-C, 1985) p. 328;
R. Brockmann and R. Machleidt, to be published.
- [130] B.D. Day, Phys. Rev. Lett. 47 (1981) 226;
B.D. Day and R.B. Wiringa, Phys. Rev. C 32 (1985) 1057.
- [131] I.E. Lagaris and V.R. Pandharipande, Nucl. Phys. A 359 (1981) 349;
J. Carlson and V.R. Pandharipande, Nucl. Phys. A 401 (1983) 59.
- [132] H. Kümmel, K.H. Lührmann and J.G. Zabolitzky, Phys. Rep. 36 (1978) 1.
- [133] R. Machleidt and K. Holinde, Nucl. Phys. A 350 (1980) 396.
- [134] P. Grangé and A. Lejeune, Nucl. Phys. A 327 (1979) 335.
- [135] M.R. Anastasio, A. Faessler, H. Müther, K. Holinde and R. Machleidt, Phys. Rev. C 18 (1978) 2416.
- [136] R. Machleidt and K. Holinde, Phys. Lett. B 152 (1985) 295.
- [137] W.W. Daehnick, Phys. Rep. 96 (1983) 317.
- [138] W.H. Dickhoff, A. Faessler and H. Müther, Nucl. Phys. A 389 (1982) 492.
- [139] Ch. Elster, PhD Thesis, University of Bonn (1986).
- [140] D. Schütte, Proc. Int. Symp. on Interaction Studies in Nuclei, Mainz, 1974, eds. H. Jochim and B. Ziegler (North-Holland, Amsterdam, 1975) p. 841.
- [141] S.S. Schweber, An Introduction to Relativistic Quantum Field Theory (Row-Peterson, New York, 1961) pp. 415–434.
- [142] M. Baranger, in: Int. School of Physics Enrico Fermi, Course XL, Varenna 1967 (Academic Press, New York, 1969) p. 511;
M.B. Johnson, Ann. Phys. (N.Y.) 97 (1975) 400.
- [143] W. Rarita and J. Schwinger, Phys. Rev. 60 (1941) 61.
- [144] D. Lurić, Particles and Fields (Interscience Publishers, New York, 1968).
- [145] J.D. Bjorken and S.D. Drell, Relativistic Quantum Fields (McGraw-Hill, New York, 1965).
- [146] R.G. Newton, Scattering Theory of Waves and Particles (McGraw-Hill, New York, 1966).
- [147] M. Jacob and G.C. Wick, Ann. Phys. (N.Y.) 7 (1959) 404.

- [148] M.I. Haftel and F. Tabakin, Nucl. Phys. A 158 (1970) 1.
- [149] J. Blatt and L. Biedenharn, Phys. Rev. 86 (1952) 399.
- [150] A. Messiah, Quantum Mechanics, Vol. II (North-Holland, Amsterdam, 1965).
- [151] C. Bloch and J. Horowitz, Nucl. Phys. 8 (1958) 91.
- [152] J.L. Friar, in: ref. [26] p. 595;
M.R. Anastasio, A. Faessler, H. Müther, K. Holinde and R. Machleidt, Nucl. Phys. A 322 (1979) 369.
- [153] M. Lacombe et al., Phys. Lett. B 101 (1981) 139.
- [154] R.M. Woloshyn and A.D. Jackson, Nucl. Phys. B 64 (1973) 269.
- [155] G. Schierholz, Nucl. Phys. B 40 (1972) 335.
- [156] F. Gross, Phys. Rev. 186 (1969) 1448.
- [157] P.M. Morse and H. Feshbach, Methods of Theoretical Physics, Vols. I and II (McGraw-Hill, New York, 1953).